FINITE ELEMENT ANALYSIS OF A LABORATORY SOIL BOX TEST FACILITY FOR EVALUATING THE STRUCTURAL RESPONSE OF CONCRETE PIPE

By

MELISSA KAY CROSBY

A THESIS PRESENTED TO THE GRADUATE SCHOOL
OF THE UNIVERSITY OF FLORIDA IN PARTIAL FULFILLMENT
OF THE REQUIREMENTS FOR THE DEGREE OF
MASTER OF ENGINEERING

UNIVERSITY OF FLORIDA

2003

Copyright 2003

by

Melissa Kay Crosby

This thesis is dedicated to my loving family, my parents, Sandra and Oler Crosby, my sister Stacy Crosby and to my loving fiancé Devin Drake. I would also like to dedicate this thesis to my loving Aunt Linda and Uncle Dewayne as they have offered their support and love throughout this endeavor. It is with the love and support of my family and friends that I am able to reach my goals.

ACKNOWLEDGMENTS

I would like to thank all of the members of my supervisory committee for their help and ideas throughout this effort. Dr. David Bloomquist, committee cochair, provided much insight, knowledge and financial support toward the completion of the work. Dr. Andrew Boyd, committee chair, provided valuable time and knowledge of the subject, as well as financial support, making this research successful.

I would also like to thank Dr. H.R. Hamilton for his contribution of time and knowledge, which provided to be invaluable assistance during this effort. An additional thank you goes to Scott Jacobs for his time and the computer expertise he provided during the research.

Above all, I would like to thank God for giving me the ability to withstand the trials and tribulations throughout this effort. It is through Him that I am able to persevere and succeed in all my endeavors.

I would also like to thank my best friend, who is also my fiancé, Devin Drake, for the support and patience he offered me during the research and writing of this thesis.

TABLE OF CONTENTS

page

ACKNOWLEDGMENTS iv

LIST OF TABLES vii

LIST OF FIGURES viii

ABSTRACT xii

CHAPTER

1 INTRODUCTION 1

2 LITERATURE REVIEW 3

Introduction to Pipes 3
Concrete Pipes 3
Concrete Pipe Testing 4
Three-Edge Bearing Strength 6
Bedding Factors and Classifications 7
History of Pipe Testing Facilities 9

3 STANDARD REINFORCED CONCRETE PIPE VS. FIBER REINFORCED CONCRETE PIPE 22

Background Information on Concrete Pipes 22
Cracking in Concrete--The Fracture Zone 23
Standard Reinforced Concrete Pipe--SRCP 25
Mechanics of SRCP 25
Reinforcement 27
Strength 27
Structural Performance 28
Fiber Reinforced Concrete Pipe--FRCP 29
Mechanics of FRCP 30
Fiber-Matrix Bond 31
Fiber-Fiber Interaction 31
Load vs. Deflection in Fiber Reinforced Concrete 32
Stages of Cracking-Fiber Intervention 33
Strength 35
Toughness 35

FRCP versus SRCP....36
Manufacturing....36
Installation....36
Performance....37

4 INSTRUMENTATION AND TESTING TECHNIQUES....38

Crack Detection and Deflection in Concrete Pipes....38
Background on Acoustic Emission Testing....38
Preamplifiers....42
Postamplifiers and Signal Processors....42
Transient Recorders....43
Spectrum Analyzers....44
LAM--Local Area Monitor....45
Minolta 3D Digitizer--VIVID 900....48
Hardware....48
Accessories....49
Operation....51

5 PLAXIS VERSION 7.2--FINITE ELEMENT CODE FOR SOIL AND ROCK ANALYSIS....53

Introduction....53
Plaxis--Input....56
Plaxis--Calculations....64
Plaxis--Output....68

6 FINITE ELEMENT ANALYSIS OF A SOIL BOX TEST FACILITY....74

Introduction....74
Plaxis 3D--Verification Analysis....77
Soil Box Analysis....83
Soil Box Analysis--No pipe....84
Soil Box Analysis--Modeled with Test Pipe....92
Four Wall Friction Analyses....99

7 RECOMMENDATIONS....102

APPENDIX PLAXIS 2D ANALYSIS AND RESULTS....105

Dimension Analysis....105
Wall Friction/ Soil Compaction Analysis....108

LIST OF REFERENCES....112

BIOGRAPHICAL SKETCH....114

LIST OF TABLES

Table		page
3.1	Typical Fiber-Matrix Pullout Strengths (Mindess, 2003).	32
4.1	Specifications of Minolta VIVID 900 3D digitizer.	52
6.1	Material Properties of the soil (Loose & Dense).	76
6.2	Material Properties of the 18” diameter concrete pipes (FRCP & SRCP).	76
6.3	Material Properties of the 24” diameter concrete pipes (FRCP & SRCP).	76
6.4	Material Properties of the 48” diameter concrete pipes (FRCP & SRCP).	77
6.5	Three Dimensional Analysis Verification of Plaxis 2D Wall Friction Analysis	83
6.7	Displacement of Pipe Length with Shear Stress Induced on the Ends.	101
6.8	Extreme Effective Normal Stresses Along the Length of Pipe with Shear Stress Induced on the Ends.	101
A.1	Wall Friction Analysis-Plaxis 2D Finite Element Analysis	111

LIST OF FIGURES

Figure page

2.1 Early Concrete Pipe Testing....5

2.2 Three edge bearing test for concrete pipe 7

2.3 Ohio University Full Scale Testing Site....13

2.4 The Center for Pipes and Underground Structures Test Facility at Ohio University.13

2.5 Hardie Pipe's Rigid Soil Box Front View....15

2.6 Hardie Pipe's Rigid Soil Box Full Image View....16

2.7 Hardie Pipe Flexible Soil 16

2.8 Hardie Pipe Flexible Soil Box Testing conducted at UCF....17

2.9 LVDT's Shown to Measure Deflection of Sidewalls....18

2.10 Flexure Crack At The Crown of Fiber Reinforced Concrete Pipe. 19

2.11 Reinforced Concrete Pipe Cracking At The Crown. 20

3.1 Coordinate system and stress components ahead of crack tip....24

3.2 Three Modes of Cracking. 24

3.3 Standard Reinforced Concrete Pipe Section Cracked. 26

3.4 Standard Reinforcing Steel Rebar. 28

3.5 Typical Fiber Reinforced Concrete Pipe 29

3.6 Typical load-deflection curve for fiber reinforced concrete in flexure 33

3.7 Schematic representation of fibers bridging across a crack. 34

4.1 Burst Acoustic emission signal with properties 39

4.2 Acoustic Emission Process....40

4.3 Pre-amplifiers 43
4.4 Transient recorder with multiple AE signals....44
4.5 Digital Oscilloscope 45
4.6 LAM--Local Area Monitor 46
4.7 Minolta VIVID 900 Non-Contact 3-D Digitizer....49
4.8 Compact Flash Memory Card 49
4.9 Rotating Stage Set for Scanning a Full 3-D image 50
4.10 Tripod (left) and Tilting Base Mount (right) for Minolta VIVID 900 50
5.1 Plaxis 7.2 Computer Aided Drafting screen used to create modeling analysis....54
5.2 General Settings window in Plaxis 7.2....56
5.3 Plaxis 7.2 Main Toolbar. 58
5.4 Tunnel Designer in Plaxis 7.2. 58
5.5 Standard Fixities in Plaxis 7.2 shown on a soil box with right half tunnel. 59
5.6 Material Sets Window in Plaxis 7.2. 61
5.7 Soil Input in Plaxis 7.2--Mohr Coulomb Model. 61
5.8 Beam Properties Input Window in Plaxis 7.2. 62
5.9 Pore Water Pressure & Initial Stress Modes in Plaxis 7.2. 63
5.10 Plaxis 7.2 Calculations Program. 65
5.11 Plaxis 7.2 Calculations Program--Parameters Tab....66
5.12 Plaxis Calculations Program--Multipliers Tab....67
5.13 Plaxis Output program with deformed mesh displayed on example model. 69
5.14 Plaxis Output Effective Mean Stresses Displayed by Mean Shading. 69
5.15 Plaxis Output Effective Mean Stresses Displayed by Contours. 70
5.16 Stress Distribution Cross Section A-A in Plaxis 7.2--Output Program 71
5.17 Horizontal Displacement Cross Section A-A in Plaxis 7.2--Output Program 72

5.18 Displacements for the Pipe and Interface--Plaxis 7.2 Output Program. 72
5.19 Bending Moment for the Pipe--Plaxis 7.2 Output Program. 73
6.1 Three Dimensional View of Total Displacements for 24” FRCP. 79
6.2 Three Dimensional View of Total Displacements for 24” SRCP 79
6.3 Left Side Interface of Soil Box Model 24” FRCP 80
6.4 18” Diameter FRCP Friction Area on Surface of Pipe. 81
6.5 18” Diameter FRCP Near Zero Frictionless Area on Surface of Pipe. 82
6.6 10’ Length Soil Box: Effective Mean Stresses with Sidewall Friction: 85
6.7 15’ Length Soil Box: Effective Mean Stresses with Sidewall Friction.....86
6.8 20’ Length Soil Box: Effective Mean Stresses with Sidewall Friction.....86
6.9 10’ Length Soil Box: Effective Mean Stresses with Frictionless Sidewalls. 87
6.10 15’ Length Soil Box: Effective Mean Stresses with Frictionless Sidewalls. 87
6.11 20’ Length Soil Box: Effective Mean Stresses with Frictionless Sidewalls. 88
6.12 10’ Length Effective Normal Stresses Left Sidewall Friction Plane. 89
6.13 15’ Length Effective Normal Stresses Left Sidewall Friction Plane. 89
6.14 20’ Length Effective Normal Stresses Left Sidewall Friction Plane. 90
6.15 10’ Length Effective Normal Stresses Left Sidewall Frictionless Plane. 90
6.16 15’ Length Effective Normal Stresses Left Sidewall Frictionless Plane. 91
6.17 20’ Length Effective Normal Stresses Left Sidewall Frictionless Plane 91
6.18 10’ Length Effective Mean Stress with Friction on Sidewalls.....93
6.19 15’ Length Effective Mean Stress with Friction Sidewalls.....93
6.20 20’ Length Effective Mean Stress with Friction Sidewalls.....94
6.21 Effective Normal Stress Imposed on Perimeter of Test Pipe. 94
6.22 10’ Length Effective Mean Stress with Frictionless Sidewalls/ Pipe. 96
6.23 15’ Length Effective Mean Stress with Frictionless Sidewalls/ Pipe. 96

6.24 20’ Length Effective Mean Stress with Frictionless Sidewalls/ Pipe. 97

6.25 10’ length Effective Mean Stress with Frictionless Sidewalls and Friction Around Perimeter of Pipe. 97

6.26 15’ length Effective Mean Stress with Frictionless Sidewalls and Friction Around Perimeter of Pipe. 98

6.27 20’ length Effective Mean Stress with Frictionless Sidewalls and Friction Around Perimeter of Pipe. 98

6.28 Plaxis 3D Test Pipe with Shear Stress Induced on Ends of Pipe 100

A.1 Plaxis 2D Symmetry Model of 24” diameter FRCP. 105

A.2 Three Different Widths Modeled in Plaxis 2D: 10, 15, 20 feet wide.....106

A.3 Example of Cross Section Used to Examine the Sidewall Stresses (20’ Width)...107

A.4 Example FRCP Cross Section of Sidewall Stresses (10’ wide box).....109

A.5 Example FRCP Cross Section of Sidewall Stresses (15’ wide box).....109

A.6 Example FRCP Cross Section of Sidewall Stresses (20’ wide box).....110

Abstract of Thesis Presented to the Graduate School
of the University of Florida in Partial Fulfillment of the
Requirements for the Degree of Master of Engineering

FINITE ELEMENT ANALYSIS OF A LABORATORY SOIL BOX TEST FACILITY FOR EVALUATING THE STRUCTURAL RESPONSE OF CONCRETE PIPE

By

Melissa Kay Crosby

May 2003

Chair: Andrew J. Boyd
Cochair: David Bloomquist
Major Department: Civil and Coastal Engineering

Two and three dimensional finite element analyses were used to examine the stresses on a laboratory soil box test facility designed to evaluate the structural response of fiber reinforced and standard reinforced concrete pipes. Boundary conditions were examined in an attempt to minimize the effects on the concrete pipe tested. The state of stress in the soil due to the applied loading was studied, along with its influence on the concrete pipe. An extensive literature search is presented on the history of soil box testing of pipes. Small and large-scale test facilities have been discussed through previous testing in the literature search. A description of the test facilities, both small and large, is presented. Plaxis, a two and three-dimensional finite element analysis program, analyzes the stresses on the sidewalls for the dimension design of a soil box properly scaled to minimize the boundary effects on the concrete pipe specimens. Comparisons were made among three different proposed box lengths. It was found that as the length

increased, the stress concentrations and intensities decreased, thus minimizing the boundary effects.

Sidewall friction and its effects on the test pipe were examined. Two and three dimensional finite element analysis was used to assign a friction angle on the sidewalls in order to model the soil structure interaction. An additional analysis was done to examine the possibility of shear stresses induced on the ends of the pipe. Friction was induced on the front and rear wall to create shear stresses on the ends of the pipe. Shear stresses were induced on the ends of the pipe in the three-dimensional analyses but very little difference in displacement occurred. A comparison of soil backfill, between a loose and dense compaction, showed a large difference in overall settlement. Maximum stresses and pipe deflections were approximately double for the loose compaction when compared to the dense backfill.

CHAPTER 1
INTRODUCTION

Structural performance testing of small diameter buried pipes dates back to the 1930's. Large scale testing of buried concrete pipes provides useful information for evaluating the soil structure response expected under field conditions. In the United States, large-scale test facilities exist at Utah State University, the University of Massachusetts at Amherst, and Ohio University. Additional facilities can be found at the University of Western Ontario in Canada and LGA Geotechnical Institute in Germany (Brachman et al., 2001). Two small-scale test facilities have been designed and constructed by Hardie Pipe, Inc. and are pending patents. Each of the testing facilities at these institutions suffers from limitations stemming from boundary conditions inherent in their respective equipment configurations. Many of the existing test facilities cannot closely approximate expected field conditions with respect to the stress states associated with small diameter buried pipes. When large scale testing is not possible at a particular location, a laboratory test facility is needed to examine the structural response of buried pipes. A soil box test facility is required to investigate small diameter buried pipes and allow a laboratory assessment of their performance under simulated field conditions.

Laboratory test facilities allow better control over monitoring and testing procedures than do field testing techniques. Boundary conditions, such as the method of loading and the geometry of the test facility, may significantly influence the results of the test. The structural response of buried pipe can be significantly affected by the boundary conditions if the test facility is not properly designed. Sufficient dimensions are

necessary, under expected loading conditions, to limit sidewall deflection and minimize boundary condition effects. The primary concern to be considered in the analysis of testing apparatus design is elimination of the influence of boundary conditions on the structural response of the concrete pipe specimen.

Both a two and three-dimensional finite element analysis program (i.e., Plaxis 7.2 and Plaxis 3D Tunnel) will be used to evaluate the boundary conditions induced by an applied distributed load. Stresses imparted by the load dissipate throughout the soil, applying load to the pipe, which is surrounded by backfill. A wall stress and sidewall friction analysis will provide dimensional information that can be used to minimize the effect of boundary conditions. Two different backfills will be evaluated, loose and densely compacted soil.

The objective of this work is to perform a finite element analysis for a laboratory test facility to be used in the evaluation of structural performance in small diameter concrete pipes, including both fiber reinforced and traditional steel reinforced concrete. The facility will be fabricated of steel and designed to limit sidewall deflections. The soil box test facility will be loaded using inflatable bladders placed on top of the soil. Attention will be focused on the influence of the boundary conditions on the soil box and how efficiently and accurately the test setup reproduces actual field conditions for small diameter buried pipe. Consideration will be given to determination of optimal test cell dimensions and, the influence of sidewall friction and boundary stiffness on the structural performance of the concrete pipe and soil behavior.

CHAPTER 2
LITERATURE REVIEW

Introduction to Pipes

Buried pipes and/or conduits have improved the standard of living for people since the beginning of civilization. Remnants of such structures from ancient civilizations have been found in Europe, Asia, and even the western hemisphere, where some of the ancient inhabitants of South and Central America established functional water and sewer systems (Moser, 2001). Buried pipes serve many purposes, including sewer lines, drain lines, water mains, gas lines, telephone and electrical conduits, culverts, oil lines, coal slurry lines, subway tunnels, and heat distribution lines. In comparing the design used in the 1800's to the design applications we have today, it is apparent that the degree of technology has increased significantly.

Engineers and planners take subsurface infrastructure into account before developing buildings and houses for a community. The underground water systems serve as arteries for cities, and the sewer systems serve as veins to carry off the waste (Moser, 2001). High quality drinking water is taken for granted by humans in today's society. To ensure adequate quality, pipes must be designed and constructed to prevent the introduction of contaminants. The same standards apply to sewer pipes so as to prevent seepage of contaminants into the ground, which may reach the water table and aquifers.

Concrete Pipes

Pipes are classified as either rigid or flexible. A flexible pipe is defined as one that will deflect at least 2 percent without structural distress. Flexible pipes, such as those

made of polyethylene plastics, do not fall within the scope of this project. A rigid pipe is one that does not meet the flexible pipe deflection criterion. The two major types of rigid concrete pipes are steel reinforced concrete pipes and fiber reinforced concrete pipes. Parameters of the pipes are analyzed to design for maximum performance. Rigid pipes must have the strength to resist wall stresses due to internal pressures or external loads that are considered critical under anticipated service conditions. Design parameters include strength, stiffness, corrosion resistance, density, durability and ease of joining. A pipe must have sufficient strength and/or stiffness to perform its intended function and also must be sufficiently durable to perform this function throughout its intended service life. Strength is defined as the ability to resist applied stress. Internal pressures, soil pressures, live loads, differential settlement and longitudinal bending moments impose stress on the pipe. Stiffness is described as a material's ability to resist deflection. The modulus of elasticity of a material is directly related to its stiffness, thus affecting deformation of the pipe wall during loading. Durability is the ability of a material to resist degradation (i.e., corrosion, chemical deterioration, abrasion) due to deleterious environmental exposures. Durability is a critical parameter when determining a design service life for performance.

Concrete Pipe Testing

In the early 1900's, concrete pipe testing consisted of placing sand bags on top of a pipe to obtain a static distributed load as shown in Figure 2.1. In 1913, Marston researched loads induced on buried pipe by the soil above the pipe. This research marked the beginning of the development of a method for calculating earth loads on buried pipes. Shortcomings include an assumption that the vertical load due to the backfill being

Figure 2.1: Early Concrete Pipe Testing (Photo courtesy of Hardie Pipe, Inc.)

uniformly distributed. Results were significantly limited by the technology available at the time and did not include such effects as pipe- soil interaction or settlement ratio. The Marston load theory, based upon the concept of a prism-shaped soil load being applied to the pipe, resulted in what is known today as the Marston load equation (2.1).

$$W_d = C_d \gamma B_d^{\,2} \tag{2.1}$$

W_d= load on conduits per unit length

C_d = load coefficient for ditch conduits

γ = unit weight of backfill

B_d = horizontal width of ditch at top of conduit

As technology progressed, more test methods were standardized for the evaluation of concrete pipe strength. Spangler conducted research in the 1930's that proposed four classifications of bedding for pipes covering normal installations in the field. In order to investigate the soil-structure interaction, the American Concrete Pipe Association (ACPA) undertook a long-range research program to examine the nature of the loading imposed on a buried pipe (Moser, 2001). Their research covered the development of a

finite element program used to simulate non-linear behavior of buried pipe, validation of the program, and analysis of the soil around the pipe. Full scale testing conducted at the Transportation Research Center in East Liberty, Ohio found the strains along the length of the pipe to be insignificant. The results were symmetric about the vertical plane of symmetry of the pipe, thus validating the use of plane strain finite element analysis.

Three-Edge Bearing Strength

Rigid nonpressure pipes are tested for strength in the laboratory using the three-edge bearing test (ASTM C 497). The performance criteria require the each pipe size and class pipe to reach specified laboratory strengths relative to the anticipated service load condition and required ultimate strength. Traditional design practice uses the three-edge bearing load that produces a 0.01-inch crack width as the design load. The failure load in three-edge bearing test is defined as the load per unit length required to cause crushing or critical cracking of the pipe test specimen. The strength thus obtained is the failure load in the laboratory only, and is not necessarily equivalent to the load that will cause failure in the field under buried conditions. Figure 2.2 shows a schematic diagram of the three edge bearing test for a rigid pipe, where W represents the distributed load, D the pipe diameter, R the radius of the wood support blocks and C the clearance beneath the pipe.

Testing of nonreinforced concrete pipes are specified in ASTM C 14. Nonpressure reinforced concrete pipe is specified by its “D-load” strength, as determined in ASTM C 76. The D- load is defined as the load applied to a pipe under three-edge bearing conditions, expressed in pounds per linear foot per foot of inside diameter.

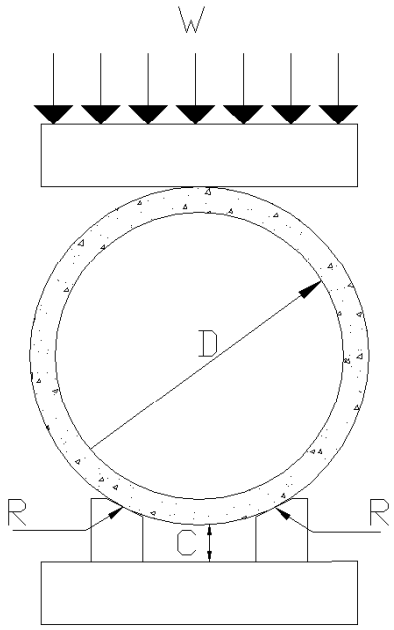

Figure 2.2: Three edge bearing test for concrete pipe

Bedding Factors and Classifications

Laboratory testing and field-testing can result in two different strengths for concrete pipes. As previously stated, the strength causing failure in the laboratory does not always cause failure in a buried condition. Past experiments show that the estimated load required to cause failure of a buried pipe, according to the Marston load equation, is greater than that resulting from the three-edge bearing strength.

The most important factor influencing this discrepancy is the method in which the pipe is bedded. Bedding factors are variables that were developed to account for the type of soil in which the pipe is installed. The bedding factor (sometimes called the load factor) is the ratio between the strength of a buried pipe and the strength of the same pipe as determined by the three-edge bearing test. Bedding conditions affect the support reaction beneath the pipe and the lateral pressure on the pipe.

Conduits used in ditch drainage have four bedding classifications. The load factors associated with these classifications have been determined empirically and do not take into account any lateral pressures exerted by the backfill. Furthermore, it has been noted that the specified soil compaction cannot be depended upon reliably. Bedding classifications in which a licensed engineer should inspect the installation are Class A, Class B, Class C and Class D.

Class A (also known as Concrete Cradle Bedding has a load factor of 2-4 and occurs when the lower part of the conduit is bedded in a cradle constructed of 2,000 psi concrete, having a minimum thickness of one-fourth the pipe's internal diameter. The cradle must extend up the sides of the pipe for a height equal to one-fourth its outside diameter.

Class B (also known as First Class Bedding) has a load factor of 1.9 and is where the pipe is carefully bedded in an earth foundation, composed of fine granular materials, that is carefully shaped to fit the lower part of the pipe. The minimum bedding width is 60 percent of the pipe diameter and the remainder of the conduit must be entirely surrounded to a height at least 1 ft above its top by granular materials that are carefully placed in order to completely fill all spaces under and adjacent to the pipe. This fill material must be thoroughly compacted on each side, and beneath the pipe, and placed in layers not exceeding 0.5 ft in thickness.

Class C (also known as Ordinary Bedding) has a load factor of 1.5, and applies to pipe bedded with "ordinary" care in an earth foundation shaped to fit the lower part of the pipe, with reasonable accuracy, for a width of at least 50 percent of its outside diameter. The remainder of the pipe is surrounded to a height of at least 0.5 ft above its top by

granular materials that are shovel-placed and shovel-tamped to completely fill all spaces under and adjacent to the pipe (Moser, 2001).

Class D (also known as Impermissible Bedding) has a load factor of 1.1. This class is where there is little or no care applied to shaping the foundation to fit the lower part of the pipe or to refill all spaces under and around it. This class of bedding is not recommended for culvert and sewage pipe. Major pipe manufacturing associations recommend bedding factors that correspond to those listed in the Water Pollution Control Federation Manual of Practice, No. FD-5, Gravity Sanitary Sewer Design and Construction (Moser, 2001).

History of Pipe Testing Facilities

A pipe's insitu performance is a function of its material properties, any applied loads, and the soil-structure interaction. Concrete pipe testing dates back to the early 1900's, when testing involved the placement of sand bags on top of the pipe to achieve static, distributed load. Traditional concrete design methods are based on research conducted at Iowa State University that dates back to the 1930's. By the 1930's, Spangler had proposed four classifications of bedding that covered the range of installations that could be anticipated in normal installations (Parmalee, 1977). Some design methods were found to be too conservative as research progressed.

Prior to the 1970's, the testing of buried pipes, along with the soil-structure interaction, did not produce accurate results. In 1970, the American Concrete Pipe Association undertook a long-range research program to determine the nature of loading imposed on buried concrete pipe and to develop a reliable design method based upon soil-structure interaction (Parmalee, 1977). This research program purported to develop a comprehensive finite element analysis program to simulate the non-linear behavior of

buried concrete pipe. The results of the research program indicated that strains along the length of the pipe were insignificant. It was also determined that results were symmetric about the vertical plane of symmetry of the pipe, thus validating the use of plane strain finite element analysis.

Soil box testing began in the 1960's. This approach consists of a three-dimensional box of known size, containing a pipe and backfilled with soil. Between 1960 and 2000, several researchers conducted large and small scale testing on pipes under simulated insitu conditions. Each of these research programs were formulated so as to design a test that would yield results similar to those found in the field.

Selander et al. evaluated reinforced plastic mortar pipe in 1972. His design for the height of overlying soil (approximately 12 feet high) proved later to be overly conservative.

Bland and Sheppard (Bland, 1985) used research findings from the Transport and Road Research Laboratory and the Clay Pipe Development Association obtained with unrealistic boundary conditions to develop a test for clay pipes using a large test pit in order to investigate structural performance. By using a large test pit, the prior limitations of unrealistic boundary conditions found in a small soil box test were eliminated.

Bishop tested buried PVC pipes in a soil cell and in a full-scale embankment. He proved it is possible to separate the long-term behavior of the pipe from the long-term behavior of the soil. In-situ load increases with time, whereas the loads applied to the soil cell will decay since the PVC pipe undergoes stress relaxation (Bishop, 1981).

In 1981, Gaube and Miller designed a sand box with 5mm thick sheet steel to test plastic sewer pipe. They placed a 'water-filled bladder' between the tops of the soil and

the soil box lid to apply pressure to the top of the soil. Their design employed a box width of eight times the diameter of the pipe. The soil box tests produced results similar to field tests and indicated that plastic pipe could withstand up to 150 feet of earth fill, assuming that compacted soil was used for the fill (Gaube, 1981).

Molin tested flexible 200mm diameter PVC pipes in a soil box, while investigating backfills of sand, compacted clay and uncompacted clay (Molin, 1981). His results showed that the vertical soil pressure above the pipe increases with increasing pipe stiffness. Molin stated that his soil box test results were similar to field tests yet claimed the field tests were more vague. Measured strains were compared to calculated strains and found to be acceptable.

In 1985, Singhal and Veliz believed that the boundary conditions and edge effects could be eliminated (Singhal, 1985). In other words, the soil surrounding the pipe in the soil box carried stresses and strains that dissipated laterally with distance. Singhal and Veliz tested cyclic torsion, axial pullout, and bending on buried pipes. In the same year Todres and McClinton used a soil box constructed of 19mm plywood panels pinned through steel channels and angles. A 4-inch diameter steel pipe was tested for performance by measuring strains on the pipe's walls. A controlled load placed on top of the fill allowed them to compare the measured bending stresses with calculated stresses, and obtained a reasonable correlation (Todres, 1985).

A finite element analysis was implemented into the design of a soil box test facility (Zanzinger, 1995). Zanzinger and Gartung based their design on the drop in modulus of elasticity of the pipe over time. When loading the surface of the soil, stresses from the pipe are distributed to the soil surrounding the pipe. A finite element analysis approach

was used to determine the required soil box width needed to eliminate stresses acting on the sides of the box. During the 1000-hour test, a laser was used to measure pipe deformation.

The size of a testing facility determines whether one needs to design a laboratory test site to simulate field conditions. Some research centers are equipped with full-scale facilities that reproduce results that would be expected in the field because the research is essentially performed in a field test site. The Center for Pipes and Underground Structures was developed by both the Ohio University and ORITE (Ohio Research Institute for Transportation and the Environment) and is shown in Figures 3 and 4. This facility is one of the largest existing test facilities of this nature. When a large test site like this is not available, a smaller facility or soil box is needed to recreate tests under laboratory conditions. Laboratory tests provide better control of the test and conditions.

As stated earlier, Ohio State University is home to one of the largest in situ pipe testing facilities. Smaller test facilities are needed for researchers unable to gain access to such large test pits. Brachman et al. states that boundary conditions, such as the geometry of testing facilities and the method of load application, may significantly affect test results. Advantages of soil box testing include better control and access for instrumentation.

Figure 2.3: Ohio University Full Scale Testing Site (Courtesy of James Hardie Pipe, Inc.)

Figure 2.4: The Center for Pipes and Underground Structures Test Facility at Ohio University. (Courtesy of James Hardie Pipe, Inc.)

Brachman et al. conducted research entitled “Interpretation of Buried Pipe Test: Small-Diameter Pipe in Ohio University Facility.” A small diameter leachate collection pipe was analyzed using two and three-dimensional analyses. Numerical analysis provides one way to assess boundary conditions on measured results when laboratory tests are conducted. Tests were performed at the Ohio University facility for small diameter high-density polyethylene leachate collection pipes. Boundary conditions of the test facility, along with the stress states in the soil and the pipe’s response to the soil interaction, were investigated.

Two large hydraulic cylinders were used to apply a vertical force to a loading platform, thus loading the soil and underlying pipe. The backfill surrounding the pipe consisted of crushed stone over clay bedding to simulate a leachate collection system. The most important boundary condition for this study was the method of load application. A platform of eight W-shaped steel beams welded together provided a rigid footing for the applied load. Results from the finite element analysis clarified the state of stress in the soil due to the overburden load induced by the platform loading. The facility results were compared to the expected results from the field installation.

The tests results were complex and required careful interpretation before drawing any conclusions concerning pipe performance for leachate collection in landfills. The stresses induced by the rigid platform differed from the expected uniform load in a landfill. It was found that, at low load levels, a portion of the backfill material at the soil-pipe interface yielded due to the crushed stone behaving as a beam in bending. This effect caused a reduction in the lateral support provided to the pipe, thus increasing pipe deformations and altering the mode of pipe deflection. The measured deflections were

higher than expected in a landfill situation. Care must be taken when interpreting the results from facility testing. Numerical analysis can be successful when correctly interpreted to evaluate boundary conditions.

James Hardie tested a *rigid* soil box constructed with lateral sidewalls of 9mm angle iron. The angle iron effectively restricted any lateral movement. Hardie's *rigid* pipe testing apparatus is shown in Figures 2.5 and 2.6.

After realizing that the rigid box was restrictive and did not accurately represent in situ conditions, Hardie developed a flexible soil box (shown in Figure 2.7). The new box was designed with moving lateral walls. Leaf springs supported the walls in an attempt to simulate in situ stiffness. The flexible soil box provided the option of changing the sidewall's lateral stiffness to reflect different burial conditions.

Figure 2.5: Hardie Pipe's *Rigid* Soil Box Front View (Courtesy of Hardie Pipe Inc.)

Figure 2.6: Hardie Pipe's Rigid Soil Box Full Image View (Courtesy of Hardie Pipe)

Figure 2.7: Hardie Pipe Flexible Soil (Courtesy of Hardie Pipe, Inc.)

Testing using this type of flexible soil (performed by Hardie Pipe) was observed on November 13, 2002 at the University of Central Florida (UCF) in Orlando, Florida as seen in Figure 2.8. This research will compare the soil box test results to in situ results. Two different types of reinforced concrete pipe were tested; Hardie Pipe's fiber reinforced concrete pipe (in both dry and saturated conditions) and standard reinforced concrete pipe. The backfill used in these tests was compacted coarse sand. Two sheets of Teflon were used to line the inside walls of the box in order to reduce the sidewall friction angle to less than 5 degrees. The box was loaded using a concrete slab placed on top of a series of parallel 2 x 4's in order to simulate a uniformly distributed load. The loading was controlled and monitored using a personal computer.

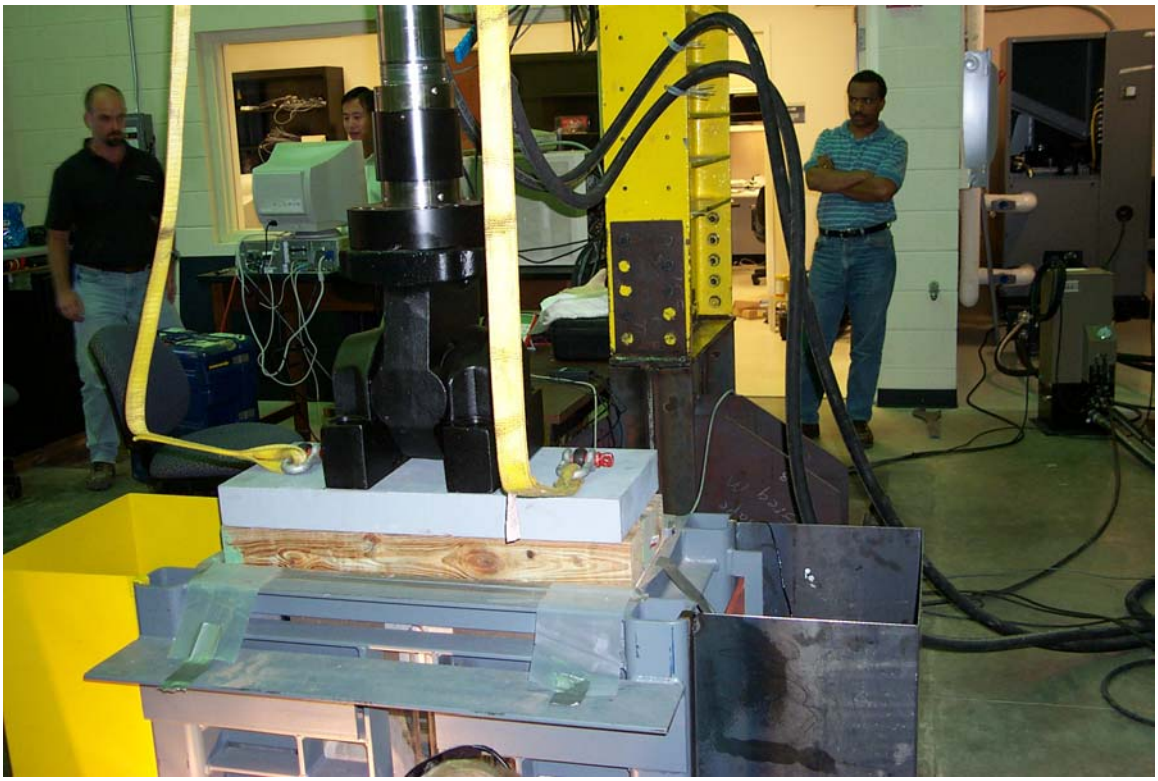

Figure 2.8: Hardie Pipe Flexible Soil Box Testing conducted at UCF.

During the test, LVDT's were used to measure the deflection of the sidewalls induced by the applied loading (Figure 2.9). The load level was noted at the point where the first crack visible to the naked eye formed and loading was then continued until multiple cracks appeared. The flexible soil box is equipped with a viewing port of plexi-glass to monitor the pipe during loading. Interior surfaces of the crown and invert of the pipe are visible from the viewing port. Cracking of the fiber reinforced concrete pipe is

Figure 2.9: LVDT's Shown to Measure Deflection of Sidewalls.

shown in Figure 2.10, as viewed through the viewing port of the soil box. Each of the tests was continued until cracks propagated across the crown and invert of the pipe. For both the dry and saturated conditions of fiber reinforced concrete pipes, the pipe was loaded until cracking occurred in flexure.

Figure 2.10: Flexure Crack At The Crown of Fiber Reinforced Concrete Pipe.

Standard reinforced concrete pipes were also tested using the flexible soil box. Compaction of the backfill was performed in accordance with the same procedure as used in the fiber reinforced concrete pipes. Cracking of the reinforced concrete pipe occurred at the crown of the pipe, as shown in Figure 2.11. Though the same loading procedure was used for the reinforced concrete pipes, it resulted in a much lower maximum load when compared to the fiber reinforced concrete pipes. The testing observed on November 13, 2002, was only a portion of the testing program being conducted at the University of Central Florida.

Figure 2.11: Reinforced Concrete Pipe Cracking At The Crown.

Brachman et al. discussed the design of a laboratory facility and the testing of buried pipe performance. Their study considered a limiting applied pressure of 1000kPa, based on a burial length of 50 m and a soil density of 20kN/m^3, and then used finite element analysis to determine the effect of sidewall friction on the soil. Symmetry about the vertical diameter of the pipe was assumed so that only one half of the test facility need be modeled. The load was applied as a uniform pressure and the soil box contained a 2,000 mm^2 soil prism that extended to a height of 1,600 mm. These dimensions allowed only small horizontal deflections under large vertical pressures. The large distance between the pipe and the sidewalls was an attempt to provide lateral stiffness, while at the same time avoiding alteration of the pipe's behavior.

Hardie stated that the effect of sidewall friction should be considered with respect to the pipe's response and not to the soil box wall. Brachman et al. stated that sidewall

friction reduces the amount of load experienced by the pipe, thus resulting in a reduction in vertical deflection of the pipe. Based on a finite element analysis, Brachman et al. concluded that a sidewall friction angle of 5 degrees best simulates in situ conditions. In order to obtain a friction angle of 5 degrees, Brachman used polyethylene sheets lubricated with DC44 silicone grease. His research highlighted the importance of recognizing that the pipe distributes both horizontal and vertical stresses and that a reasonable model of the soil stresses can be achieved when the top and bottom of the soil is at least a distance of one diameter from the pipe. Research conducted at the University of Florida will provide a bedding depth below the pipe of one pipe diameter.

In the early years of soil box testing, the boundary conditions induced by the equipment caused poor correlation with in situ condition results. Boundary conditions were later revised to better represent such conditions. From the literature review conducted, it has become apparent that boundary conditions and pipe installation technique are of high importance when trying to simulate in situ performance with pipes tested in a soil box. Therefore when designing a soil box, controlling boundary conditions and soil stiffness is fundamental to producing accurate and acceptable results.

CHAPTER 3
STANDARD REINFORCED CONCRETE PIPE VS. FIBER REINFORCED CONCRETE PIPE

Background Information on Concrete Pipes

Presently, concrete pipes are fabricated in a variety of sizes, ranging from 4 inches to over 16 feet of inner diameter. Concrete pipes are used to transport liquids under gravity flow and are implemented as highway culverts, storm drains and sanitary sewers. The evaluation of concrete pipes for use as storm drains under gravity flow is the focus of this project.

Concrete pipes are reinforced against crushing when the inner diameter is greater than 24 inches. Standard reinforced concrete pipes (SRCP) are fabricated in accordance with ASTM C76 "Standard Specification for Reinforced Concrete Culvert, Storm Drain, and Sewer Pipe." ASTM C76 covers a size range diameter from 12 inches to 108 inches, with an exception for larger pipe diameters. SRCP are heavy products and require lifters capable of proper placement and installation. The SRCP used for this research will come from Rinker Materials.

Hardie Pipe introduced fiber reinforced concrete pipes (FRCP) into the civil construction market for large drainage pipes in early 2002 under the company's trademark Fiber Reinforced Concrete Speed Drain Pipes.

The concrete properties for each type of pipe include compressive strength, density, absorption, water-cement ratio, cementious materials, aggregates and versatility.

Cracking in Concrete--The Fracture Zone

Cracking in concrete begins at the micro level. The fracture zone is defined as the state when the stress or the strain is increased to the point where the atomic bonds within the matrix are broken and the solid material is cracked or fractured. As the stress load increases, cracks will develop and propagate. In concrete, cracks typically propagate due to tensile stresses, as a result of the low tensile strength of concrete. Though tensile strength is not considered in concrete design, is the cause of most crack initiation and propagation. Failure of concrete is due to tensile stresses induced by loads and/ or environmental changes. Concrete failure is often the end result of microcracking associated with the interfacial region between the hydrated cement paste and aggregates or other inclusions (reinforcing steel, fibers, etc.). Cracks are initially localized but increase in size as the applied stress is increased. In certain circumstances, cracks can propagate very fast. Cracks propagate in three different modes.

Cracking modes are classified as either plane strain modes or anti-plane strain modes. Mode I and Mode II deformation are plane strain and Mode III is anti-plane strain. The deformation of the crack is discussed using the coordinate system shown for Mode I displacement in Figure 3.1 below. A description of the three modes of cracking will follow the coordinate system shown in Figure 3.2. In Figure 3.1, an isotropic solid is shown with the origin of the coordinate system at the tip of the crack. It is important to note that the solid shown in Figure 3.1 represents an isotropic solid only. Anisotropic solids are quite complicated when analyzing the fracture of the solid.

Mode I deformation occurs when a transverse plane stress is applied to the crack forcing the crack to open up along the y-axis. Mode I is the most prevalent type of cracking in a brittle material. Mode II deformation is a result of a shear stress applied on

the cracked solid that forces the faces of the crack slide over one another parallel to the xy plane. Mode III occurs when a shear stress is applied resulting in the crack faces sliding over each other perpendicular to the xy plane. Cracking of concrete occurs in different stages beginning at the micro level.

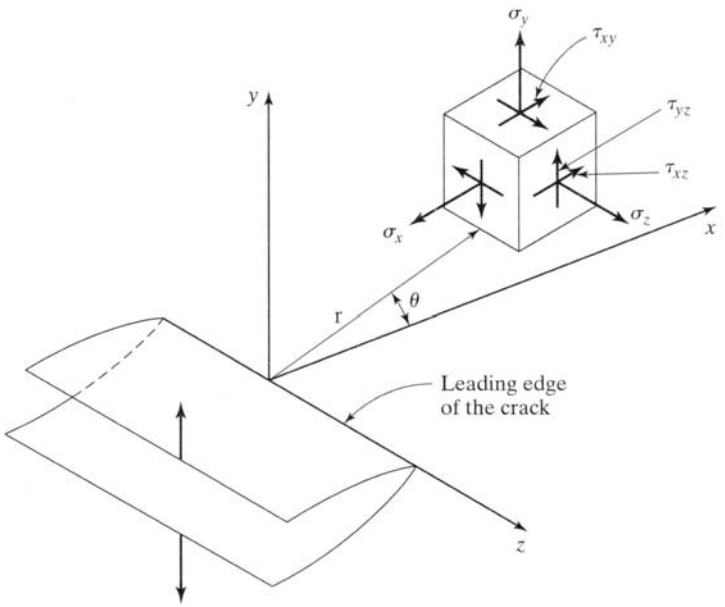

Figure 3.1 Coordinate system and stress components ahead of crack tip (Mode I displacement) (Mindess, 2003).

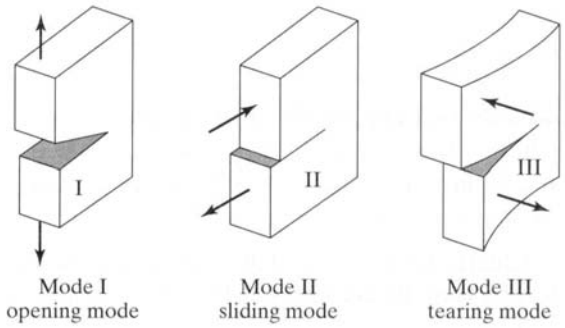

Figure 3.2 Three Modes of Cracking (Mindess, 2003).

Standard Reinforced Concrete Pipe--SRCP

SRCP is widely used in the construction market today. Uses include highway culverts, storm drains and sanitary sewers. Pipes without reinforcement are used where the application is suitable for such products. The majority of applications require reinforcement in order to increase overall strength and resist loads applied over the service life of the pipe. For example, a highway culvert located under a bridge would be subjected to cycling of live loads from traffic. Reinforcement would increase the amount of live load capability prior to failure.

SRCP uses steel rebar for reinforcement. The rebar is oriented within the pipe as a longitudinal spiral or linear section placed around the perimeter, parallel to the length of the pipe. Welded wire mesh is also used for additional reinforcement, allowing for increased bonding of the concrete to the rebar reinforcement. An SRCP is shown in Figure 3.3 with the steel reinforcement visible. This pipe section was tested in Hardie Pipe's soil box apparatus located at the UCF. The aggregates are also visible, along with the cracking induced by the load applied.

Properties that will be discussed for SRCP include durability, such as the ability to resist corrosion of rebar and proper bonding of the concrete to the rebar. Without sufficient bonding of the concrete and rebar, the reinforcement cannot properly carry the tensile stresses and prevent cracking of the concrete matrix.

Mechanics of SRCP

Different sizes of steel rebar are used to reinforce cement based concrete structures. In this research, concrete pipes will be tested for ultimate strength. Concrete is weak in tension, strong in compression. When tensile stresses are induced in the

Figure 3.3 Standard Reinforced Concrete Pipe Section Cracked.

concrete, the use of steel bars or wires carries the tensile stresses. Sufficient bond between the concrete and steel is necessary to allow transfer of the tensile stresses to the steel. The structural performance of SRCP thus relies on the bond between the steel and concrete. Steel design for concrete structure is specified in ACI 318.

Steel rebar left unprotected from the environment will corrode, resulting in a loss of strength. In reinforced concrete structures, the steel rebar is placed within the concrete matrix to provide protection from corrosion.

Reinforcement

The most commonly used reinforcements for non-prestressed members are hot-rolled deformed bars and wire fabric. Hot-rolled deformed steel bars are basically round in cross section with lugs or deformations rolled into the surface to aid in developing anchorage or bond with the concrete. Steel reinforcing bars are manufactured according to ASTM specifications: ASTM A615-85 Specification for Deformed and Plain Billet-Steel Bars for Concrete Reinforcement; ASTM A616 Specification for Rail-Steel Deformed and Plain Bars for Concrete Reinforcement; ASTM A617 Specification for Axle-Steel Deformed and Plain Bars for Concrete Reinforcement; ASTM A706 Specification for Low-Alloy Steel Deformed Bars for Concrete Reinforcement.

Strength

Reinforcing steel bars are manufactured in three grades; 40, 50, and 60, with yield strengths of 40, 50 and 60 thousand pounds per square inch (ksi). The 40-ksi bar is the most ductile of the three. Hot rolled steel bars are shown in Figure 3.4. Steel reinforcement is classified by its nominal diameter, expressed in eights of an inch.

ASTM specifications for reinforcing bars define the yield strength as the stress carried by the bar at a strain of 0.005. ACI Sections 3.5.3.2 and 3.5.3.4 to 3.5.3.6 define the yield strength as the stress carried at a strain of 0.0035. ACI's definition is based on the strain at which concrete crushes when bars are in compression, a situation where a strain of 0.005 may never be reached. ASTM specifications for yield strength are based on mill tests that are carried out at a high rate of loading.

Figure 3.4 Standard Reinforcing Steel Rebar.

Structural Performance

Structural performance is affected by several factors, such as bond, temperature and surrounding environmental conditions. The bond between the concrete matrix and the steel defines the stress transfer within the concrete. Tensile stresses are absorbed by the structural steel, providing tensile strength to the concrete structure. Debonding of the concrete and steel results in lower overall strength and performance of the concrete. Temperature affects the strength and performance of steel. The concrete cover over the steel resists heat penetration into the concrete, preventing temperature rise and decreased strength in the steel. Steel temperatures exceeding about 850°F result in a significant drop in both yield and ultimate strength.

Adverse environmental conditions can cause corrosion of the steel reinforcing bars, thus decreasing performance. Water and oxygen penetration into the concrete from the surrounding soil or water increases the possibility of steel corrosion, especially in the presence of chlorides. Concrete pipe serving as storm drains are susceptible to water penetration from both inside and outside the pipe. Increasing strains applied to the pipe will induce stresses and result in cracks forming throughout the pipe. Once a crack occurs, channels are created throughout the concrete, allowing water to enter at a much

higher rate and accelerating corrosion of the steel reinforcement. Once the steel corrodes, the strength of the concrete structure is impaired.

Fiber Reinforced Concrete Pipe--FRCP

The fibers in fiber reinforced concrete pipe serves as the reinforcement used to carry tensile stresses. A diameter range of 12" to 48" is produced, with a standard length of 16'. Pipe strengths within each size category are divided into five different classes, based upon wall thickness (I – V, with I being standard and V extra heavy). FRCP is manufactured in accordance with ASTM Standard C1450 and FDOT Standard 941, with designs from AASHTO Section 17 or LRFD Section 12. A typical FRC pipe is shown in Figure 3.5.

Figure 3.5 Typical Fiber Reinforced Concrete Pipe

Mechanics of FRCP

Different types of fibers are used to reinforce cement-based matrices. Fibers offer a more economical means of reinforcement for concrete structures of small size. Economically, fibers are cheaper than the usual steel reinforcing bars used, although fibers cannot be considered a replacement for traditional structural reinforcement of massive structures. The ACI 318 design code is based solely on concrete strength as the design criteria, considering only the peak loads a structure can withstand. Fibers are used very little in conjunction with structural steel due to the lack of consideration for post peak behavior. Fibers are most effective in the post peak phase of loading, since the fibers do not carry significant load until after the first crack occurs. They thus do no affect the first-crack strength of concrete and have very little effect on ultimate load.

Fibers are generally randomly distributed throughout the cross section. Most fibers are short and closely spaced within the matrix to allow formation of a bond between the fiber and the matrix. Stresses are sometimes transferred from fiber to fiber within the matrix, thus resulting in fiber-fiber interaction.

Fibers are primarily used to control crack propagation by bridging across cracks as they begin to open when the concrete strain exceeds its ultimate capacity. An important factor used to determine fracture properties of a material is the stress intensity factor. Cracking occurs after the critical value of the stress intensity factor is reached. Without going into the detail necessary to solve for the stress intensity factor, a simple overview will be provided to explain its importance.

The stress intensity factor K is considered to be a single-parameter description of the stress and displacement fields in the region of a crack tip (Mindess, 2003). When the

stress intensity factor reaches a critical value, unstable fracture will occur, resulting in cracks forming.

Fibers contribute to a more ductile concrete matrix. Fracture toughness is increased due to the bridging of fibers across the crack as they resist crack opening. As the applied load is increased, fiber reinforcement is designed to absorb the maximum amount of energy possible before unstable behavior of the matrix occurs.

Fiber-Matrix Bond

In properly designed cement composites for maximum performance, fibers are randomly dispersed throughout the matrix. The fiber matrix bond is a function of both the fiber and matrix properties. Fiber-matrix bond strength is determined from fiber pullout tests and reported as an average value over fiber surface area. Stresses are induced on the fiber-matrix bond, resulting in fiber pullout or debonding from the matrix after the maximum strength is reached. Typical fiber-matrix pullout strengths are shown in Table 3.1.

When using cement as a matrix, the fiber-cement interface can become complicated if a chemical reaction occurs between the cement and fiber. Formation of water around the fibers can occur due to bleeding in fresh concrete or insufficient packing of cement grains around the fibers. Under such conditions, the matrix becomes porous near the surface of the fibers than in the bulk cement paste.

Fiber-Fiber Interaction

A high ratio between fiber modulus of elasticity and matrix modulus of elasticity facilitates stress transfer from the matrix to the fiber. Fiber to fiber interaction occurs when stress is transferred between fibers. Fibers take on the tensile stress induced within the fibrous composite material. Stress concentrations will arise at the fiber ends if they

are discontinuous. The tensile stress that would be assumed by the fiber without the discontinuity must be taken up by the surrounding fibers in the composite.

Table 3.1 Typical Fiber-Matrix Pullout Strengths (Mindess, 2003).

Matrix	*Fiber*	*Pullout Strength Mpa (lbs/in2)*	
Cement Paste	Asbestos	0.8-3.2	(115-460)
	Glass	6.4-10.0	(930-1450)
	Polycrystalline alumina	5.6-13.6	(810-1970)
	Steel	6.8-8.3	(990-1200)
Mortar	Steel	5.4	(780)
Concrete	Steel	3.6	(520)(first crack)
		4.2	(610)(failure)
	Nylon	0.14	(20)
	Polypropelene	1	(150)

The effect of fiber-fiber interaction on stress transfer is described by Riley's theory (Beaudoin, 1990), which states that discontinuous fibers can contribute a maximum of only 6/7 of their strength to the strength of the composite, decreasing to 1/2 for badly flawed fibers.

Load vs. Deflection in Fiber Reinforced Concrete

As the applied load on a material increases, the strain will increase as well resulting in deformation and deflection. A typical stress-strain curve for fiber reinforced concrete is shown in Figure 3.6. Point A indicates load at which the first crack occurs in the matrix, known as the first-crack strength. The stress at which the first crack occurs is the same in fiber reinforced concrete, traditionally reinforced concrete and plain concrete. The strength of fiber reinforced concrete in the post-cracking zone comes from the transfer of loads across the cracks by the fibers, increasing the strength of fiber reinforced concrete over that of the matrix. Fibers increase the toughness by providing energy absorption mechanisms through the gradual debonding and pull out of the fibers bridging across the cracks (Mindess, 2003).

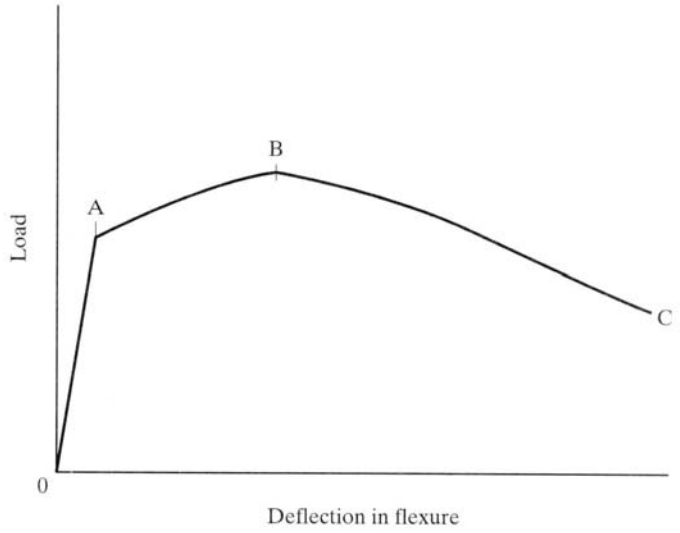

Figure 3.6 Typical load-deflection curve for fiber reinforced concrete in flexure (Mindess, 2003)

Stages of Cracking-Fiber Intervention

The first stage of cracking is the development of microcracks. Microcracks form due to high stress concentrations in specific regions of the concrete matrix. The microcracks lengthen, meet and coalesce to form one or more macrocracks. The final stage corresponds to the propagation of cracks. Much research has been done to find out how fibers intervene during the various stages of cracking. During the first stage, the fibers respond to the uniformly distributed microcracking creating a stitching effect on the micro-cracks and preventing propagation. The intervention of the fibers retards the microcracking coalescence phase and the creation of macro-cracks. Once macrocracks develop, the fibers will bridge across them and serve as reinforcement similar to the steel in reinforced concrete. This bridging mechanism is illustrated in Figure 3.7.

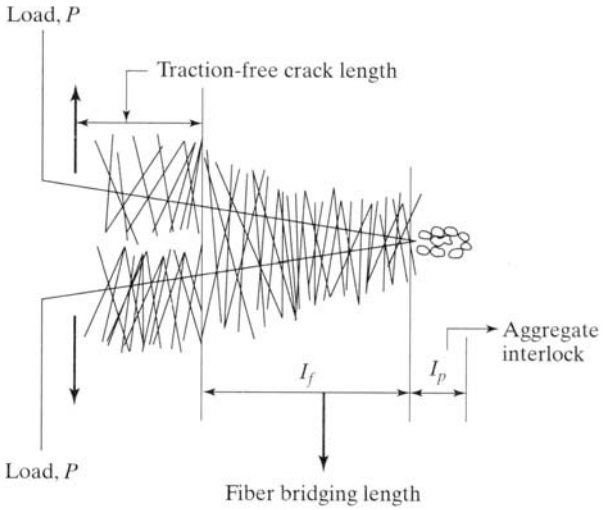

Figure 3.7 Schematic representations of fibers bridging across a crack (Mindess, 2003).

Fibers bridge across the cracks as they open within the matrix. The stress field around the crack is shown along with the traction-free crack length, fiber bridging length and the aggregate interlock. Stresses are absorbed by the fibers in three different areas shown in figure 3.7. The traction free zone is where fibers have pulled out due to the crack opening up wide enough to overcome the pull out strength. Stresses are absorbed by the fibers and transferred across the fibers by frictional slip in the fiber-bridging zone. Aggregates also absorb energy as their interlocking is distributed to the matrix itself in the microcracked matrix process zone.

As stated previously, fibers intervene at two levels; the material level (during macrocracking) and at the structural level (during stress redistribution). In order for the fibers to respond effectively, fiber dimensions and properties must be optimized for the matrix material. The volume proportion of fibers also needs to be optimized to provide maximum mechanical performance. Two approaches are considered during the mix design stage. Since only discontinuous fibers are used, one possibility is to mix in a high percentage of relatively short fibers, resulting in an increase in the strength of the FRC, as the dimensional scale of the fibers is the same as that of the microcracks. Another

possibility is to mix in a low percentage of long fibers, resulting in improved ductility of the structure. This is effective, with regard to macrocracking, since the fibers have sufficient anchorage length on either side of the crack as it opens across the fibers.

Strength

The role of fibers in concrete is not to increase the overall strength. Some minimal increase in strength will occur in compression and flexure. Research shows that in direct tension, where it would be expected that fibers should be most effective in terms of strength, strength increases are limited to about 30% for a steel fiber volume of 1.5% (Mindess, 2003). Fibers are reported to have no major effect on shear and torsional strength or on elastic modulus.

Toughness

Fibers have an enormous effect on toughness. If the fibers possess sufficient strength and stiffness, and bonded well with the matrix, they will minimize cracking. This allows the fiber reinforced concrete to withstand significant stresses over a relatively large strain capacity in the post-cracking (or strain-softening) stage, thus providing a considerable amount of post-cracking ductility (Mindess, 2003). Certain fibers have a greater effect on increasing the toughness of fiber reinforced concrete. Deformed fibers tend to have a greater effect on increasing toughness since they bond to the matrix better, increasing the overall pullout strength. Increasing the bond strength past the point where the fibers themselves begin to fail in tension, however, is counterproductive. More energy is required to pull a fiber out of the surrounding matrix than to actually break the fiber across a crack. Thus, designing fibers and FRC for fiber pullout, instead of breakage, is the key to maximizing energy absorption and ductility during failure.

Mindess shows that steel fibers are more effective that polypropylene fibers in improving toughness because of their higher stiffness.

FRCP versus SRCP

Performance of a pipe is based on its ability to maintain shape under service loads, resist cracking from applied stresses, and resist deterioration of the pipe material due to environmental exposure. Concrete drainpipes are subjected to a number of deterioration mechanisms. Stresses will induce microcracking that eventually coalesces into macrocracks within the concrete matrix. These cracks provide openings for water and other deleterious materials to penetrate into the concrete. In traditional steel reinforced concrete pipe, such ingress can induce corrosion of the steel reinforcement, leading to a decrease in the ultimate strength of the pipe. Though not susceptible to corrosion, the durability concerns related to cellulose fiber reinforced concrete pipe have not yet been fully investigated. A comparison of the properties and characteristics of FRCP and SRCP will be discussed.

Manufacturing

FRCP is manufactured using high-pressure autoclaving, allowing higher concrete strengths to be obtained for a given set of ingredients. SRCP is manufactured with a low water to cement ratio concrete mix, which is cast into forms during an automated fabrication sequence.

Installation

The unit weight of a concrete pipe has a significant impact on the installation process. A lighter pipe is easier and quicker to install than a heavy pipe. For a given size and class, an FRC pipe is about half the weight of a corresponding SRC pipe, making it easier to install and handle.

The standard length of SRCP is six feet. FRCP, on the other hand, comes in a standard length of 16 feet. The installation work required for FRCP, compared to SRCP, is cut in half due to this longer standard length. FRCP is also easier to cut when length adjustments are needed, requiring less time than SRCP.

An important part of the installation of concrete pipes is the joint seal at the ends of the pipes. Both pipes use rubber gaskets at joints to provide a tight seal, preventing the flow of liquid into, and out of, the pipe system.

Performance

A vital property affecting mechanical performance is the bond of the concrete to the reinforcement. Steel rebar is more difficult to bond to than cellulose fibers, which are randomly dispersed throughout the concrete mix. This random dispersion allows for increased bonding due to the small size of the fibers and the increase in total surface area inherent in smaller particle sizes. Even with these improvements in bond performance, it still must be remembered that fiber reinforcement cannot be considered a complete replacement for the reinforcement of concrete structures.

Both FRCP and SRCP will be tested in the soil box designed by the University of Florida for research funded by the Florida Department of Transportation. The FRCP will come from Hardie Pipe, Inc. while Rinker Materials, Inc will provide the SRCP. Following design and construction of the soil box testing apparatus, each type of pipe will be evaluated as to its insitu performance.

CHAPTER 4
INSTRUMENTATION AND TESTING TECHNIQUES

Crack Detection and Deflection in Concrete Pipes

During the testing, the two primary parameters, other than applied load, that will be monitored include cracking and deflection. The ultimate failure of a pipe specimen will eventually be define relative to one or both of these serviceability limits. There are many test methods used today to detect cracks and measure deflection of a structure under load. Determining which of these to implement comes down to applicability, accuracy, and ease of use.

Since the pipes are to be tested in a buried condition, detecting cracks occurring on the outer face of the pipe may prove problematic. With current advances in technology, crack detection is more easily accomplished using acoustic emission monitoring techniques. This should allow detection of crack formation without the need to actually observe the crack.

The deflection of the concrete pipes is an observation of the pipe's deformation while subjected to an applied load. A novel method will also be used to observe and record pipe deflection during testing, specifically three-dimensional imaging of the inner surface of the pipe with a laser based digitizing system.

Background on Acoustic Emission Testing

Acoustic emission is defined as an acoustic wave generated by a material when subjected to an external stimulus causing an irreversible change in the material. There are two types of acoustic emission signals, continuous and burst signals. A continuous

emission is a sustained signal level produced by rapidly occurring emission events such as plastic deformation. A burst emission is a discrete signal related to an individual emission event occurring in the material, such as a crack forming or propagating in a brittle material, such as concrete.

An acoustic emission burst signal is shown in Figure 4.1. The term "acoustic emission signal" is often used interchangeably with simply "acoustic emission". An acoustic emission signal is defined as the electrical signal received by the sensor in response to the acoustic wave moving through the material. This emission is picked up by the sensor and transformed into an electrical signal, then analyzed by acoustic emission instrumentation, resulting in information about the material that generated the emission.

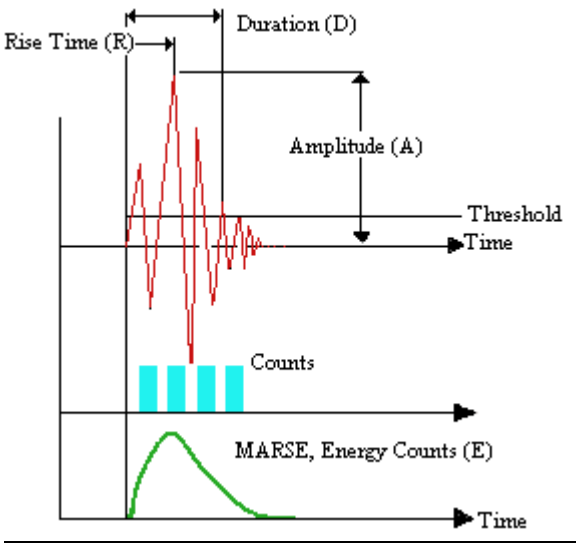

Figure 4.1: Burst Acoustic emission signal with properties

Acoustic emission is a passive, non-destructive monitoring technique. This means that there is no input from an outside source; the technique purely monitors the material being tested. Acoustic emission is typically used to detect cracking, delamination (slip between concrete and steel reinforcement), failure of strands in prestressing tendons, and

fracture or debonding of fibers in fiber reinforced concrete. A typical acoustic emission system setup is shown in Figure 4.2.

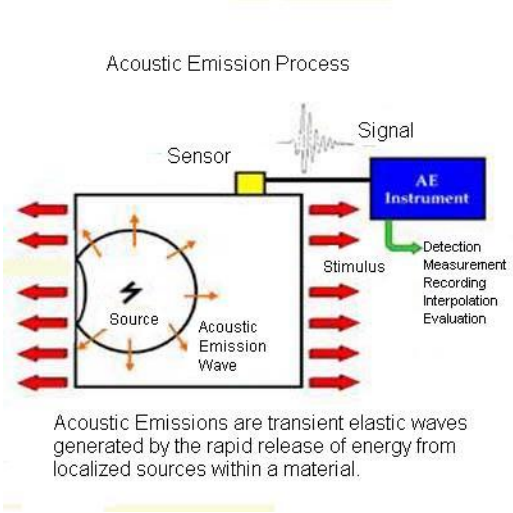

Figure 4.2: Acoustic Emission Process

Equipment and Instrumentation

An Acoustic emission system includes at least one sensor and a preamplifier. Most systems also include postamplifiers and signal processors. The system to be used in this research project is a LAM – a Local Area Monitor that consists of eight sensors, which will be mounted on the pipe during load testing. More specialized equipment often associated with such a system includes transient recorders, spectrum analyzers, distribution analyzers and spatial discrimination circuits (Beattie, 1993). Microprocessor based systems have become more widely used in recent years that can perform single channel analysis along with source location for up to eight AE channels.

Sensors

The Acoustic emission sensor is the most important part of the instrumentation and must be properly mounted to assure the required sensitivity. Selection of sensors and or transducers will depend on test parameters and desired results. Sensors are calibrated

using test methods stated by societies. ASTM states that annual calibration and verification of pressure transducer, AE sensors, preamplifiers (if applicable), signal processor (particularly the signal processor time reference), and AE electronic simulator (waveform generator) should be performed. Equipment should conform to manufacturer's specifications. Instruments should be calibrated in accordance with National Institute for Standards and Technology (NIST) specifications.

An AE electronic simulator, used in making evaluations, must have each channel respond with a peak amplitude reading within ± 2dBV of the electronic waveform output. A system performance check should be done immediately before and after an AE examination. The preferred technique for this is the pencil lead break test. A complete description of this test can be found in ASTM E 570.

One very important factor affecting sensor performance is location. Determination of the number of sensors required for the test, their placement strategy and location on the specimen to be monitored is critical. A single sensor used near the expected source of AE is sufficient when background noise can be controlled or does not exist. When background noise is limited, the use of a single AE data sensor near the expected source plus a guard sensor(s) near the background source will suffice. ASTM defines a *guard sensor* as sensors whose primary function is the elimination of extraneous noise based on arrival sequences.

Another technique involves the placement of two or more sensors to perform spatial discrimination of background noise and allow AE events to occur. ASTM defines *spatial discrimination* as the process of using one or more (guard and data) sensors to eliminate extraneous noise based on arrival sequences.

In situations where irrelevant noise cannot be controlled during testing and could be emanating from any and all directions, a multiple sensor location strategy should be considered. Using a linear or planar sensor configuration will allow for accurate source location of the acoustic emission event. Applications of spatial filtering and/or spatial discrimination will only allow data emanating from the region of interest to be processed as relevant AE data.

Preamplifiers

Preamplifiers (as shown in Figure 4.3) are used to prevent loss of sensor activity. Loss occurs when one sensor is connected through a long coaxial cable to an amplifier. The amplifier is split into a fixed gain preamplifier located close to the sensor. The preamplifier consists of a low noise input stage, bandpass filters and a low impedance output stage capable of driving a 50-ohm cable (Beattie, 1993). Power for the preamplifier is received from the main instrument group. AE preamplifiers are designed to have a relatively flat frequency response between about 20 kHz and 2MHz, without the bandpass filters (Beattie, 1993).

Preamplifiers can be included in the sensor package. The advantages of this arrangement are the elimination of cable capacity effect and being able to tailor the preamplifier characteristics to match the sensor. The disadvantages of such units, besides their higher cost, are that they are restricted to temperatures near 20°C (the preamplifier will not work properly at higher or lower temperatures) and that a separate preamplifier has to be purchased for each sensor (Beattie, 1993).

Postamplifiers and Signal Processors

Most AE systems use variable gain postamplifiers. This allows the use of signal processors with fixed input ranges or thresholds in conjunction with fixed gain

preamplifiers (Beattie, 1993). The systems total gain is the sum of the preamplifier and postamplifier gains, expressed in decibels. Additional noise reduction can be achieved through postamplifiers from bandpass filters.

Signal processors are typically included in the system's capabilities. These include voltage controlled gates that allow data to be collected only on certain portions of a load cycle, envelope processors which attempt to filter out high frequencies leaving only the signal envelope to be counted, logarithmic converters which allow the output of the signal analyzer electronics to be plotted in logarithmic form and a unit which allows the combination of outputs from several preamplifiers so that several sensors can be monitored by one channel of electronics (Beattie, 1993).

Figure 4.3: Pre-amplifiers (PAC)

Transient Recorders

Transient recorders are used to study individual AE burst signals. A signal is digitized in real time, and then stored into memory. A transient recorder is used in sequence with an oscilloscope or spectrum analyzer to display AE signals at visible speeds. Digital rates vary on transient recorders. The fastest rate of the recorder is ultimately the limiting rate, with some instruments sampling up to 1 word/nano-second (Beattie, 1993).

Sampling rates can be modified for testing purposes. One advantage of transient recorders is an additional mode of triggering and pretriggering, where the input signal is continuously digitized and the data stored in the memory (Beattie, 1993). This feature allows a digitized picture of the signal to be displayed as it is received. More advanced systems allow recording of two or more signals simultaneously. The recording of more than one AE signal is shown in Figure 4.4.

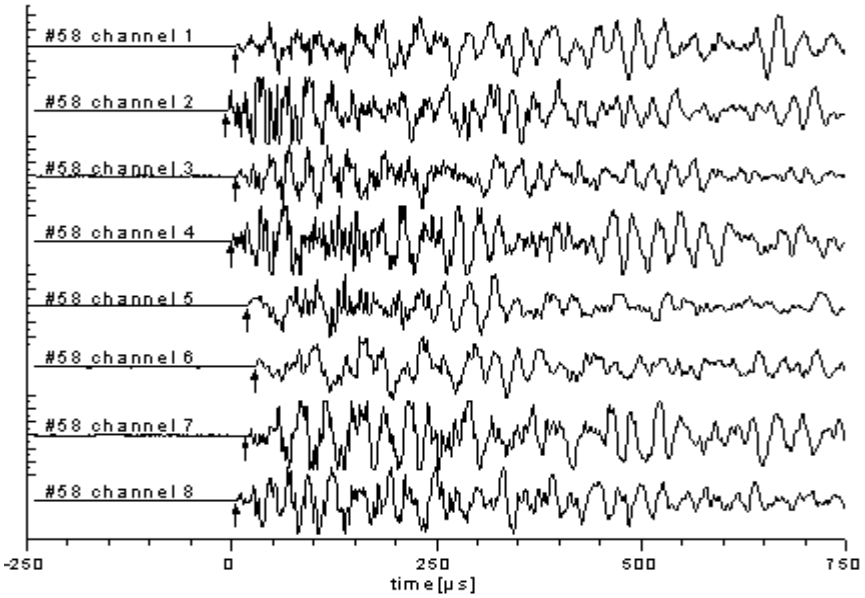

Figure 4.4: Transient recorder with multiple AE signals

Spectrum Analyzers

The ideal spectrum analyzer has horizontal and vertical signal outputs, allowing an X-Y plot of the AE signal. Spectrum analysis is done either directly with analog electronics or by digitally viewing a continuous signal. A local oscillator signal is mixed with the input signal and the highest frequency is passed through a chain of intermediate frequency (I.F.) amplifiers, after which it is measured by a voltmeter (Beattie, 1993). The oscillator is swept through a frequency range so that the frequency components of the signal selected by the I.F. amplifier are continuously changing (Beattie, 1993). The

voltmeter output is plotted on the vertical axis of the oscilloscope. A typical oscilloscope is shown in Figure 4.5. A synchronized signal is displayed for the horizontal axis through the local oscillator frequency. The final result is a plot of signal strength vs. frequency.

Spectrum analyzers range in frequencies from at least 10kHz to 2MHz. The width and speed of the local oscillator and the sharpness of the I.F. amplifier filters are all under the direct control of the operator (Beattie, 1993). An AE burst signal emission is not suitable for spectrum analysis. AE burst signals must be captured on a tape recorder and played repetitively onto the spectrum analyzer for analysis. This essentially simulates a continuous signal for spectrum analysis.

Figure 4.5: Digital Oscilloscope

LAM--Local Area Monitor

LAM is the world's first acoustic emissions system to allow remote condition monitoring of structures. Physical Acoustics Corporation developed the LAM, as shown in Figure 4.6, in conjunction with the U.S. Federal Highway Administration. The system

is portable and easy to handle weighing only 25 pounds including one battery pack.

Features of the LAM used in this research project are:

- Modular 8 channel DSP-based AE system with 16-bit A/D
- User-friendly software
- AC/DC powered
- 4 high-speed and 8 low-speed parametrics
- Digital AE features and waveforms processed simultaneously
- Software programmable filters
- Resistant to harsh environmental conditions

Figure 4.6: LAM-Local Area Monitor

The LAM is useful for monitoring many structures including bridges for defects, chemical/ petrochemical tanks for leaks and deterioration, transformers for partial discharge and most structures (including concrete pipes) during fatigue tests.

The LAM was originally designed for monitoring defects in steel bridges. The LAM's modularity lends itself to many other applications, as stated before, to monitor fatigue cracks and other discontinuities in structures, pressure vessels and transformers. This research will use the LAM to monitor microcracking in the walls of fiber reinforced and steel reinforced concrete pipes.

The LAM offers up to 8 channels of digital AE for short-term condition monitoring, long-term integrity monitoring, laboratory fatigue testing or incipient failure detection monitoring through user selections. The unit operates from an external 12 Volt DC battery or 110 Volt AC power supply. An optional feature is remote access through traditional phone line or cellular phone. This feature allows the user to monitor the apparatus from an office or other location remote from the test site.

Advantages of the LAM over other acoustic emission instrumentation include a reduction in the extensive cabling normally required for operation. The unit is placed on site with the structure/ object to be monitored. For this project, the concrete pipes will be instrumented with the eight sensors to monitor microcracks occurring inside the walls. Data analysis for this research will be performed with the NOESIS 3.1 software published by Physical Acoustics Corporation.

NOESIS 3.1 is an MS Windows based advanced data analysis pattern recognition and neural networks software used for acoustic emission applications. It provides all necessary tools for analyzing, filtering and classifying acoustic emission hits and waveforms that are acquired with the LAM unit. NOESIS is equipped to handle data saved in a DTA file format produced by the LAM unit. The software utilizes PAC (Physical Acoustics Corporation) file libraries to load and save data in the DTA file format.

NOESIS allows multiple DTA files to be loaded simultaneously for direct comparison, statistical analysis and filtering or merging. Direct export of data files to MS EXCEL and MS WORD is also possible. Any number of windows can be displayed, limited only by the resolution of the viewing window for adequate visibility. Navigation

throughout the program, along with data selection, is done with the mouse. Data point selection is available using the mouse on scatter plots, cumulative plots, waveform plots, FFT plots and tabular data views. NOESIS allows graphs and plots to be customized for presentation of data and analysis.

Waveforms and AE hits can be selected and displayed on any graph or data table. Comparison of the data can be superimposed or viewed in three dimensions. Graphical and other data filtering are applied to waveform views for presenting the collected data. Any changes made to hardware settings are immediately reflected in the waveforms.

Minolta 3D Digitizer--VIVID 900

Minolta is the world's largest manufacturer of 3-D non-contact digitizing instruments, providing a 3-D scanner with a simple point and shoot camera that scans 300,000 points in less than 3 seconds. This project will use Minolta's newest 3-D scanner, the VIVID 900, shown in figure 4.7. The VIVID 900 is an easy to use scanner with simplicity, flexibility and portability. Minolta offers simplicity by a point and shoot camera with excellent results. The VIVID 900 includes interchangeable lenses, for variable scanning volumes, for flexibility. The camera unit is compact, measuring 8-3/8"x16-1/4"x 10-11/16" and weighs only 24 lbs. Scans can be saved and stored on a compact flash memory card or viewed immediately after scanning on the rear-panel's color LCD viewfinder. Color images are equivalent to a 3 CCD digital camera displaying full 24-bit color depth.

Hardware

The Minolta VIVID 900 offers variable volumes for digitizing between 110 x 80 x 40 mm and 1200 x 900 x 750 mm. There are three interchangeable lenses included as standard accessories for scanning; telephoto, medium and wide angle. The VIVID 900 is

an independent instrument that does not require a host computer for operation. Scanned images are saved to a flash memory card (Figure 4.8) or viewed immediately after scanning on the LCD viewfinder. The Minolta VIVID 900 also offers an autofocus function that eliminates the need to move the unit back and forth to achieve optimal focus for the scan.

Figure 4.7 Minolta VIVID 900 Non-Contact 3-D Digitizer

Figure 4.8 Compact Flash Memory Card (40MB capacity)

Accessories

Minolta offers accessories to improve the outcome of the scan. When scanning a complete 360° view of an object, the rotary specimen stage shown in Figure 4.9 will

prove helpful. A rotating disc is set to rotate at a specified speed while the VIVID 900 scans the object, resulting in a full 3-D image of the object. To ensure level scans and stability, Minolta offers a tripod accessory with the option of a tilt mounting base unit as shown in figure 4.10. Other accessories available are a PC card adapter allowing direct transfer of the scanned images to a personal computer for analysis.

Figure 4.9 Rotating Stage Set for Scanning a Full 3-D image

Figure 4.10 Tripod (left) and Tilting Base Mount (right) for Minolta VIVID 900

Operation

The Minolta VIVID 900's basic theory of operation is described through LASER triangulation. A laser source from the VIVID 900 emits a horizontal light stripe through a cylindrical lens onto the object being scanned. The plane of light is swept across the field of view by a rotating mirror. The light is reflected from the scanned object, captured, and observed by a single frame through the CCD camera. Once received by the CCD, the light is converted through triangulation into distance information. Each scan line is captured and observed by the CCD camera. The shape of the image of each reflected scan line is derived to produce the contour of the surface. The selected area in the view is captured in 2.5 seconds (0.3 seconds in FAST mode), and the surface shape is converted to a lattice of over 300,000 vertices or connected points (Minolta, 2001).

The VIVID 900 produces polygonal-mesh with all connected information, eliminating geometric ambiguities while improving detail. Minolta's VIVID 900 uses an X, Y, and Z coordinate axis. The x coordinate is the horizontal dimension of the focal plane, the y coordinate is the vertical axis and the z coordinate is the distance from the sensor. The VIVID 900 creates no parallax error. Specifications for the VIVID 900 are displayed in Table 4.1 below.

Table 4.1 Specifications of Minolta VIVID 900 3D digitizer.

Type	Non-contact 3D digitizer VIVID 900
Measuring method	Triangulation light block method
AF	Image surface AF (contrast method), active AF
Light-Receiving Lens (Exchangeable)	TELE: Focal distance f=25mm MIDDLE: Focal distance f=14mm WIDE: Focal distance f=8mm
Image Input Range	0.6 to 2.5m (2m for WIDE)
Measurement Input Range	0.6 to 1.2m
Laser Output	"Eye-safe", Class I (FDA), Class 2 (IEC), Maximum 30mW 690 nm
Laser Scan Method	Galvano mirror
Input Time	0.3 sec (FAST mode), 2.5 sec (FINE mode), 0.5 sec (FINE mode)
Transfer Time to Host Computer	Approx. 1 sec (FAST mode, 1.5 sec (FINE mode)
Ambient Light Condition	Office Environment, 500 1x or less
Imaging Element	3-D data: 1/3-inch frame transfer CCD (340,000 pixels) Color data: 3-D data is shared (color separation by rotary filter).
Number of Output Pixels	3-D data: 640 x 480 (for FINE mode); 320 x 240 (for FAST mode) Color data: 640 x 480
Output Format	3-D data: Minolta format, & (STL, DXF, OBJ, ASCII points, VRML) (Converted to 3-D data by the Polygon Editing Software/ standard accessory) Color data: RGB 24-bit raster scan data
Recording Medium	Compact Flash memory card
Data File Size	Total 3-D and color data capacity: 1.6MB per data (for FAST mode), 3.6MB per data (for FINE mode)
Viewfinder	5.7-inch LCD (320 x 240 pixels)
Output Interface	SCSI II (DMA synchronous transfer)
Power	Commercial AC power100 to 240V (50 to 60Hz), Rated current 0.6A (when 100Vac is input)
Dimensions (WxHxD)	213 x 413 x 271 mm (8-3/8 x 16-1/4 x 10-11/16 in.)
Weight	Approx. 11 kg.
Operating environment	Temperature: 10-40°C (50-104°F); relative humidity 65% or less with no condensation, Pollution degree:2, Installation category:II
Storage Temperature	-10 to 50°C (14-122°F); relative humidity 85% or less (at 35°C/95°F) with no condensation

CHAPTER 5
PLAXIS VERSION 7.2--FINITE ELEMENT CODE FOR SOIL AND ROCK ANALYSIS

Introduction

Plaxis was developed in 1987 at the Technical University of Delft, initiated by the Dutch Department of Public Works and Water Management. Initially, Plaxis was developed to analyze river embankments in the soft soils of the Dutch lowlands. Throughout the original development and later improvements, Plaxis extended its applicability to cover most areas of geotechnical engineering. Plaxis excelled over the years forming a company in 1993, Plaxis BV.

Plaxis is a computer program designed to provide a practical analysis tool for use by engineers who are not specialists in finite element analysis. Non-linear finite element computations done without a computer can be too time-consuming for regular analyses. Plaxis 7.2 is an MS Windows-based program with easy-to-use tabs used to navigate through the analysis.

Plaxis is a finite element program designed for the analysis of deformation and stability in geotechnical engineering projects. Geotechnical engineering uses advanced models for the simulation of non-linear and time dependent behavior of soils. Soil is a multiphase material with properties that can change with a changing environment. Plaxis is equipped to deal with hydrostatic and non-hydrostatic pore pressure in the soil. Even though modeling of the soil itself is important, modeling of soil-structure interactions is

the application seen in many engineering projects today. Plaxis is also equipped with features to analyze a number of aspects dealing with complex geotechnical structures.

Plaxis is made up of four internal programs, Input, Calculation, Output and Curves. Graphical input of geometry models consists of soil layers, structures, construction stages, loads and boundary conditions all created with drafting procedures on a CAD (Computer Aided Drawing) screen, as shown in Figure 5.1. The CAD interface allows accuracy and detailed modeling of real engineering situations. From the geometry entered, a finite element mesh is generated. The automatic mesh generation feature allows for fully automated mesh generation of unstructured finite element meshes.

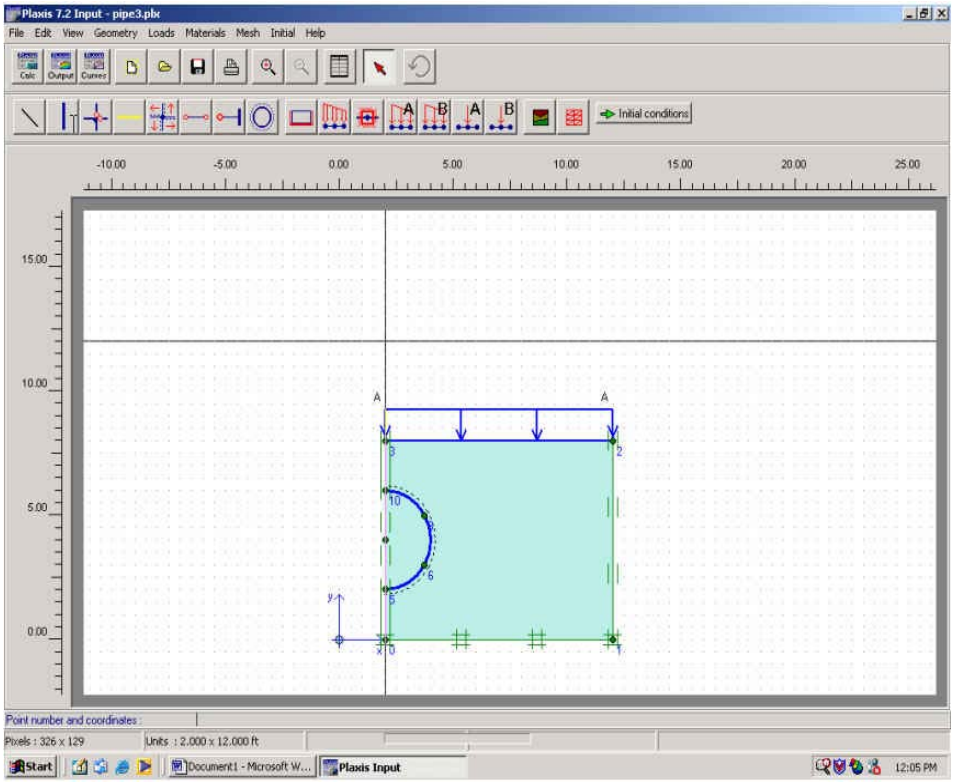

Figure 5.1: Plaxis 7.2 Computer Aided Drafting screen used to create modeling analysis.

Beam elements are used to model retaining walls, tunnel linings and other structures. Pipes are modeled using the tunnel feature. Behavior of each element is defined as flexural rigidity, normal stiffness and/or ultimate bending moment. Assigned

to the beam elements is a feature called “interface.” Interfaces are joint elements used in calculations of soil-structure interactions. For example, interfaces can simulate a zone of intense shearing stresses located at the contact plane of footings, piles, geotextiles, retaining walls and pipe surfaces. Values of friction angle and adhesion properties can be assigned to interface elements. Anchors and geotextiles are additional features available for modeling. The tunnel feature option creates circular and non – circular tunnels composed of arcs. Beams and interfaces may be added for analysis of tunnel linings or interactions with the surrounding soil.

A number of soil models are used in Plaxis for analysis of soil performance. Mohr-Coulomb, a simple non-linear model, is the most used model based on soil parameters encountered in everyday practical situations. Other advanced soil models are also available for analyses.

Pore pressures are analyzed within the Plaxis model. Steady state and excess pore pressures are defined by the water table location in the model. There are two approaches for steady state pore pressures. Complex pore pressure distributions are generated on the basis of a two-dimensional groundwater flow analysis. For simple conditions, multi-linear pore pressure distributions can be directly generated by a simple phreatic line in the model. Excess pore pressures are computed during plastic calculations when pores are full of water and subjected to loads.

A typical analysis with Plaxis finite element modeling involves input parameters and specifications of model types. The input model is then run through the calculation phase to produce output results for analysis. Plaxis is also equipped with a curves

program that produces graphs for analysis results, such as stress/strain curves and load/displacement curves.

Plaxis--Input

The input program is the first step of a Plaxis analysis. At the start of a new project, the *General Settings* window appears (as shown in Figure 5.2), prompting the user to set the basic parameters of the project. The *General Settings* window has two tabs: Project and Dimensions. The project tab allows the user to enter a description of the project, the type of model used (i.e. plane strain) and the number of nodes to be used in the finite element analysis (i.e., 6 and 15 node). The *Dimensions Tab* specifies units of length (ft), force (lbs.) and time (day); and the geometry dimensions for the CAD screen and grid spacing.

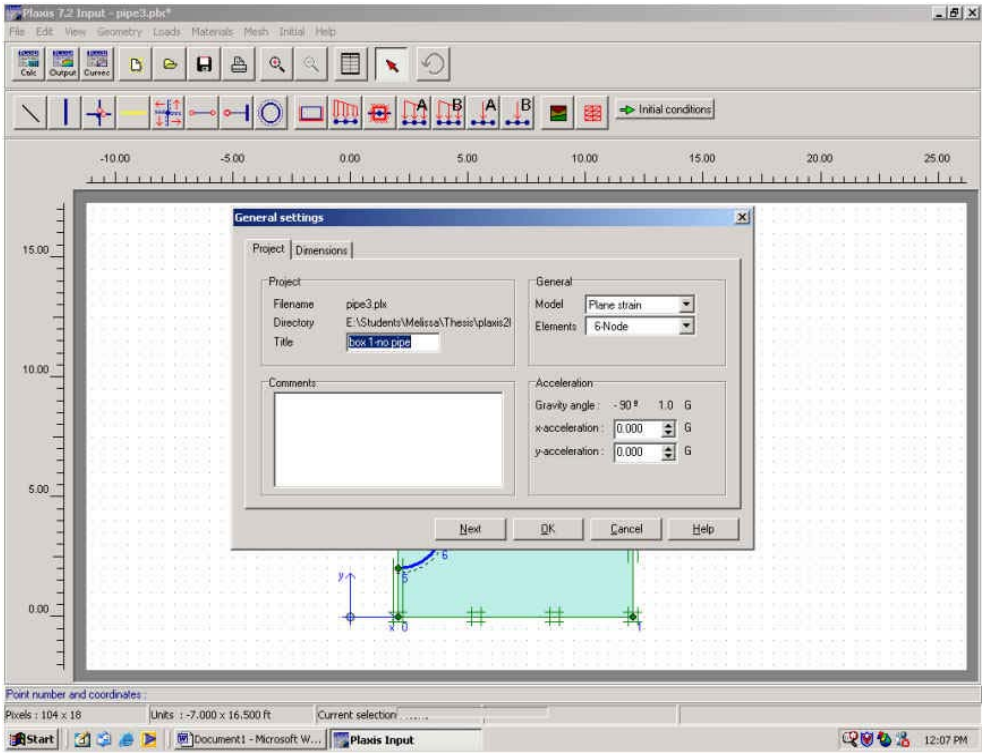

Figure 5.2: General Settings window in Plaxis 7.2.

Once the general setting parameters are entered into Plaxis, the CAD screen appears for geometric creation of the model. An example of a tunnel model, as used in this research, will be used to demonstrate a typical run-through of a Plaxis 7.2 finite element modeling. The tunnel model can be used to simulate buried pipes for analyses. The model described in the example is a four-foot diameter reinforced concrete pipe, located within a soil box. Ultimately, a steel framed box will be designed to test concrete pipes. Plaxis modeling will be performed on the soil structure interaction and in analyzing the stresses induced on the sidewalls and pipe, thus defining the design parameter for the box.

After the general settings are complete, the geometry of the model is created in the input drawing area using the points and lines feature. With the Windows based program the creation of a model is accomplished by working from left to right with the icons at the top of the screen, as shown in Figure 5.3. Points and lines are used to create an enclosed box of dimensions 20’ x 10’ x 10’. The tunnel option is then used to create a circular tunnel representing the four-foot diameter concrete pipe, composed of arcs defined by a radius and a radial increment (angle). By clicking on the tunnel feature, the user is prompted with a choice to use a whole tunnel or a half tunnel. After this choice is made, a window is opened as shown in Figure 5.4 to allow input of the radius and radial increment. In this same window an interface and lining material is assigned to the tunnel model.

For the example, a radius of 4 feet is entered and a tunnel and interface lining is assigned to the tunnel. An interface is used to model soil-structure interaction and the

lining material provides the option to assign concrete properties to the tunnel lining. The next step in the model is load and boundary conditions.

Figure 5.3: Plaxis 7.2 Main Toolbar.

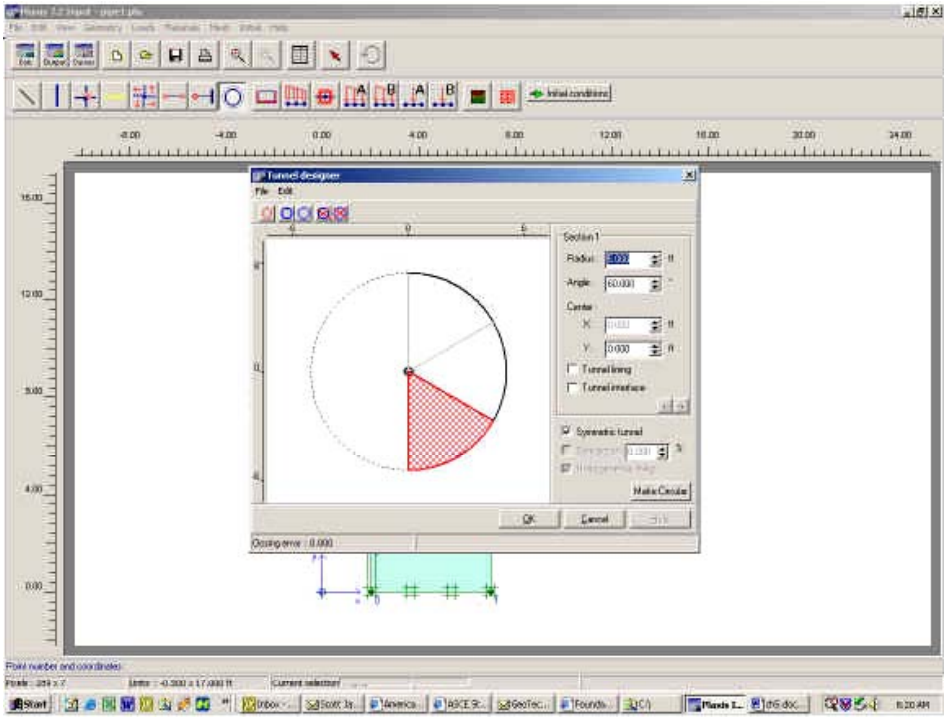

Figure 5.4: Tunnel Designer in Plaxis 7.2.

The load and boundary conditions used for this model are standard fixities and traction loads (distributed loads). Both features are chosen from the standard toolbar as shown in Figure 5.3. The soil box will be modeled as a rigid box with minimal deflection. Fixities are prescribed displacements equal to zero. These fixities can be applied to points or lines. By clicking on the standard fixities button on the toolbar, the two sidewalls and the bottom of the box were assigned both horizontal and vertical fixities as shown in Figure 5.5 below.

After the standard fixities are assigned, moving to the left on the toolbar, the loads are assigned through the traction icon as shown in Figure 5.5. A distributed load was assigned using traction A, assigning the load to the two top points of the box on the CAD drawing area. Plaxis will ask the user to enter a multiplier for loading steps in the calculation phase. The default is 1.00, representing a true value for the load entered in the calculation phase. A multiplier of 1.00 was used in the example.

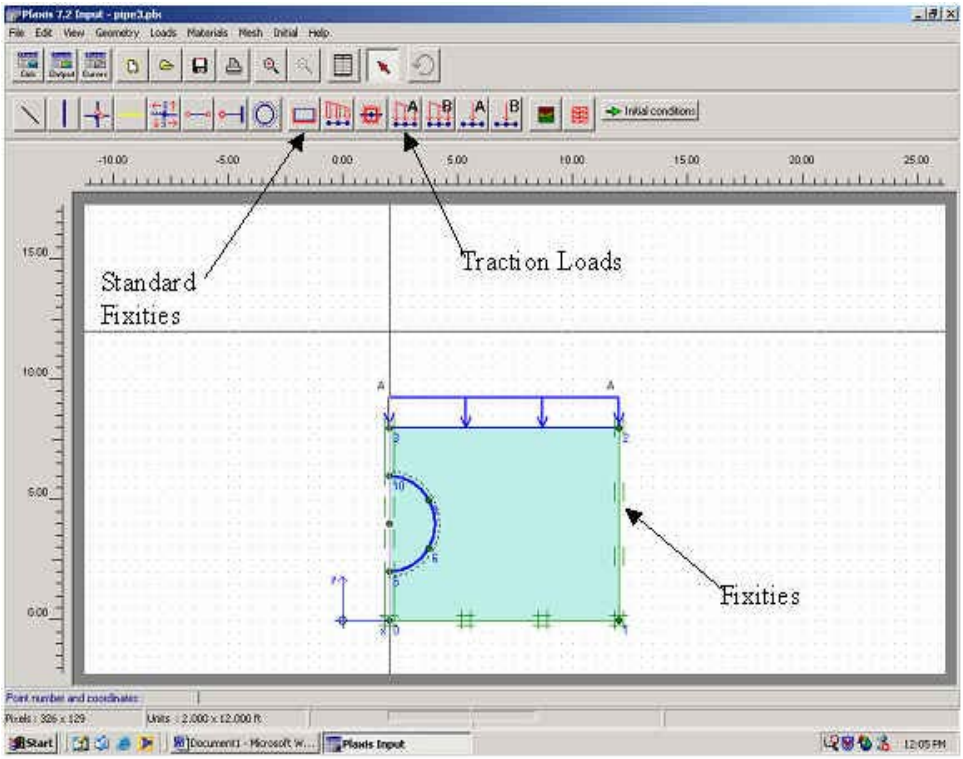

Figure 5.5: Standard Fixities in Plaxis 7.2 shown on a soil box with right half tunnel.

Once geometric definition of the model is finished, with all beam elements defined, fixities assigned and loads designated, the material properties need to specified and added to the model. Material data sets for soil, interfaces and beams are entered using the material data set icon located on the main toolbar. When the icon is clicked, a *Material Sets* window will open with choices for the project database as shown in Figure 5.6.

The example requires material data sets for soil & interfaces and beams. The first step is to set the parameters for the soil & interfaces. Input parameters for the soil are entered in the window shown in Figure 5.7 and include material model, unit weight, permeability, stiffness, poisson's ratio, cohesion, friction and dilatancy angles and interface properties. The input parameters used for the example soil model are as follows:

- Model used: Mohr Coulomb
- Material type: drained
- Unit weight: 120 pcf
- Permeability: 0 (both vertical and horizontal)
- Stiffness (E): 489,600 psf
- Poisson's ratio (ν): 0.3
- Cohesion (c): 1×10^{-5}
- Phi angle (φ): 35.00°
- Dilatancy angle (ψ): 5.00°

Specified along with the input parameters for the soil model are the settings for the interface. The soil interface is specified as either rigid or set manually. This feature is used for soil-structure modeling. The example model shown is modeling the soil-structure interaction between the soil and a concrete pipe. Both rigid and manual settings for the interface are used. *Rigid* assigns the soil properties to the interface and *Manual* allows the user to specify a friction angle for modeling two materials in contact with one another, such as concrete and soil or steel and soil.

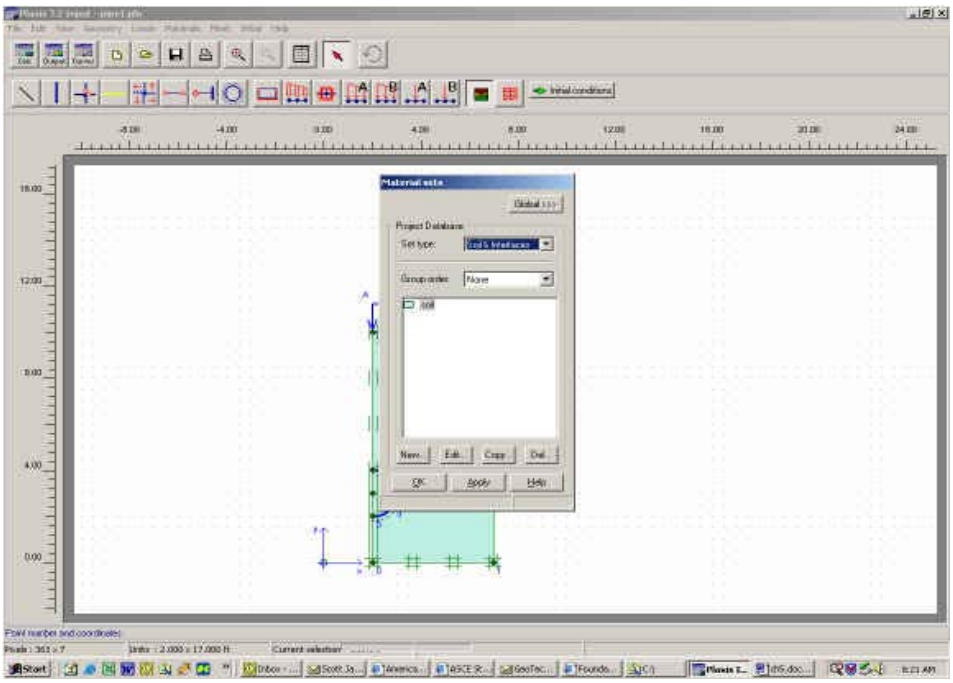

Figure 5.6: Material Sets Window in Plaxis 7.2.

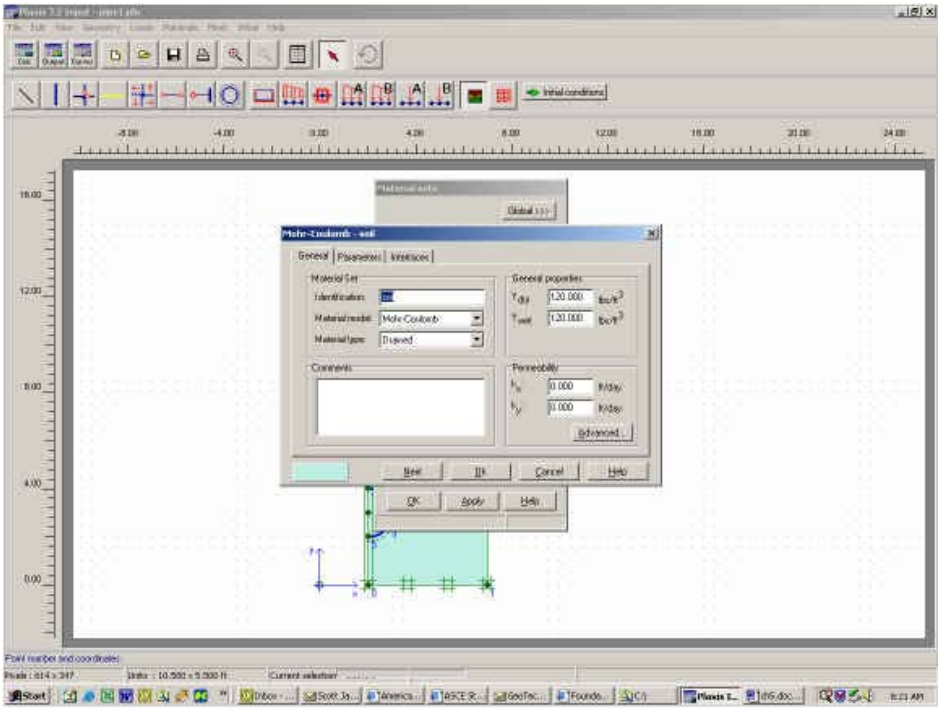

Figure 5.7: Soil Input in Plaxis 7.2 – Mohr Coulomb Model.

The material set for beams is specified when the user selects beams from the material set window and assigns the parameters. Input parameters are entered in the

window as shown in Figure 5.8. The input parameters used for the beam material model representing the concrete pipe are:

- Axial Stiffness (EA): 107.3×10^6 lb/ft
- Flexural Rigidity (EI): 193.5×10^6 lb-ft/ft
- Unit weight: 150 pcf
- Poisson's ratio: 0.15

The axial stiffness and the flexural rigidity are calculated using the modulus of elasticity and the cross sectional area of the concrete pipe along with the moment of inertia of the pipe. An estimate for the unit weight was obtained from a concrete manual.

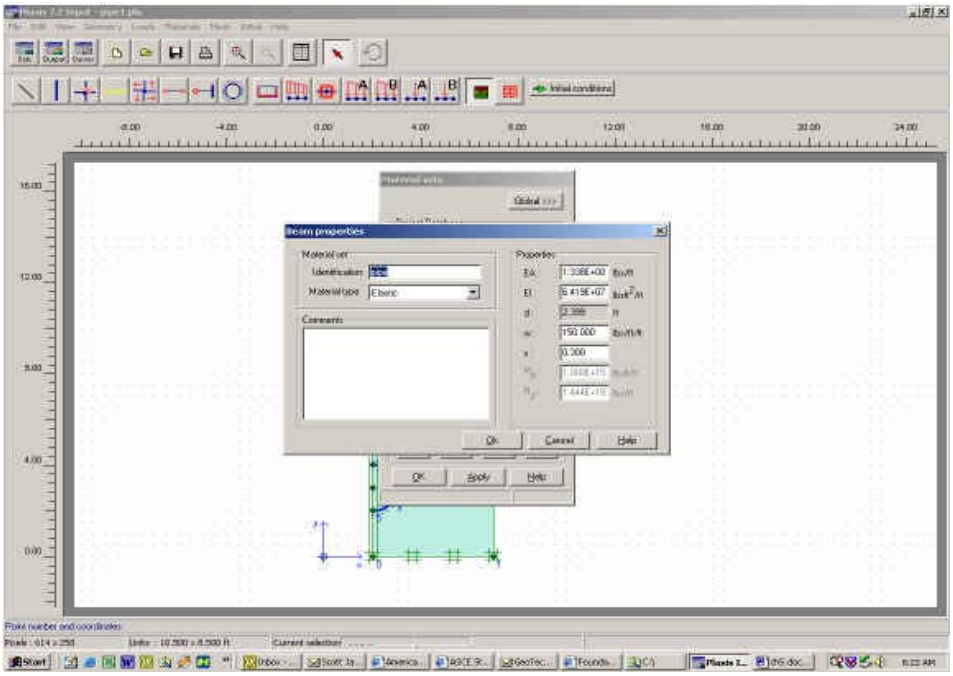

Figure 5.8: Beam Properties Input Window in Plaxis 7.2.

After the material parameters are assigned to the model, the material sets window appears once more to click and drag the material properties onto the model. Once this task is complete the window is closed. At this point, the model setup is complete.

In order for the finite element analysis to proceed, however, the geometry must be divided into elements called a finite element mesh. The mesh generation icon is the last icon on the main tool bar, located to the far right. Plaxis is equipped with a self-

generating mesh tool. Once the mesh is generated, a plot is displayed through the output program. The mesh can be defined as very coarse, coarse, medium, fine and very fine. A finer mesh is used where large stress contributions might be seen due to loading. After the mesh is generated the initial conditions are entered as shown in Figure 5.9.

Initial conditions involve an initial stress state before loading and an initial situation. This process is still part of the input program. The initial conditions consist of two different modes; one for the generation of initial water pressures (water conditions mode) and one mode for the specification of the initial geometry configuration and the generation of an initial effective stress field (geometry configuration mode). Switching between these two modes is done by clicking on icons as shown in Figure 5.9.

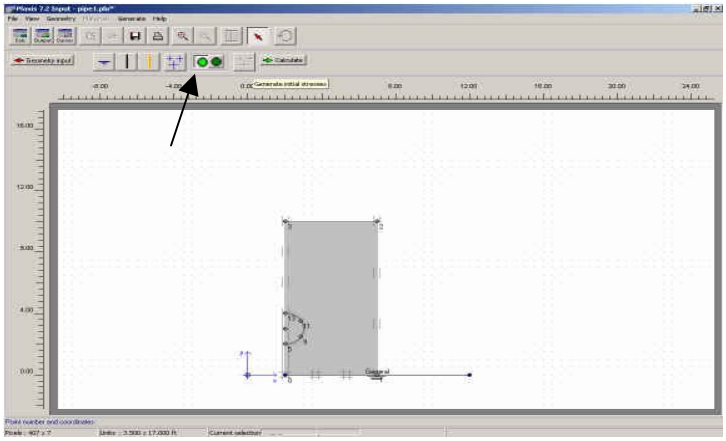

Figure 5.9: Pore Water Pressure & Initial Stress Modes in Plaxis 7.2.

Water conditions are specified by means of the water weight and phreatic lines. The model used for this example was in a dry state, thus there were no phreatic lines or water pressures to generate.

The screen is then switched to initial geometry configuration. In this step the example model is shown with the soil box and concrete pipe inside the box. The initial geometry configuration allows the user to select geometry objects that are not active in

the initial situation. This means that the beam elements can be turned off to determine the initial stresses before addition of the concrete pipe to the soil box.

The initial stresses are calculated using the K_0 procedure with a default value of 0.426 when the stress icon is chosen on the tool bar. An initial vertical stress is calculated using the coefficient of lateral earth pressure K_0. After the initial stresses are generated, a window is displayed with the initial stresses showing the plane of direction. Once the input stage is completed, the next step is the calculation stage.

Plaxis--Calculations

After the mesh is generated, the finite element calculations can be specified and executed in the calculations program. In this program each type of calculation to be performed is defined, along with the type of loading activated during the calculation. Initiating the calculation program will open a window as shown in Figure 5.10. The three tabs (general, parameters and multipliers) will allow the user to navigate through to the end calculate command. The only settings to define in the calculation program are the calculation type, selecting the calculation phases and multipliers. The other input areas in the calculations program were set to default and were used as default for the example model.

Figure 5.10: Plaxis 7.2 Calculations Program.

In the calculation program under the general tab the calculation type is specified along with the setup of the calculation phase(s) using the insert button as seen in Figure 5.10. The insert button will add additional phases for calculation. In the example model, three phases were setup; initial phase, phase 1 and phase 2. Phases are assigned parameters and multipliers when highlighted in the phase display box located at the bottom of the calculations window. The initial phase represents the starting conditions of the project as defined in the initial conditions mode of the Input program. For the example model, two phases were added: staged construction and total multipliers. The staged construction represents the installation of the concrete pipe with loading coming from overburden soil above the pipe. The total multipliers stage is where the assigned distributed load is activated and applied to the model.

Under the parameters tab (as shown in Figure 5.11) the default modes are used. The parameters tab is where the staged construction phase is defined. The loading input group is used to specify which type of loading is considered in a particular calculation

phase. Loading input was set to stage construction. The define button, located at the bottom right, will open the input window of the model allowing the user to deactivate and activate soil clusters and structural objects that define the construction of the model. After the staged construction phase is defined, the update key will return the user to the calculation program.

The multipliers tab is where loads are assigned for the total multipliers stage. There are two types of multipliers: incremental and total as shown in Figure 5.12. In the example model shown, the total multiplier assigned in the input program is ∑MloadA at a value of 16,000 with units of pounds per square foot. ∑MloadA controls the magnitude of the traction loads as defined in the *Load System A* of the input program.

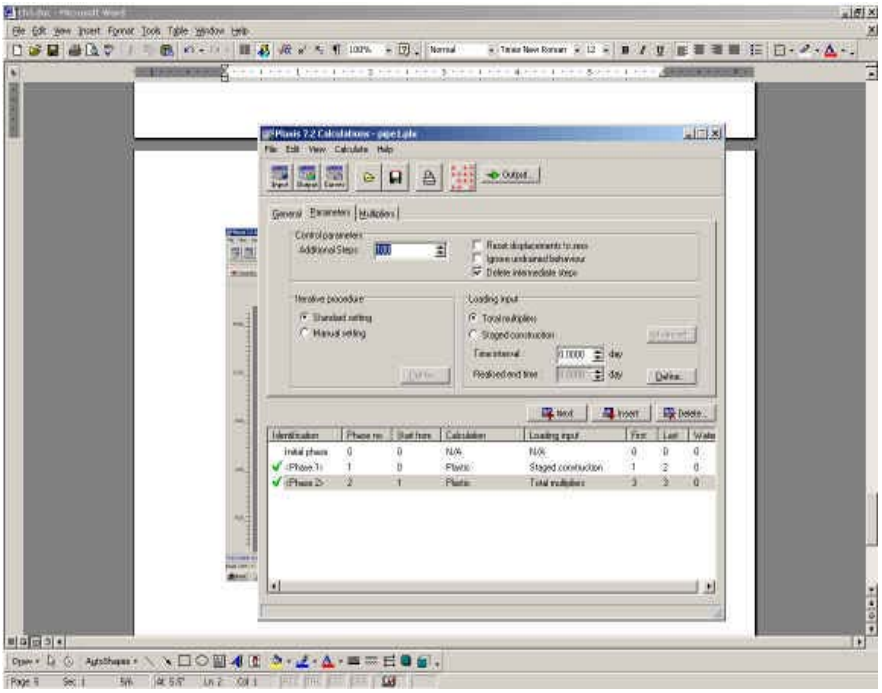

Figure 5.11: Plaxis 7.2 Calculations Program – Parameters Tab

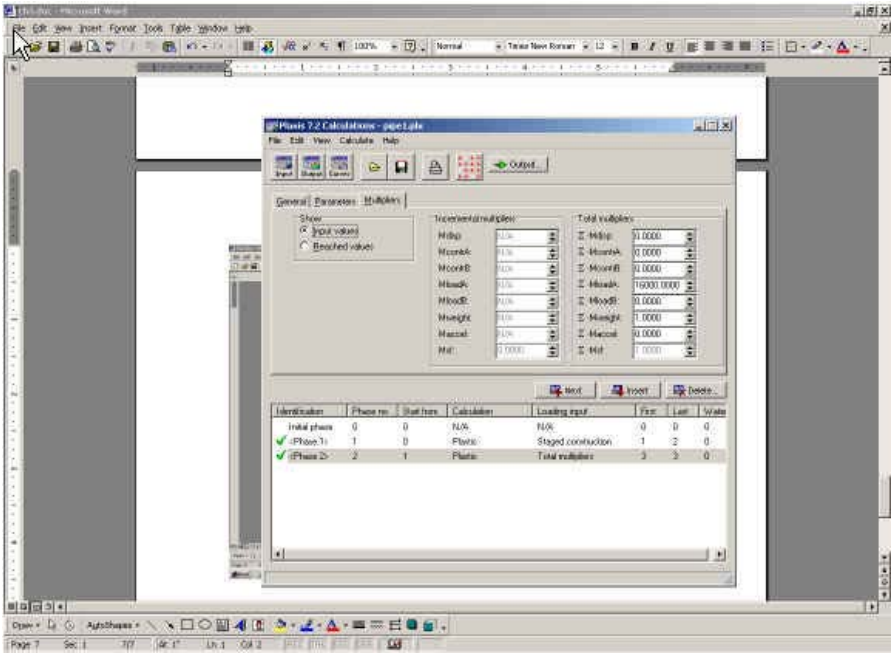

Figure 5.12: Plaxis Calculations Program – Multipliers Tab

Another feature in the calculation phase sets up points for curves generated in the curves program. The points can be entered by selecting the *Select Points For Curves* option from the *View* menu or by clicking on the corresponding button in the tool bar. Selection occurs when the output program opens showing a plot of the finite element mesh displaying all of the nodes. Nodes are selected by left clicking the mouse on the node of interest. Each node selected is characterized in the curves program by an alphabetical letter. A node can also be deselected by clicking on it again with the mouse.

In the example model shown, points were selected to create curves for load displacement and stress/strain curves. After selecting the points for curves the calculate button will run the calculation program. A window is opened to view the loading increments displaying different properties. Once the calculation is completed the calculation window appears with green checks beside the phases of calculation. Output of the calculation is viewed with the output program, which is opened by clicking on the output button located at the top of the calculation window.

Plaxis--Output

The main output quantities of a finite element calculation are the displacements at the nodes and the stresses at the stress points. When a finite element model involves structural elements, structural forces are calculated in these elements. The output program is equipped to display the results of a finite element analysis. The resulting program window is displayed in Figure 5.13, showing the deformed finite element mesh due to the load.

Results are viewed via the output program, displaying deformations, deformed mesh, total displacements, total increments, total strains, incremental strains, stresses, effective stresses, total stresses, plastic points, active pore pressures, excess pore pressures, groundwater head, flow field, structures and interfaces, beams, geotextiles, interfaces and anchors. In the example model (a four foot diameter concrete pipe modeled in a 20' x 10' x 10' soil box) the only outputs of interest are deformed mesh, total displacements (how much the pipe and soil settled), stresses, structures and interfaces and beams (concrete pipe). Each of the output results can be viewed as a picture, table or curve.

The first plot the user views in the output program is the deformed mesh plot as seen in Figure 5.13. From this plot the user can navigate to other results by selecting from the menu at the top of the output window. In the example model, the first thing to analyze is the stress distribution throughout the soil contained in the box. Figure 5.14 displays the stress distribution throughout the soil box by means of shading, with red indicating the highest stresses. Shading provides a colorful way of presenting results for effective mean stresses. Another way to display stress distribution results is through the contour plot of effective mean stresses as shown in Figure 5.15. The contour plot

displays a legend on the right side of the window that identifies each contour. A scan line, labels the contours with respect to the legend.

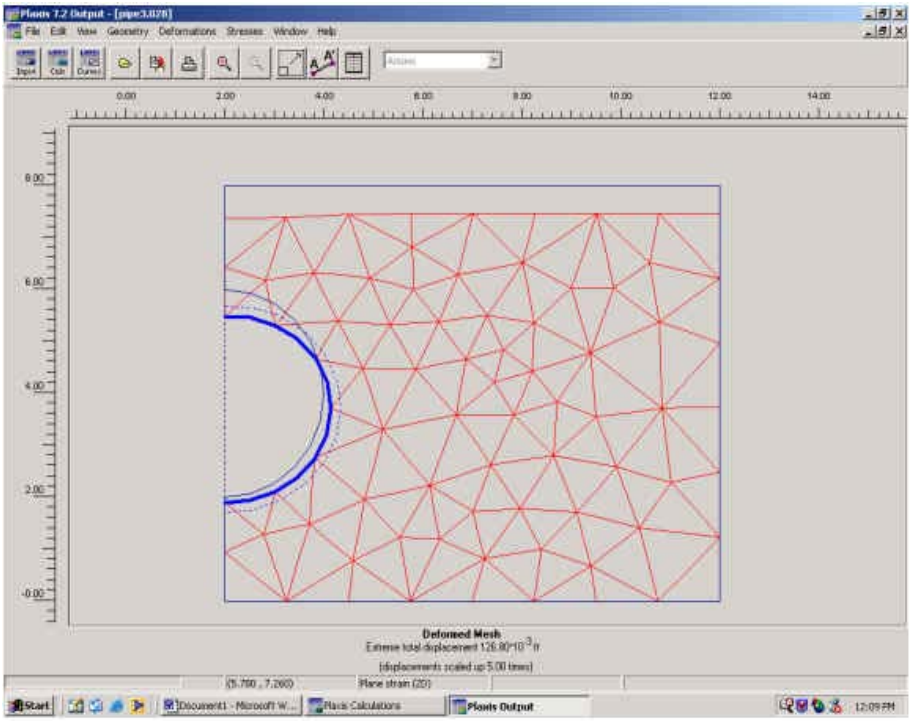

Figure 5.13 Plaxis output program with deformed mesh displayed on example model.

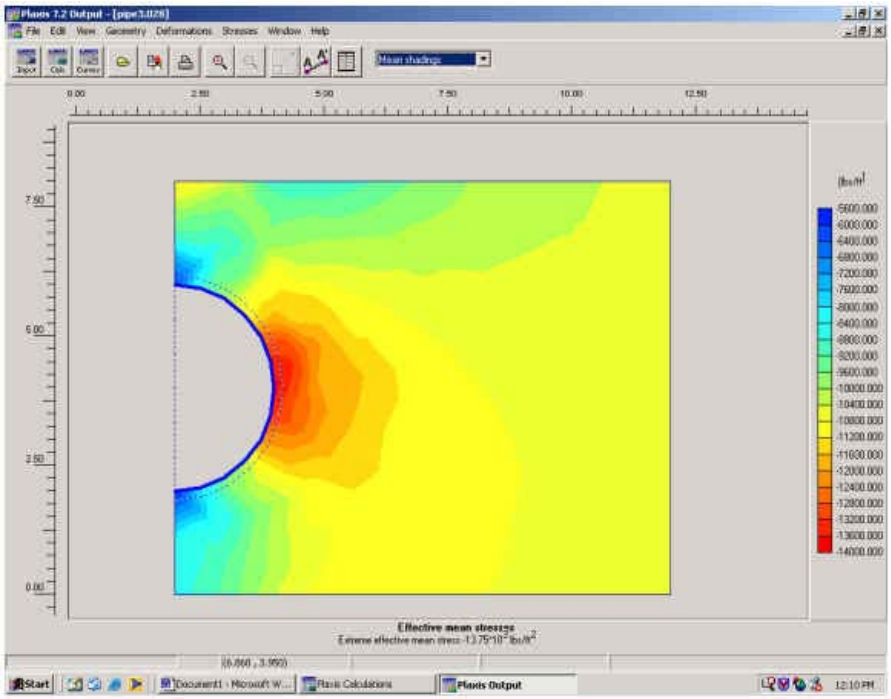

Figure 5.14: Plaxis Output Effective Mean Stresses Displayed by Mean Shading.

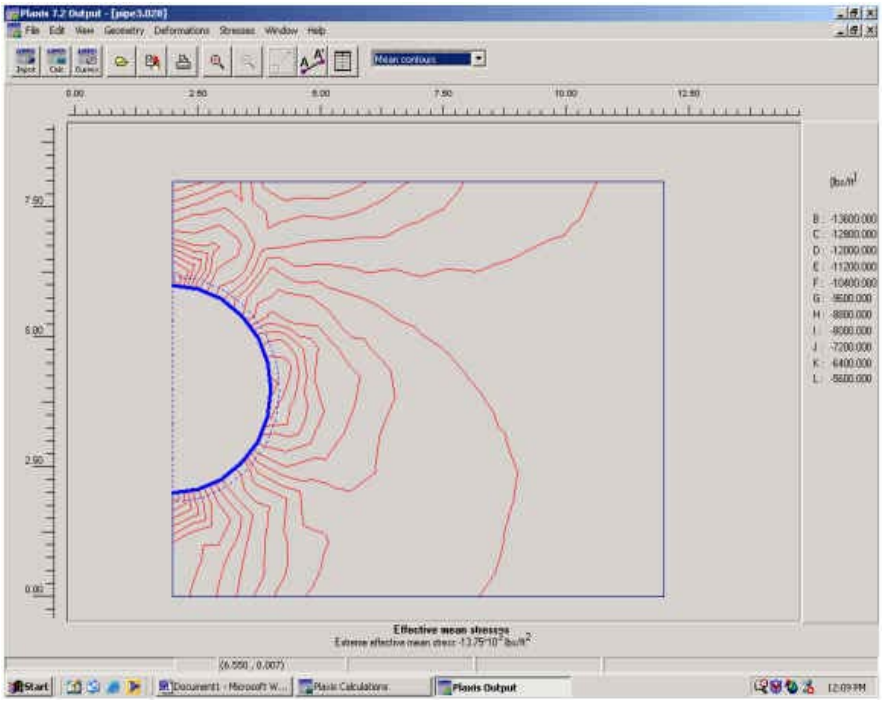

Figure 5.15: Plaxis Output Effective Mean Stresses Displayed by Contours.

Cross sections through the model can be used to present results of displacement and stress distributions. Viewing output in a cross section allows the user to gain insight into the distribution of a certain quantities calculated by the model. Cross sections are created in the model by selecting the cross section button and then clicking and dragging a line through the model where desired. In the example model stress distribution on the sidewalls was desired, requiring a plot of stress distribution along the sidewalls of the soil box. The cross section at the sidewall is shown in Figure 5.16. Also shown with the cross section tool are the horizontal displacements along the cross section shown in Figure 5.17.

Beam elements, as created by the input program, are viewed in the output program with element and interface results. Element results are the beam forces, displacements and bending moments. Interfaces assigned to the element will show displacements and stresses acting at or within that interface. Displacement output for the beam element –

concrete pipe and the interface assigned to the concrete pipe are shown in Figure 5.18. Plaxis will specify the extreme displacement for the beam elements and the interfaces. The bending moment of the concrete pipe in the example model is shown in Figure 5.19. Beam element properties are displayed in the output program by double clicking on the element itself. The various display choices are activated from the sub menu found at the top of the screen.

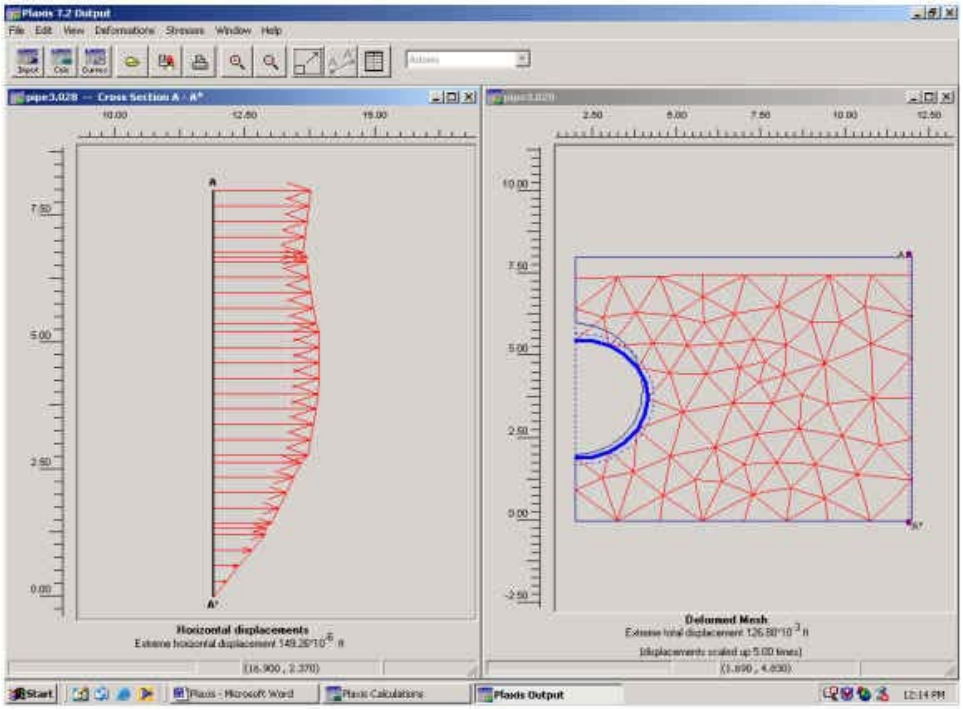

Figure 5.16: Stress Distribution Cross Section A-A in Plaxis 7.2 – Output Program

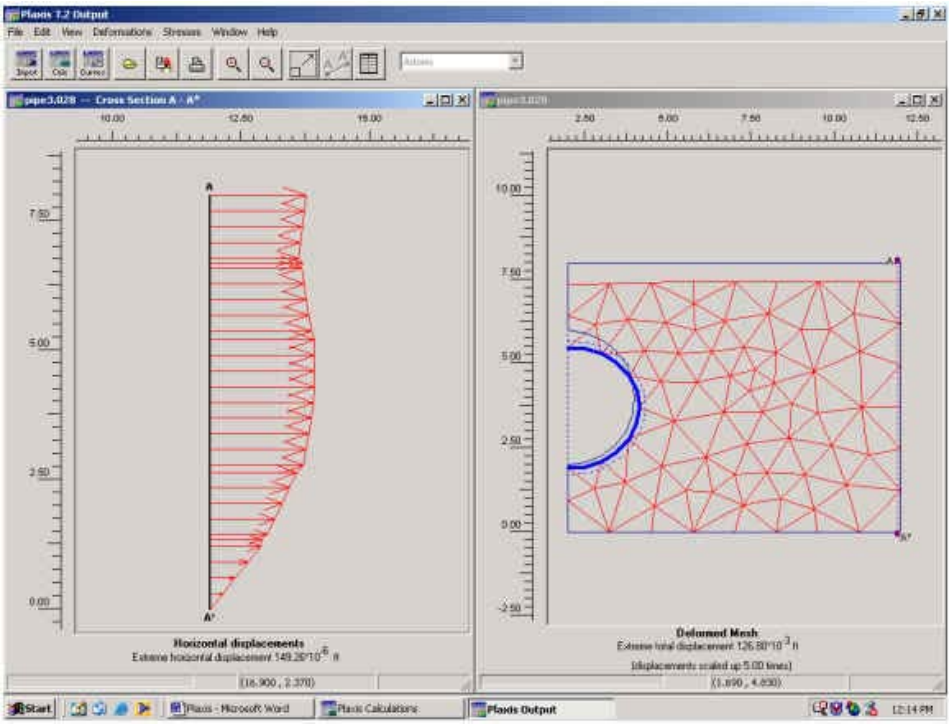

Figure 5.17: Horizontal Displacement Cross Section A-A in Plaxis 7.2 – Output Program

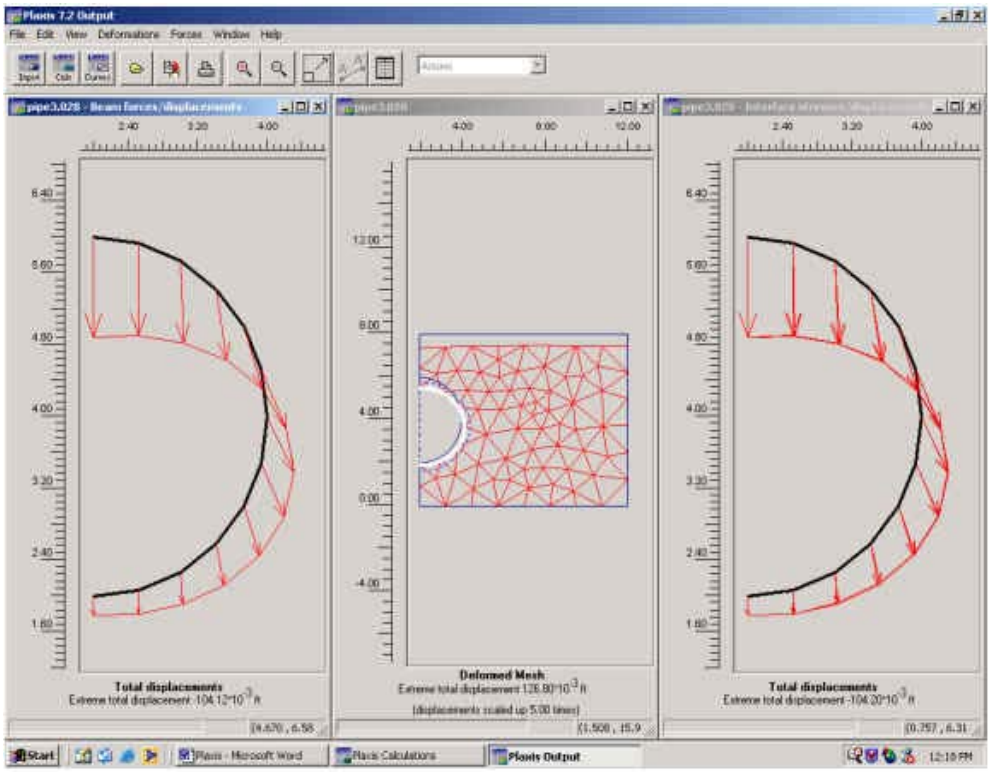

Figure 5.18: Displacements for the Pipe and Interface – Plaxis 7.2 Output Program.

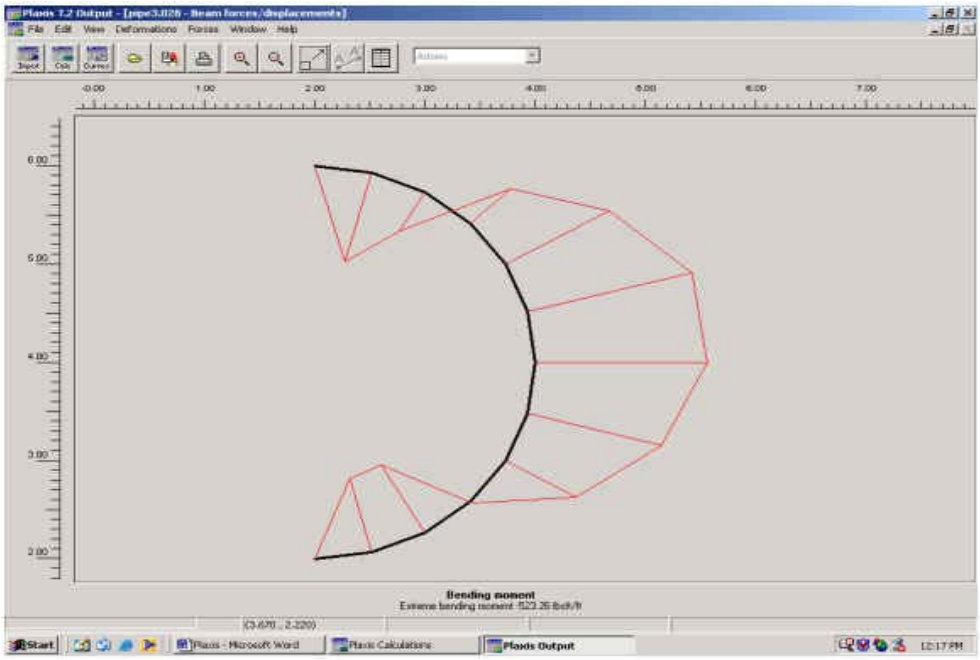

Figure 5.19: Bending Moment for the Pipe – Plaxis 7.2 Output Program.

The output program is also capable of producing tabular data for analysis. The numerical data can be viewed in output tables for all types of graphical output by clicking on the *Table* button in the main tool bar or by selecting the Table option from the *View* menu. A menu is available to view selections of other quantities. Tables available in Plaxis include displacement, stresses and strains, and stresses and forces. In the research example used, tabular data was not used directly. Output data was fed into the curves program to allow generation of different graphs.

CHAPTER 6
FINITE ELEMENT ANALYSIS OF A SOIL BOX TEST FACILITY

Introduction

A finite element analysis was performed in order to provide the necessary information for the design and fabrication of a soil box for testing two different concrete pipes, fiber reinforced and standard reinforced. Two and three-dimensional finite element analyses were done in order to evaluate the stress on the sidewalls due to the applied load and the effect of boundary conditions (i.e., friction on the sidewalls and around the perimeter of the test pipe).

The soil box will be fabricated of steel and filled with compacted soil similar to that used by the State of Florida in highway right-of-ways. The two-dimensional program used, Plaxis 2D, is a finite element analysis for soil and rock. Plaxis 2D evaluated the stresses on the sidewalls and the soil structure interaction between the soil and concrete pipes as well as between the soil and steel structure sidewalls. From the two dimensional analysis, the box dimensions were examined and the stresses evaluated using an interface between the soil and concrete pipe and the soil and the sidewalls. In the analysis, boundary conditions were evaluated in order to determine size requirements that would not induce lateral stresses on the test pipe. The results from the two-dimensional analysis are included in Appendix A.

A three-dimensional finite element analysis, Plaxis 3D Tunnel was used to evaluate the two-dimensional analysis, plus stresses in the z direction, the third dimension. Plaxis 3D analyzed the stress distribution throughout the box while varying the friction angle at

the soil-sidewall and soil-pipe interfaces to examine the stress concentrations induced within the soil box. Each of the three possible lengths to be considered (10', 15', and 20') was evaluated while varying the friction angle and analyzing the boundary conditions. Displacements of the concrete pipes were evaluated with and without friction on the sidewalls. Stresses were examined along the length of the pipe to ensure that no shear stresses were induced on the ends of the pipes near the front and rear walls.

Two different manufactured pipes will be tested inside the soil box, fiber reinforced and standard reinforced concrete pipes. The proposed pipe diameters to be used for testing are 18" and 24" with the further possibility of sizes as large as 48" in diameter. In order to ensure proper bedding, a depth of at least one diameter below the pipe inside the soil box will be used in the analysis. For example, the 24" diameter pipe will need two feet of underlying soil, resulting in an approximate height of six feet above the crown of the pipe to the top of the box. An overburden soil depth of six feet will allow a distribution of stresses that simulates *in-situ* conditions. The maximum load applied on the soil will be 16,000 lbs/ft^2.

The two types of backfill used in the analysis (shown in Table 6.1) were loose and dense compacted soil. For the loose compacted soil, a Young's Modulus of 216,000 lbs/ft^2 was used, while the dense compacted soil had a Young's Modulus of 489,600 lbs/ft^2.

Input parameters for the different sizes of SRCP and FRCP are displayed in Tables 6.2-6.4. Young's Modulus for the FRCP and SRCP were obtained from previously published literature. The SRCP modulus value was calculated using the American Concrete Institute (ACI 318) relationship between elastic modulus and compressive

strength, as shown in Equation 6.1. Compressive strength for concrete pipe normally ranges from 4000 lbs/in^2 to 6000 lbs/in^2 (Rinker Materials, 2003). Elastic modulus for the SRCP was calculated using a compressive strength (f'$_c$) of 4000 lbs/in^2. The elastic modulus for the FRCP, used to determine normal stiffness and flexural rigidity was 25 Gpa or 3.62 x 10^6 lbs/in^2.

$$E_c = 57{,}000 * \sqrt{f'_c} \tag{6.1}$$

Table 6.1 Material Properties of the soil (Loose & Dense).

Parameter	Name	Loose	Dense	Unit
Material Model	Model	Mohr-Coulomb	Mohr-Coulomb	-
Type of material behavior	Type	Drained	Drained	-
Soil weight above phr. level	γ_{unsat}	120	120	lbs/ft^3
Soil weight below phr. level	γ_{sat}	120	120	lbs/ft^3
Young's modulus	E_{ref}	216,000	489,600	lbs/ft^3
Poisson's ratio	ν	0.3	0.3	-
Cohesion	c_{ref}	0.00001	0.00001	lbs/ft^3
Friction angle	φ	35	35	DEG.
Dilatancy angle	ψ	5	5	DEG.

Table 6.2 Material Properties of the 18" diameter concrete pipes (FRCP & SRCP).

Parameter	Name	FRCP	SRCP	Unit
Type of behavior	Material type	Elastic	Elastic	-
Normal stiffness	EA	147,372,845	280,303,765	lbs/ft
Flexural Rigidity	EI	38,138,787	66791264	lbs-ft^2/ft
Weight	W	150	150	lbs/ft^2
Poisson's ratio	ν	0.15	0.15	-

Table 6.3 Material Properties of the 24" diameter concrete pipes (FRCP & SRCP).

Parameter	Name	FRCP	SRCP	Unit
Type of behavior	Material type	Elastic	Elastic	-
Normal stiffness	EA	198,636,143	382,227,687	lbs/ft
Flexural Rigidity	EI	93,303,588	168,720,067	lbs-ft^2/ft
Weight	W	150	150	lbs/ft^2
Poisson's ratio	ν	0.15	0.15	-

Table 6.4 Material Properties of the 48" diameter concrete pipes (FRCP & SRCP).

Parameter	Name	FRCP	SRCP	Unit
Type of behavior	Material type	Elastic	Elastic	-
Normal stiffness	EA	665,723,216	1,228,267,715	lbs/ft
Flexural Rigidity	EI	1,263,829,838	2,322,073,435	lbs-ft^2/ft
Weight	W	150	150	lbs/ft^2
Poisson's ratio	ν	0.15	0.15	-

Plaxis 3D--Verification Analysis

A three-dimensional analysis was performed to verify the results obtained from the two-dimensional analysis, as well as to analyze the stresses and displacements in the third dimension. Plaxis 3D introduces a third dimension of analysis allowing stresses in the z-direction to be examined. From the two-dimensional analysis, results showed that the use of well-compacted soil (90% proctor) provided proper stability with half as much settlement as that of the loose compacted soil. It is important to obtain proper compaction during the installation of the pipe to produce maximum performance of the pipe.

Three-dimensional finite element analysis was used to verify eight analyses performed with the two-dimensional finite element program (Appendix A). Verification of the stresses and displacements throughout the soil box were done for the 18" and the 24" diameter FRCP and SRCP. The ability to test a 48" diameter pipe in the soil box is questionable according to the two-dimensional analysis due to the limited depth of soil cover on top of the test pipe.

Verification of the 18" and 24" diameter pipe was done using the three dimensional version of Plaxis. Four different analyses of the 18" and 24" pipe were performed using dense compacted soil and varying the friction angle along the wall within the interface for each of the SRCP and FRCP. The three-dimensional analyses differed very little from

the two-dimensional analyses, through the three-dimensional results provided better stress distribution throughout the soil box in the third dimension. Varying the soil-wall friction angle from a value equal to the soil friction angle of 35 degrees to less than 5 degrees doubled the amount of total displacements throughout the whole soil box. Assigning a value of 5 degrees to the interface resulted in higher displacements within the soil upon loading.

Friction on the sidewalls equal to that of the soil resulted in a total displacement of 0.236' while a friction angle of less than 5 degrees on the sidewalls results in a total displacement of 0.433'. When comparing the 18" and 24" diameter pipes, the total displacements were the same. Figure 6.1 shows the total displacements for the 24" FRCP and Figure 6.2 shows the total displacement for the 24" SRCP, both with a friction angle equal to that of the soil. It is visually apparent on the sidewalls that there is friction. The load is distributed throughout the third dimension and the friction along the wall is visible through the shading.

The effective mean stress reported from the three-dimensional analysis differed little from the two-dimensional analysis. For example, the extreme effective mean stress for the 18" SRCP, friction sidewalls, measured 12,690 lbs/ft^2 in the two-dimensional and 12,520 lbs/ft^2 in the three-dimensional analysis. The three-dimensional analysis distributes the stresses more efficiently in the z direction (i.e., the third dimension).

The analysis of the box focuses on the maximum stress on the sidewalls as a result of the 16,000-lbs/ft^2 load. Each of the two-dimensional wall friction analyses examined the effective mean stress on the sidewalls. When verified by the three-dimensional finite

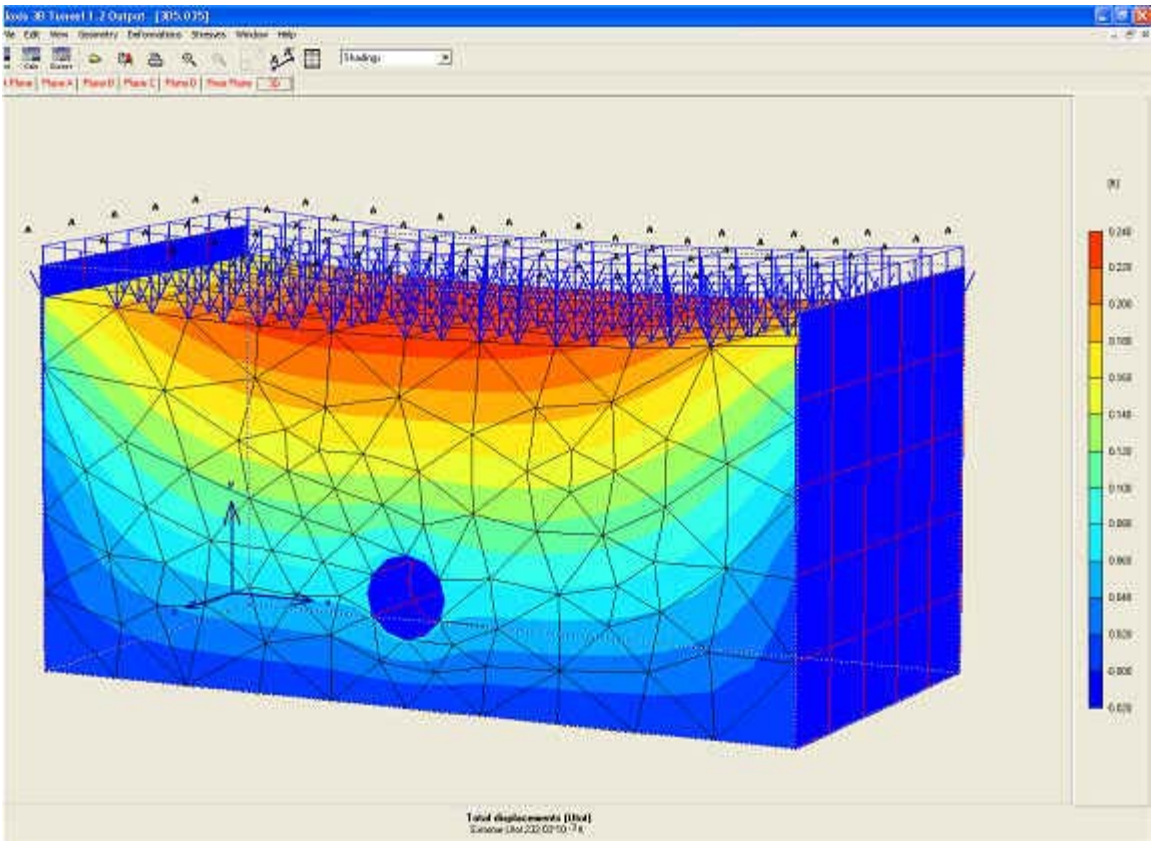

Figure 6.1 A Three Dimensional View of Total Displacements for 24” FRCP.

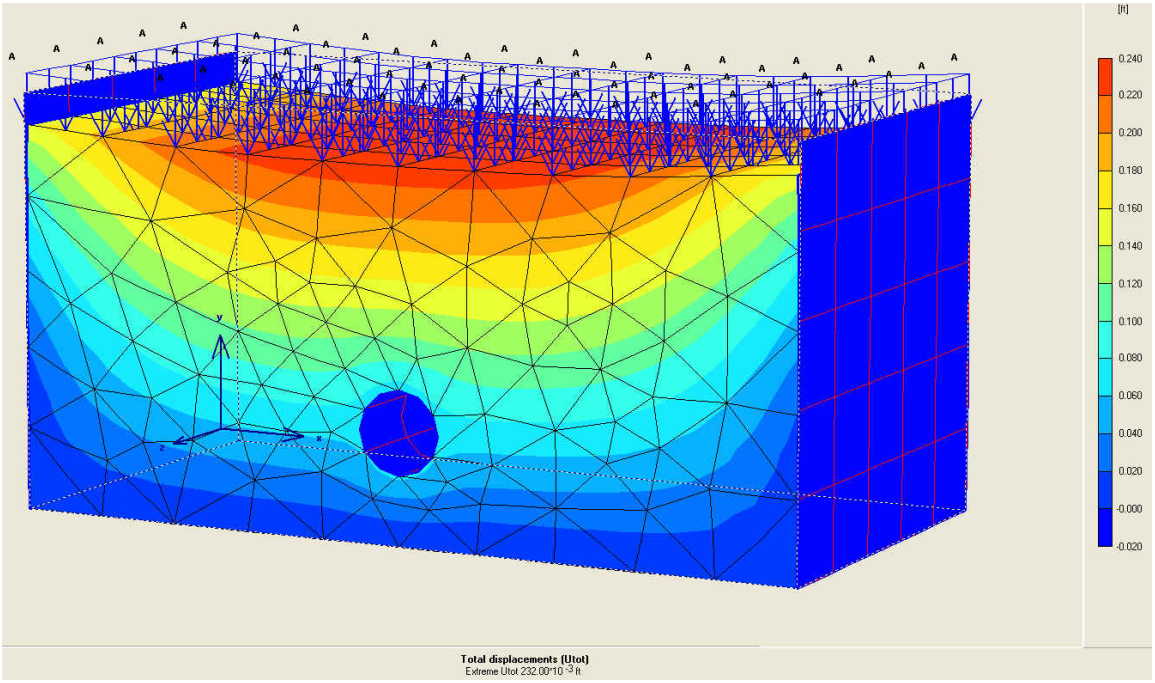

Figure 6.2 Three Dimensional View of Total Displacements for 24” SRCP

element program, it was found that the sidewall stresses were slightly smaller. Sidewall stresses examined through the interface along the sidewall increased when the friction angle was set to 35 degrees.

For example, the interface wall stress for the 18" diameter SRCP with friction was 7,070-lbs/ft^2 compared to an interface without friction of 4,470-lbs/ft^2. The soil was unable to move freely upon load application when friction occurred at the sidewalls, therefore creating higher stresses on the sidewalls. Figure 6.3 shows the left sidewall of the soil box displaying the effective normal stresses.

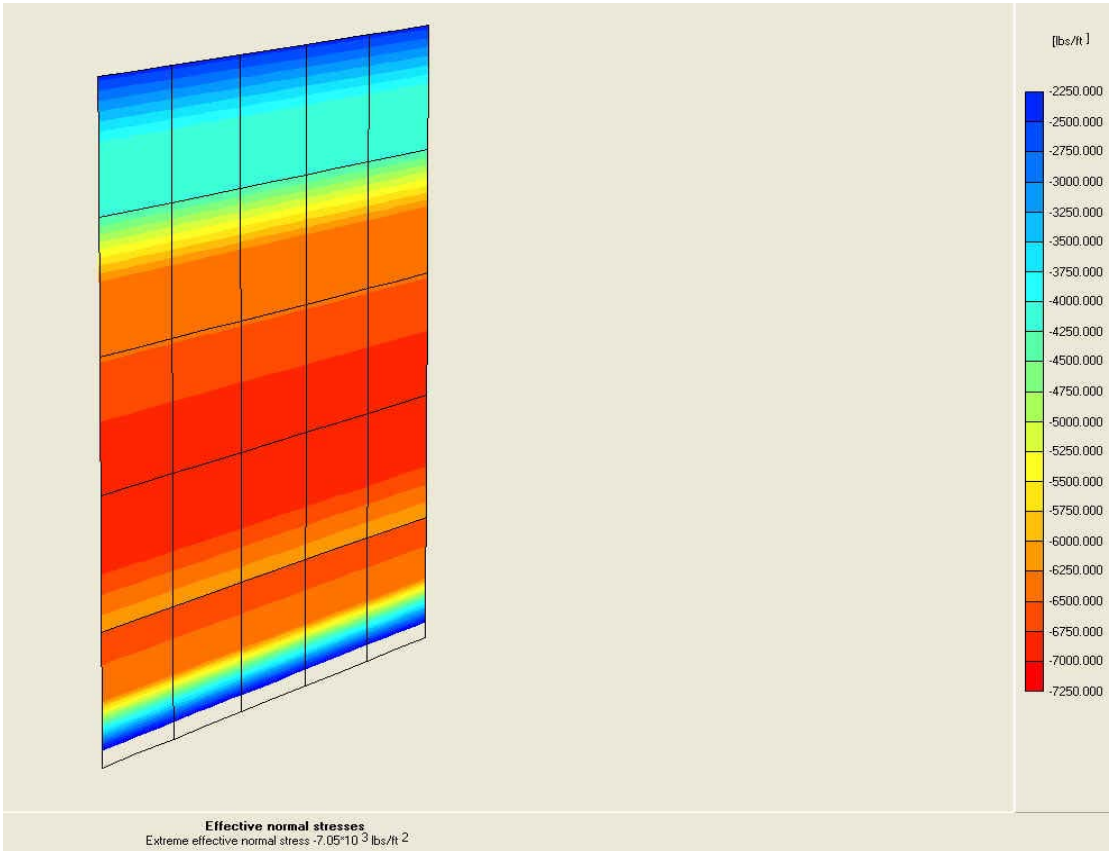

Figure 6.3 Left Side Interface of Soil Box Model 24" FRCP

An interface was also assigned to the perimeter of the pipe inside the soil box for soil-structure interaction modeling. The friction angle associated with this interface was also varied in the same manner as the sidewalls. The extreme effective mean stress

around the pipe and the extreme total displacement around the pipe are reported for each of the tests. There was very little difference between the FRCP and the SRCP modeled. In varying the friction angle at the interface around the perimeter of the pipe, the effective mean stress increased greatly, from -2,860 lbs/ft^2 for a friction angle of less than 5 degrees to -27,870 lbs/ft^2 when the friction angle was set to the same value as the soil. Results are depicted graphically in Figures 6.4 and 6.5.

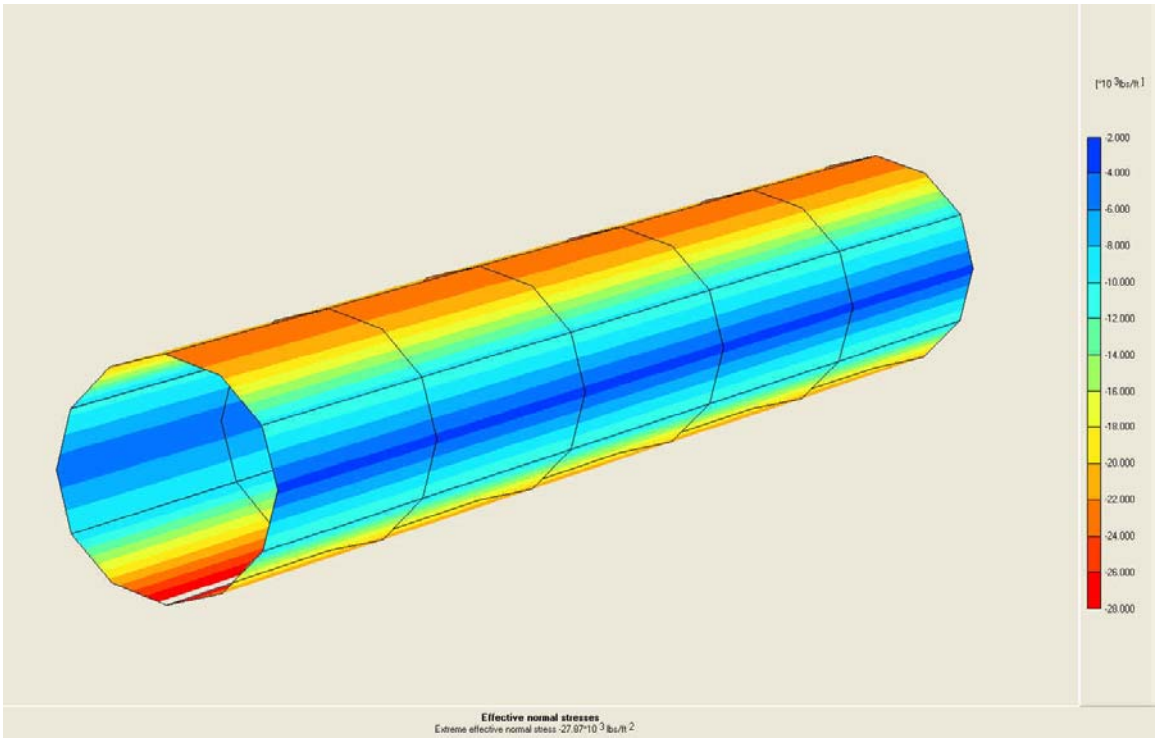

Figure 6.4 18" Diameter FRCP Friction Area on Surface of Pipe.

In situ conditions reflect a soil interacting with a concrete surface and soil-soil interaction around the pipe. In an attempt to model this, the friction analysis along the sidewall is justified but the friction around the perimeter of the pipe is questionable. It is impossible to have near zero friction around the perimeter of the pipe that would result in a stress decrease, as seen in the three-dimensional analysis for a friction angle less than 5 degrees. FRCP is a smoother pipe, when compared to SRCP, yet the friction will not be

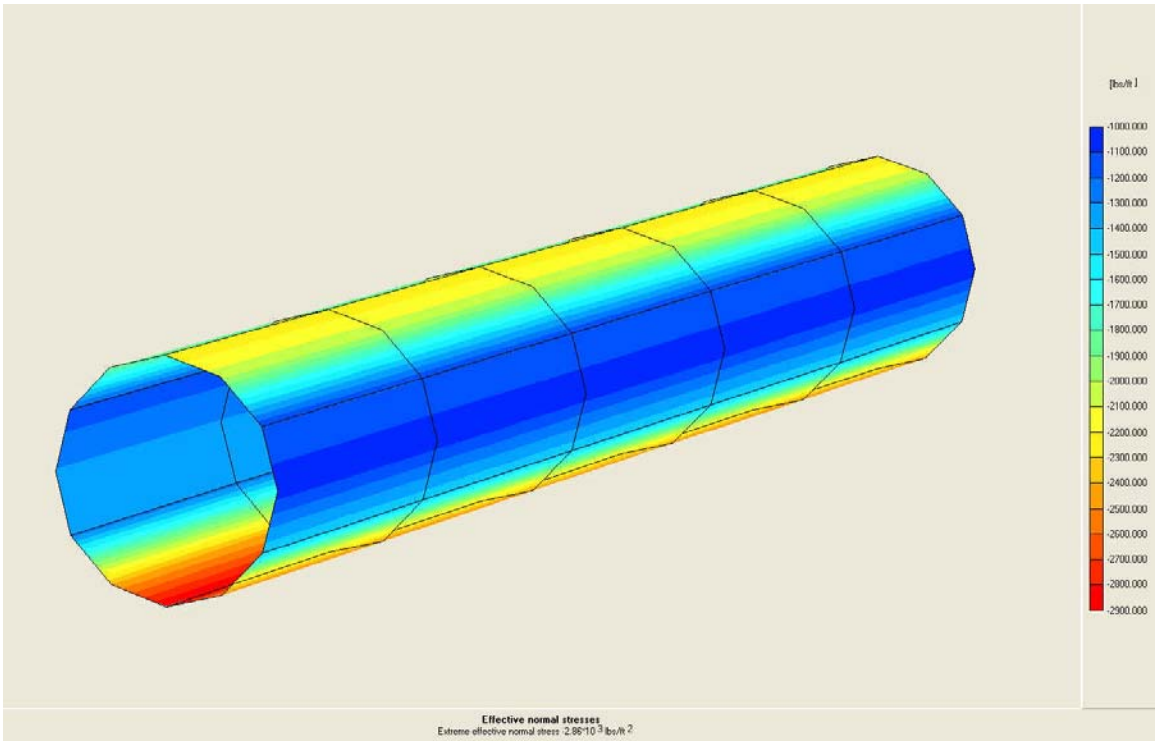

Figure 6.5 18" Diameter FRCP Near Zero Frictionless Area on Surface of Pipe.

near zero. Thus using a friction angle equal to that of soil around the perimeter of the pipe produced more justified results. More stress is induced as friction is encountered throughout the soil depth under the load.

The displacement for the interface reacted in the same manner increasing, for example, from 0.072' to 0.211' when the friction angle was increased to a value equal to that of the soil friction angle, 35 degrees. This is a direct result of the soil encountering a rough friction surface along the pipe. Table 6.5 presents the results of the three-dimensional analysis verification of the two-dimensional analysis. Note that the negative values refer to compression.

Other concerns that were addressed with three-dimensional finite element analysis included stresses along the length of the pipe as a result of a possible shear stress induced on the ends of the pipe due to wall friction and displacement of the entire pipe as a result of both wall friction and service load.

Soil Box Analysis

A three-dimensional finite element analysis was conducted with and without the pipe inside the soil box to analyze the box dimensions while varying the friction angle through four different analyses. An approximate height of ten feet was used for the height of the soil box based on providing proper bedding needs for each of the 18" and 24" diameter pipe. A bedding depth of one pipe diameter below the invert of the pipe was used in the finite element analysis. Three different lengths of soil box were analyzed, ten, fifteen and twenty feet. Full-scale models were used for analyses eliminating any concerns of the results.

Table 6.5 Three Dimensional Analysis Verification of Plaxis 2D Wall Friction Analysis

Pipe	D[1]	C[2]	R[3]	EPS[5]	EMS[6]	$Disp_1$	IEWS[7]	IEPS[8]	$Disp_2$	PM[9]	$Disp_3$
FRCP	18"	Dense	1	-23650	-13830	0.236	-7340	-24630	-0.060	-6170	0.057
SRCP	18"	Dense	1	-21600	-12690	0.237	-7280	-22440	-0.065	-5230	0.064
FRCP	18"	Dense	0.05	-24430	-15400	0.331	-4840	-4590	-0.143	-961	0.090
SRCP	18"	Dense	0.05	-24440	-15400	0.331	-4840	-4550	-0.143	-877	0.090
FRCP	24"	Dense	1	-24520	-14690	0.230	-7410	-24960	-0.696	-11090	0.067
SRCP	24"	Dense	1	-22180	-13380	0.234	-7380	-22610	-0.077	-9600	0.076
FRCP	24"	Dense	0.05	-26430	-14760	0.333	-4790	-5800	-0.194	-2220	-0.113
SRCP	24"	Dense	0.05	-26450	-14750	0.333	-4790	-5740	-0.195	-2070	0.113

*All values reported are extreme values (i.e., the maximum values).

1. D is the pipe diameter in inches.
2. C is the compaction of the backfill.
3. R is the interface value of strength. A value of 1 represents a friction angle the same as the backfill soil. A value of 0.05 represents a friction angle less than five degrees.
4. DM is the deformed finite element mesh after loading 16,000 lbs/ft^2
5. EPS is the effective principal stress for the entire model box in lbs/ft^2
6. EMS is the effective mean stress for the entire model box in lbs/ft^2
7. IEWS is the interface effective normal wall stress in lbs/ft^2
8. IEPS is the interface effective normal pipe stress in lbs/ft^2
9. PM is the pipe bending moment in lbs-ft/ft

$Disp_1$ is the total displacements for the entire box in feet.

$Disp_2$ is the total displacements for interface around the perimeter of the pipe in feet.

$Disp_3$ is the total displacement of the concrete pipe in feet.

The first analysis group examined the three different lengths with soil backfill only and no test pipe in the box. In this analysis, the friction angle was varied from 35 degrees to less than 5 degrees. This friction angle was assigned to the sidewalls. The remaining three analyses examined boundary effects with a 24" FRCP inserted in the soil box. Again each of the three soil box lengths was analyzed while varying the friction angle at the sidewalls and around the perimeter of the test pipe. Note that the decision to use the FRCP is not due to preference; it is merely an example to model the boundary effects since Young's modulus for both SRCP and FRCP are similar in magnitude.

Soil Box Analysis--No pipe

A three-dimensional analysis was done on three different lengths of the soil box to determine the stress and displacement of the soil due to a maximum distributed load of 16,000 lbs/ft^2. An interface was assigned to the sidewalls to all variation of the friction angles. Dense compacted backfill soil was used since it provides better bedding for the test pipe than the loose compacted soil. Six models, two for each length, were analyzed with a friction value of 35 degrees and less than 5 degrees.

Figures 6.6-6.8 show the stress distribution for the effective mean stresses throughout the entire soil box with sidewall friction angle 35 degrees. Figures 6.9-6.11 show the stress distribution for a sidewall friction of less than 5 degrees. For the soil box model with sidewall friction, the extreme effective mean stresses decreased as the length of the soil box increased. For the friction value of less than 5 degrees, the extreme effective mean stresses increased as the length of the soil box increased. A higher displacement resulted in higher load concentrations throughout the soil box, thus the increase in stress with an increase in length. Another observation is the stress concentration and distribution throughout the soil. In comparing the 10' soil box with

friction to the 15’ soil box with friction, the stress concentration around the middle of the box increases approximately 2,000 lbs/ft^2. This is important in dimensioning the soil box for the maximum load needed for proper testing results.

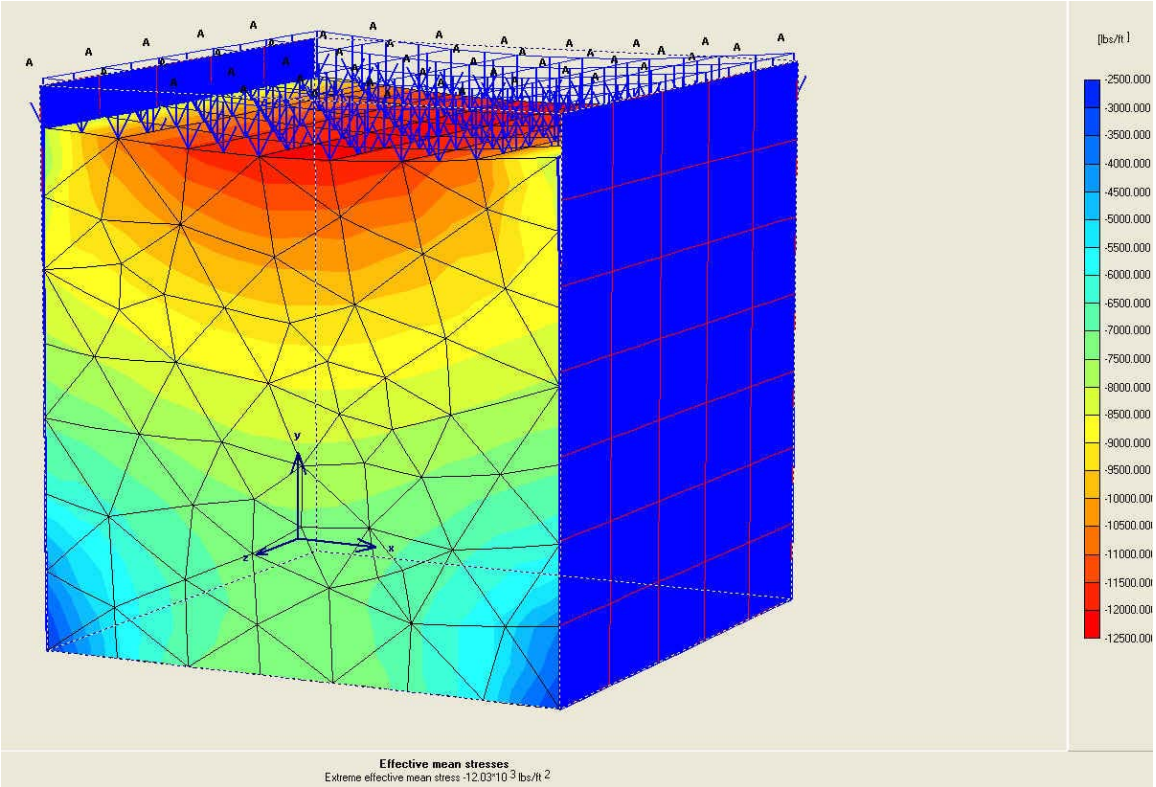

Figure 6.6 10’ Length Soil Box: Effective Mean Stresses with Sidewall Friction:

Stresses were modeled along the sidewall. Figures 6.12-6.14 show the left sidewall deformation plane with a friction angle of 35 degrees. The sidewall interface with the largest effective normal stress occurs in the 15’ soil box at a value of 7,280 lbs/ft^2. The 10’ soil box has a sidewall interface stress value of 6,620 lbs/ft^2 and the 20’ length a value of 7,150 lbs/ft^2. The 10’ box contains only half the volume of soil as the 20’ length box, resulting in the lower stress value. Also, the surface area of the 10’ box exposed to the distributed load is half the area of the 20’ box. Figures 6.15-6.17 show the left sidewall deformation plane with a friction angle less than 5 degree. The mean effective

normal stress along the sidewall of the soil box with a friction angle of less than 5 degrees

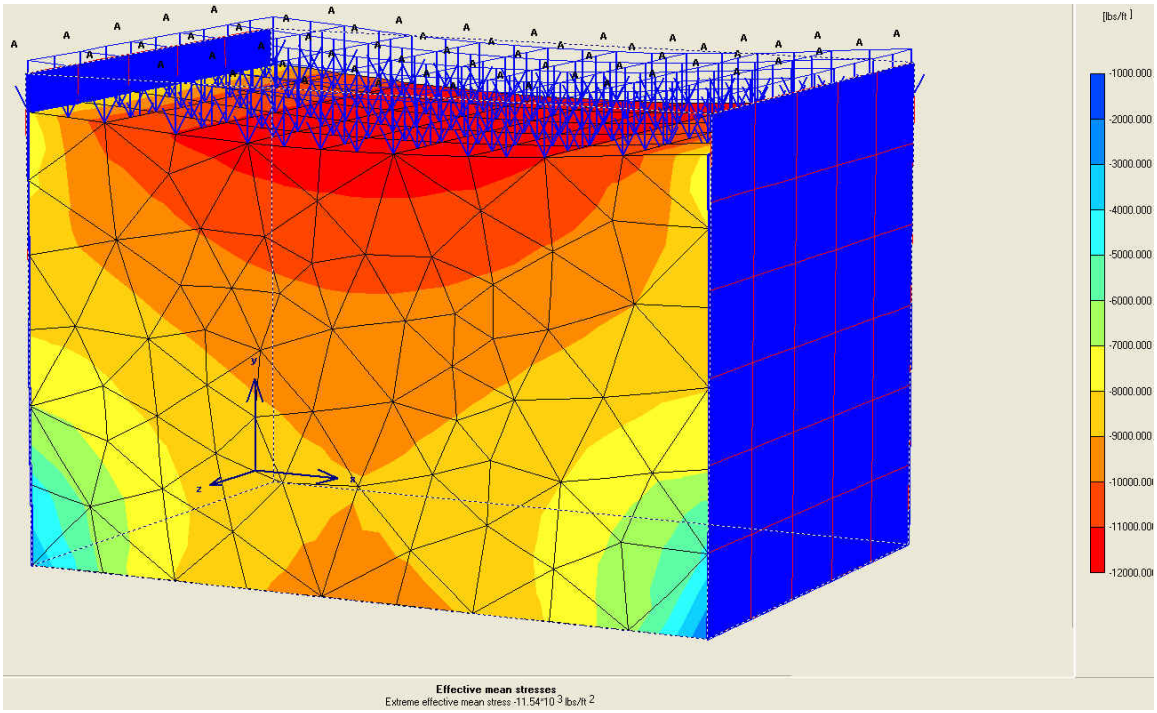

Figure 6.7 15’ Length Soil Box: Effective Mean Stresses with Sidewall Friction.

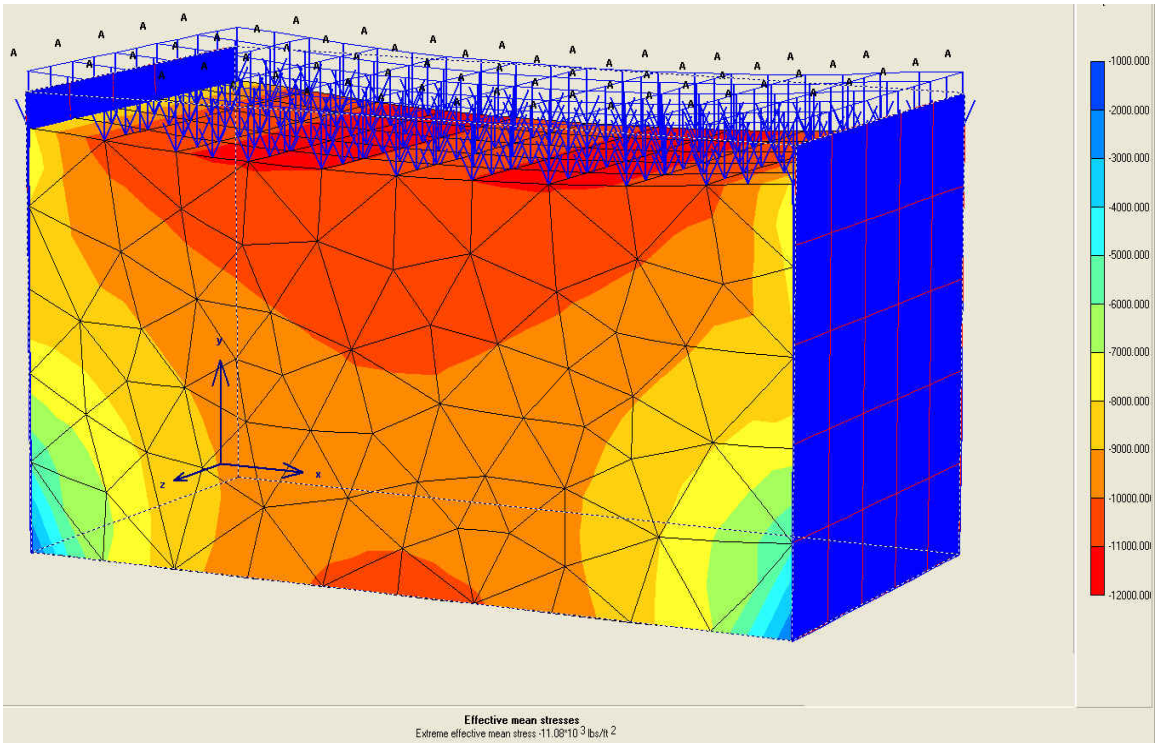

Figure 6.8 20’ Length Soil Box: Effective Mean Stresses with Sidewall Friction.

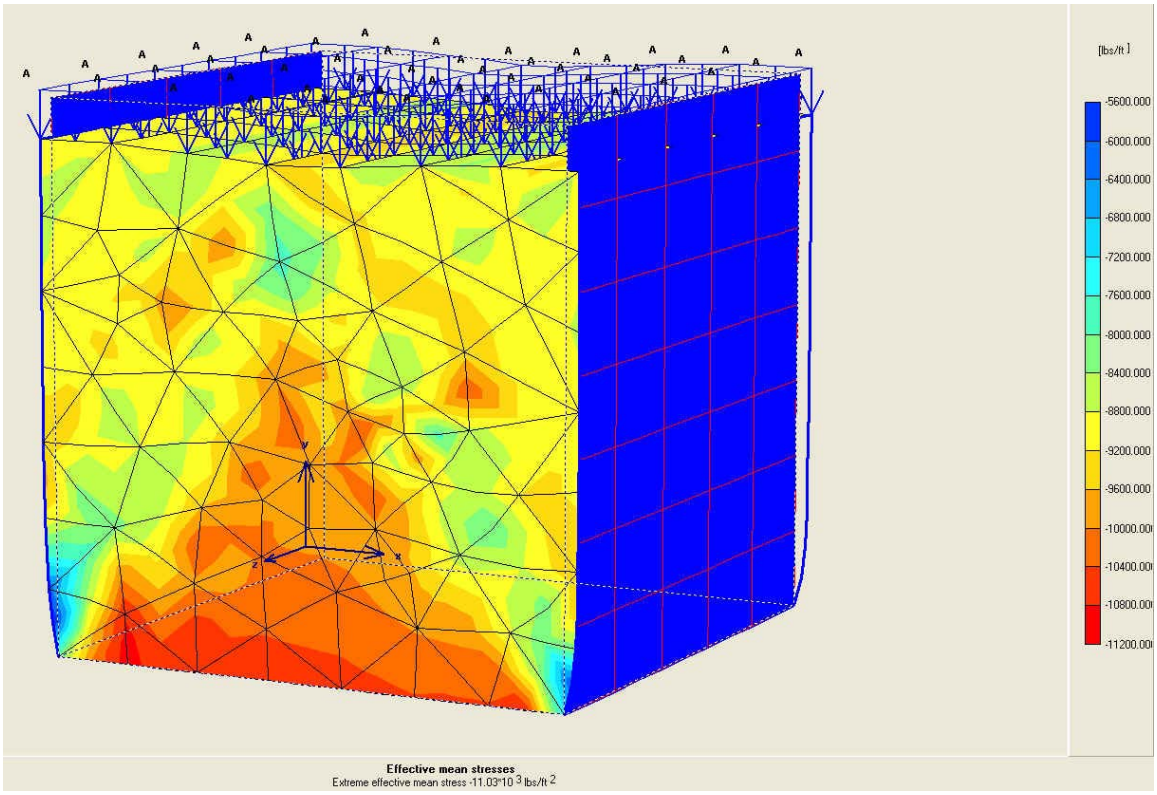

Figure 6.9 10’ Length Soil Box: Effective Mean Stresses with Frictionless Sidewalls.

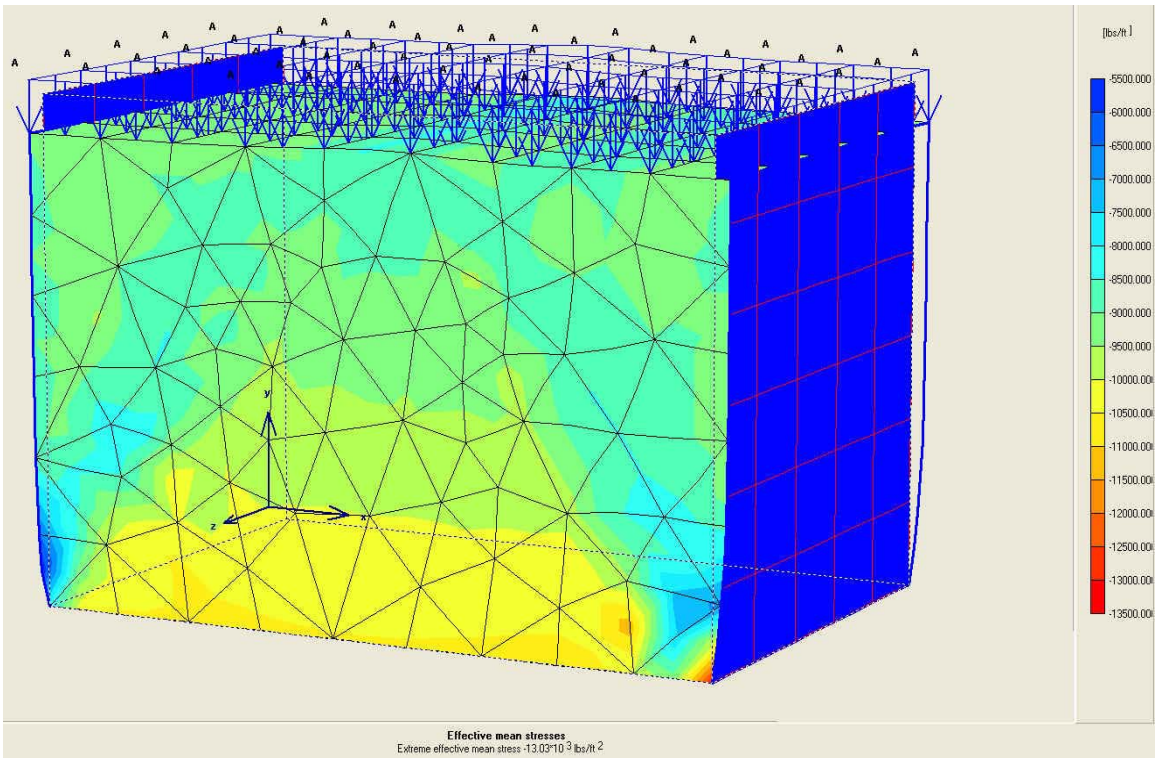

Figure 6.10 15’ Length Soil Box: Effective Mean Stresses with Frictionless Sidewalls.

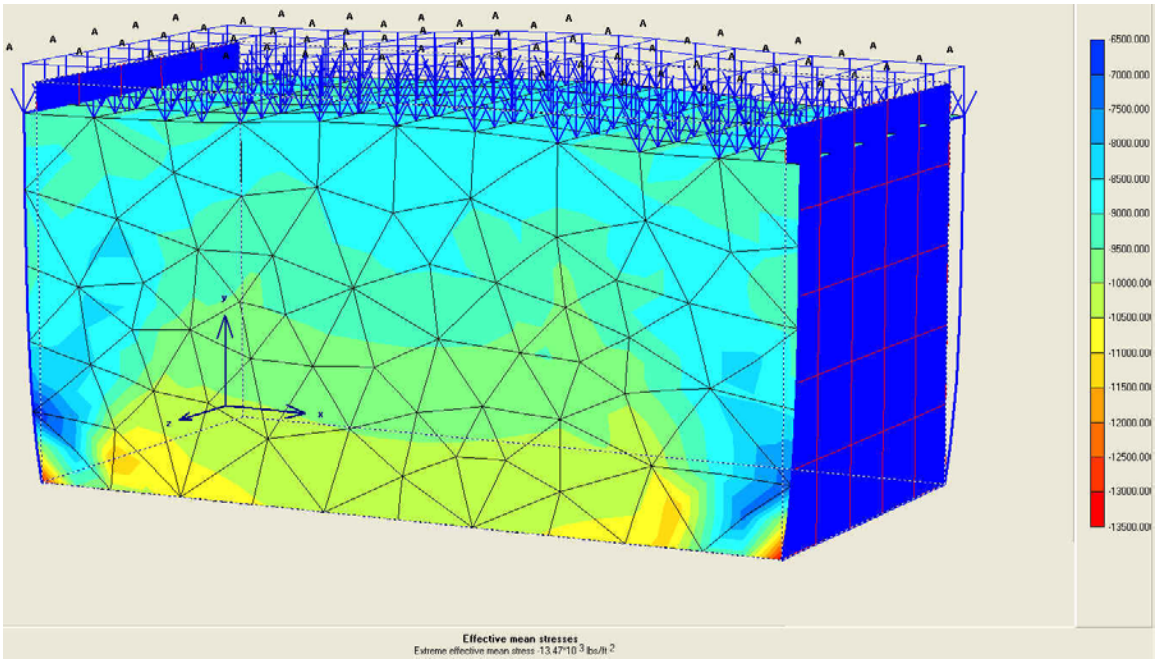

Figure 6.11 20' Length Soil Box: Effective Mean Stresses with Frictionless Sidewalls.

decreases as the length of the soil box increases. The stress value for the 20' soil box was 4,790 lbs/ft^2. With almost frictionless sidewalls, the soil is free to settle upon loading releasing stress from the sidewalls.

In comparing the sidewall stress deformation plane for the friction wall and the frictionless wall, the former deformation plane was jagged, representing the friction on the sidewall. The frictionless wall's deformation plane is smooth, representing the transition of deformation after loading.

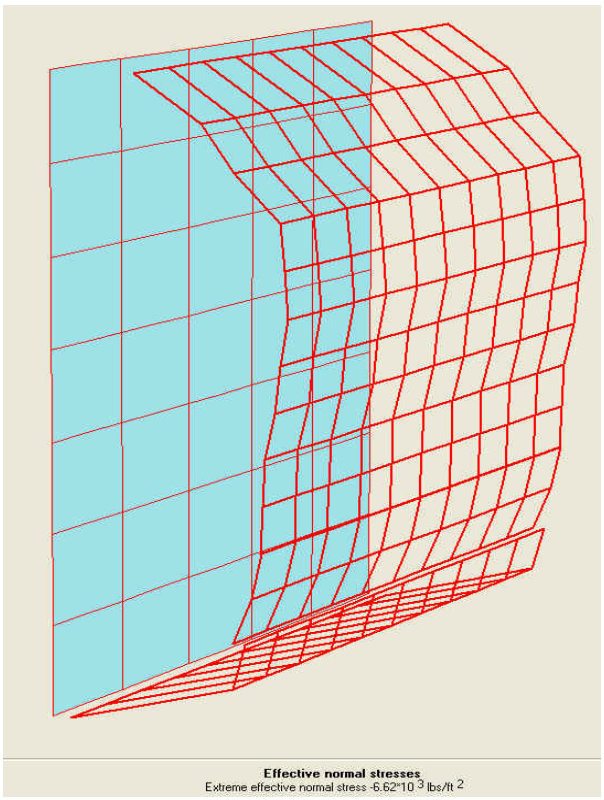

Figure 6.12 10’ Length Effective Normal Stresses Left Sidewall Friction Plane.

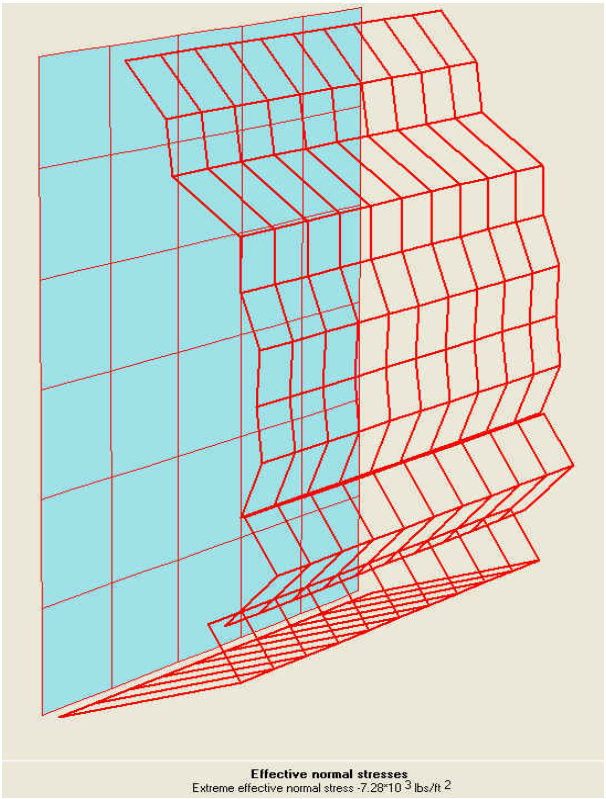

Figure 6.13 15’ Length Effective Normal Stresses Left Sidewall Friction Plane.

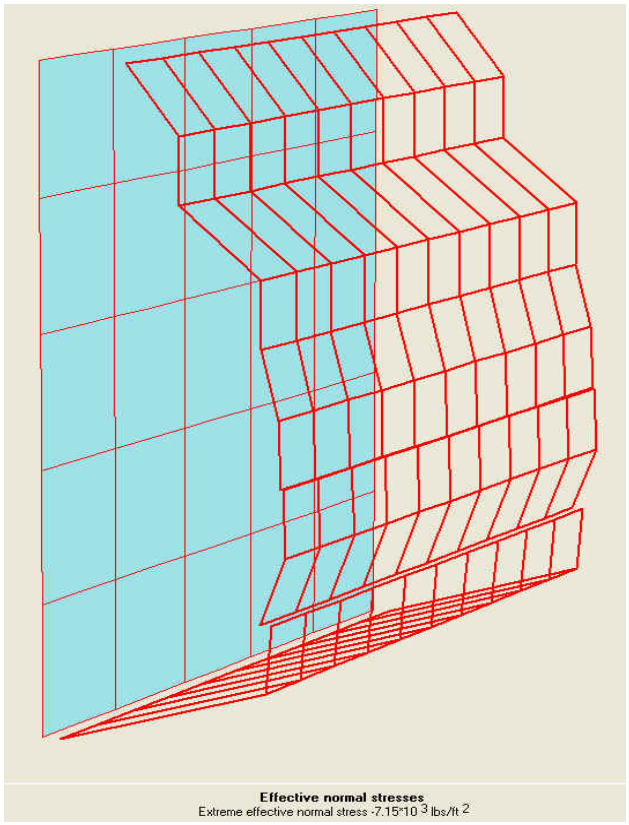

Figure 6.14 20’ Length Effective Normal Stresses Left Sidewall Friction Plane.

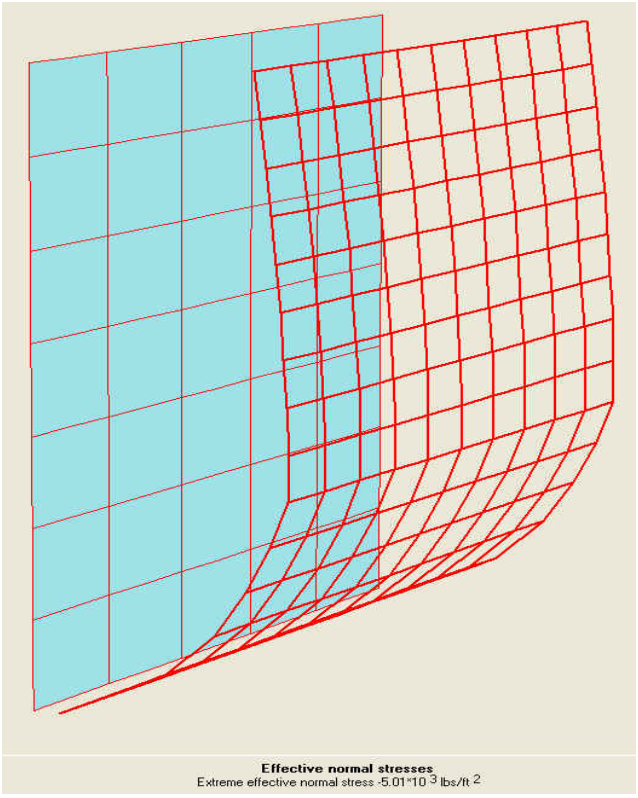

Figure 6.15 10’ Length Effective Normal Stresses Left Sidewall Frictionless Plane.

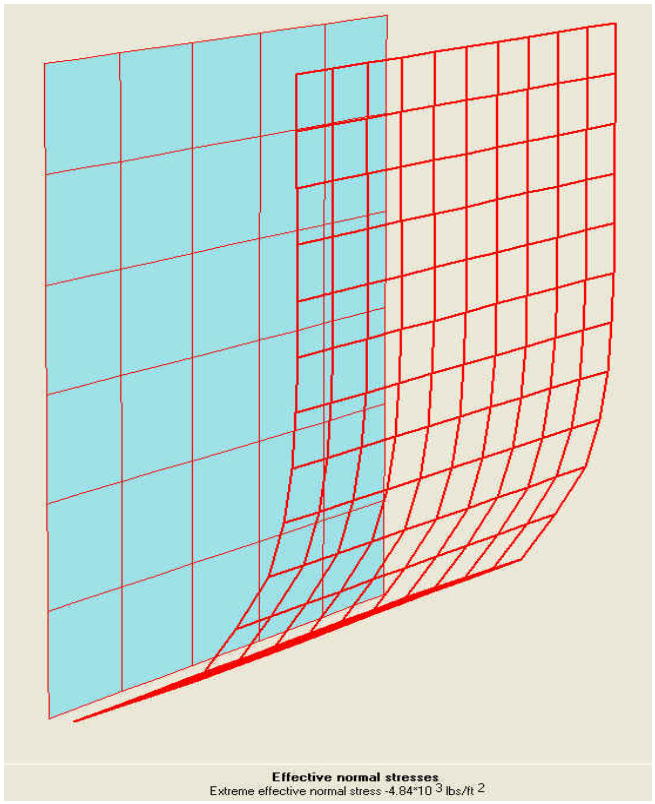

Figure 6.16 15’ Length Effective Normal Stresses Left Sidewall Frictionless Plane.

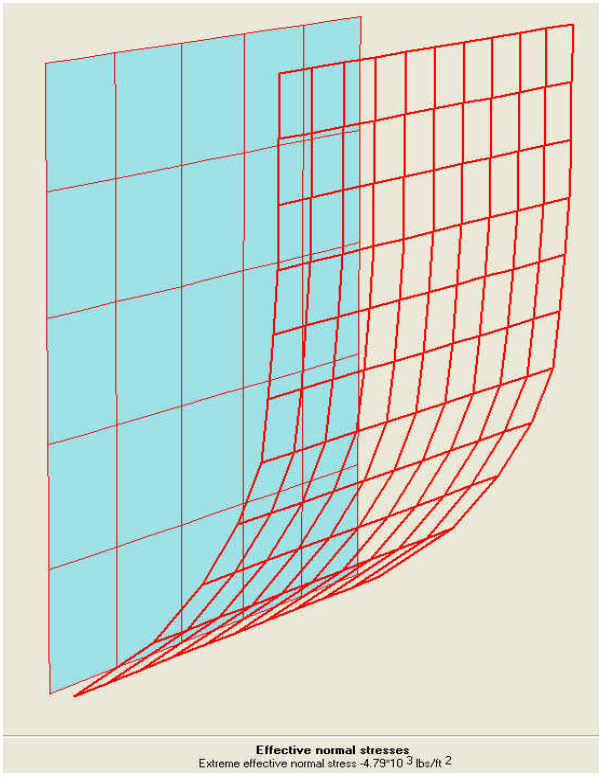

Figure 6.17 20’ Length Effective Normal Stresses Left Sidewall Frictionless Plane

Soil Box Analysis--Modeled with Test Pipe

A three-dimensional analysis was done with a 24" concrete pipe inserted inside the box. As stated above, the depth of bedding used was one diameter of the test pipe and a dense compacted soil backfill was used. In this analysis, the area around the perimeter of the pipe and the area on the sidewalls were modeled with both a friction angle of 35 degrees and a friction angle of less than 5 degrees.

Three lengths of soil box (10', 15', and 20') were analyzed using a friction angle of 35 degrees assigned around the perimeter of the pipe and along the sidewalls of the soil box. The stresses within the soil box and at the soil-structure interface were examined. The displacements of the soil and test pipe were also examined. Figure 6.18-6.20 shows the effective mean stress distribution for the entire soil box. The result of friction on the sidewalls shows a high stress concentration around the crown and invert of the pipe. In comparing the stress level between the haunch, the crown and invert of the pipe, the difference in stress values is approximately 7,000 lbs/ft^2.

With a friction surface on the sidewalls, the soil is restricted in movement resulting in a more concentrated load in the center of the soil box. The sidewall maximum stress value is seen in the 20' length box. The difference in stress from the 10' to the 20' length is approximately 600 lbs/ft^2. Figure 6.21 shows the stresses for the 20' soil box, for example, imposed on the perimeter area of the test pipe. The red shading on the crown and invert of the test pipe shows a high concentration of stresses. This concentration is a result of the friction on the sidewall and the soil displacing more at the center due to the applied load.

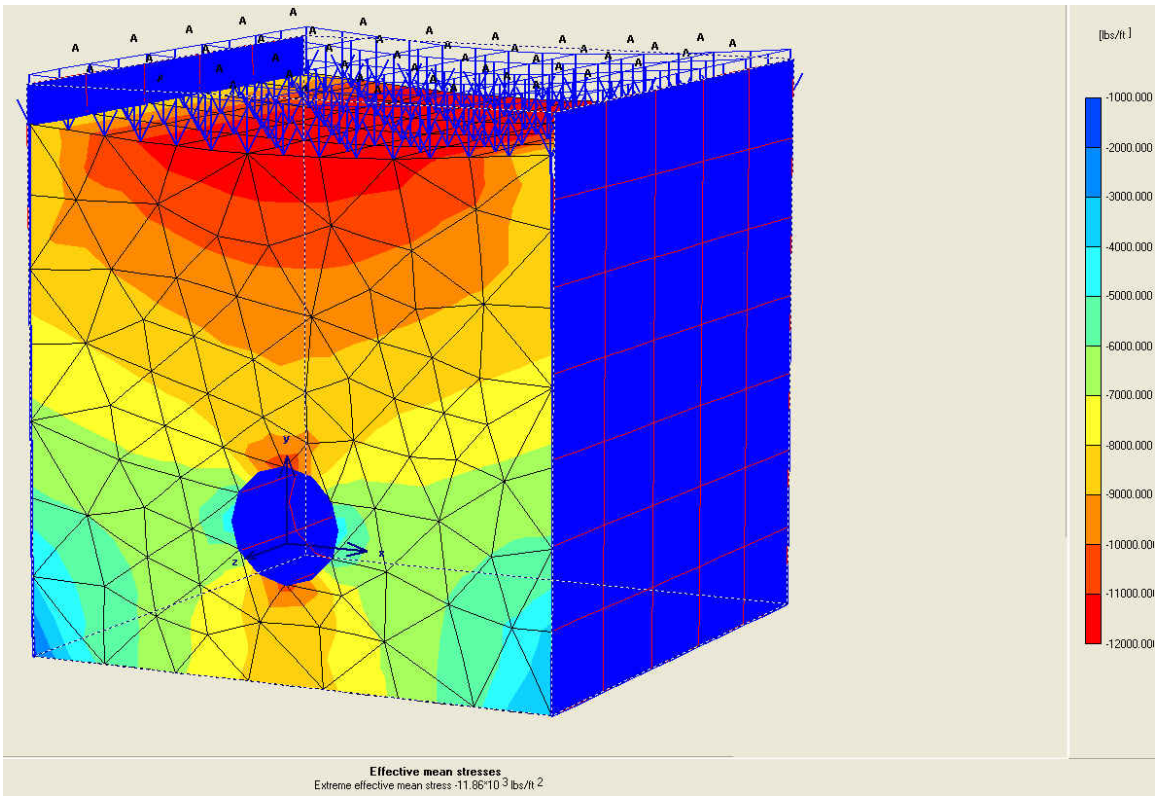

Figure 6.18 10’ Length Effective Mean Stress with Friction on Sidewalls.

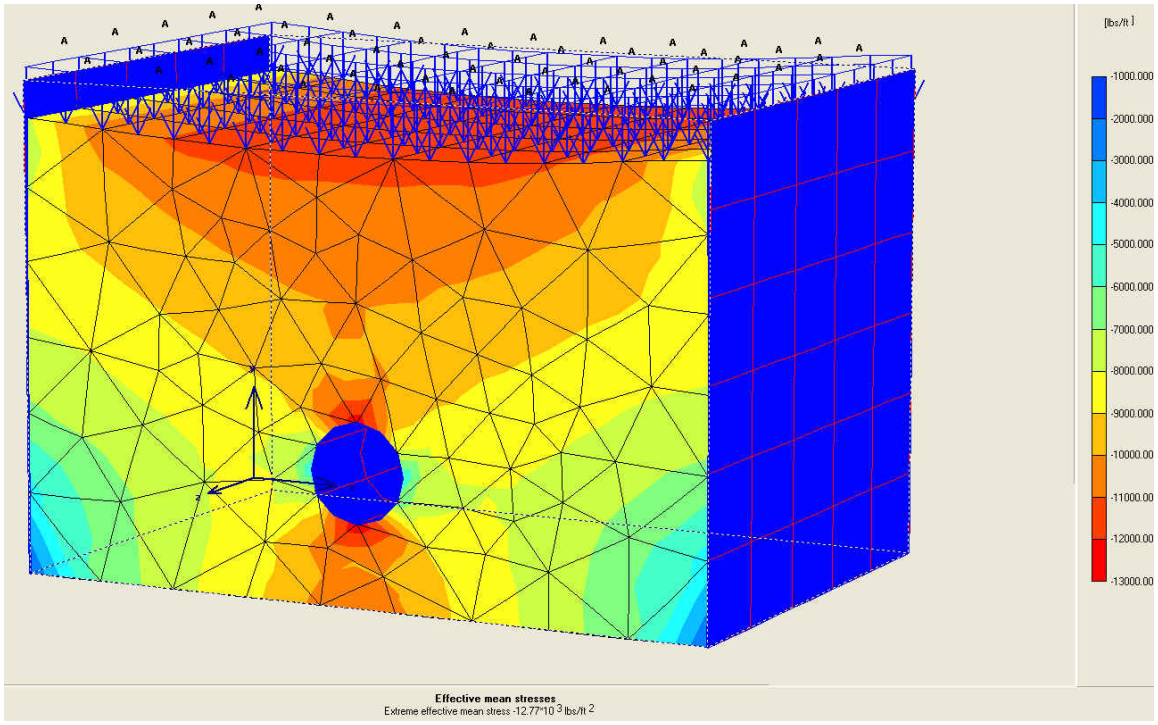

Figure 6.19 15’ Length Effective Mean Stress with Friction Sidewalls.

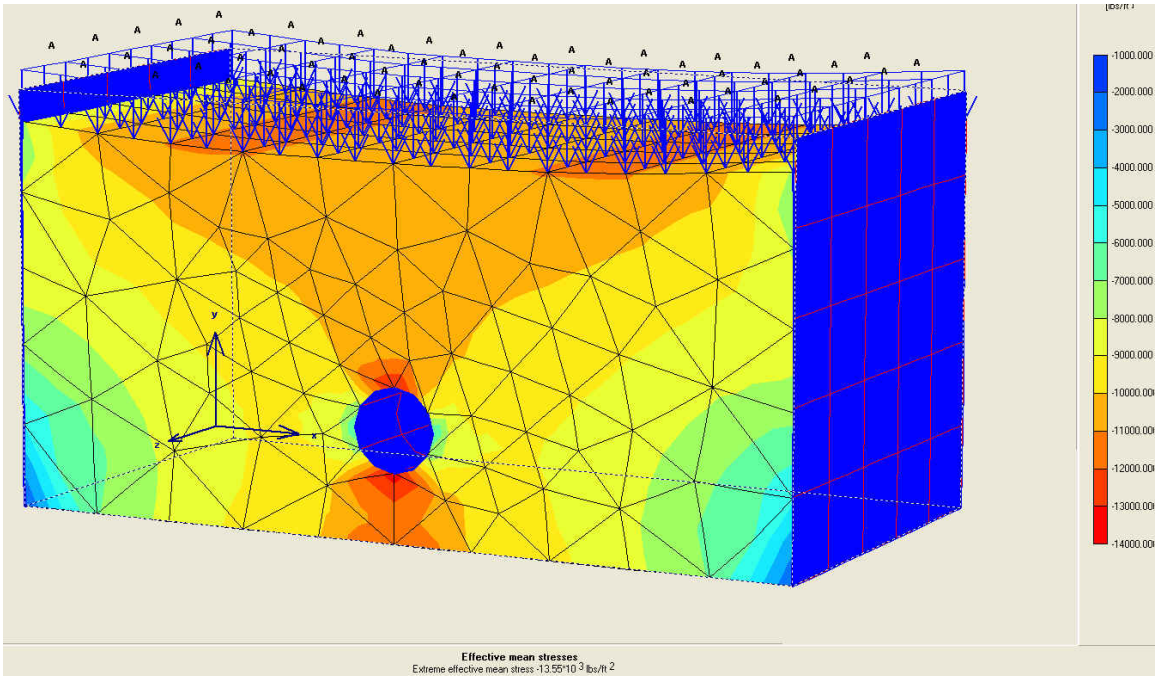

Figure 6.20 20’ Length Effective Mean Stress with Friction Sidewalls.

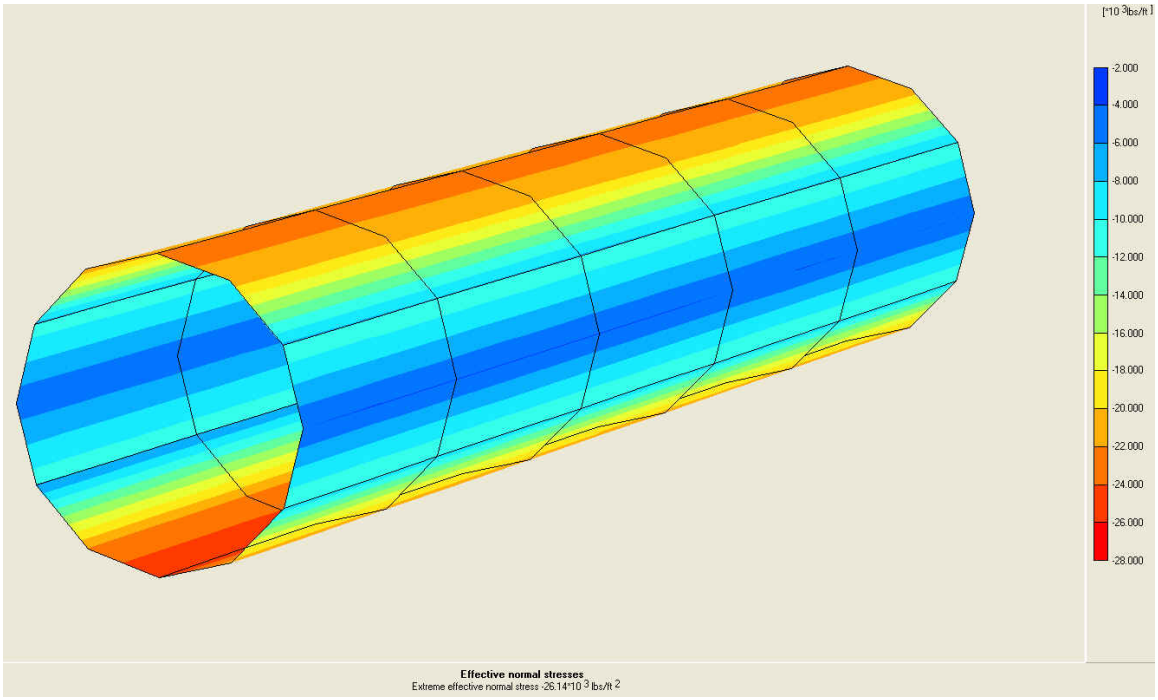

Figure 6.21 Effective Normal Stress Imposed on Perimeter of Test Pipe.

Another three-dimensional analysis was performed with a friction angle of less than 5 degrees assigned to the sidewalls and the perimeter area of the pipe. With the sidewalls having near zero friction, the soil is free to slide along the walls and also around the

perimeter of the pipe. This analysis was done to model the stress behavior difference between the friction analyses as stated previously and the near frictionless performance of the soil. Figures 6.22-6.24- show the effective mean stress concentration throughout the entire soil box due to the distributed load of 16,000 lbs/ft^2. The high stress values are concentrated around the haunches of the test pipe. Extreme effective mean stress for the 10' length is 17,320 lbs/ft^2, for the 15' length is 14,220 lbs/ft^2, and for the 20' length is 14,610 lbs/ft^2. The stress concentration decreases with increasing length.

When comparing the friction and frictionless analyses, the stress concentration modeled around the perimeter of the pipe decreased by a large amount when removing the friction from around the pipe. Another observation was the doubled increase in soil displacement. This is a direct result of the soils ability to move and displace freely along the sidewalls. Total displacements for the friction surface analysis ranged from 0.2' to 0.24'. The increase in displacement for the near frictionless analysis ranged from 0.4' to 0.6'.

A frictionless surface at the perimeter of the test pipe does not represent an accurate model for analysis. In order to examine this effect more precisely, a friction angle of less than 5 degrees was assigned to the sidewalls and a friction angle between a recommended soil/ steel structure interaction and a soil/ soil interaction was assigned to the perimeter of the pipe. An average was taken to represent a friction surface of less than the soil-soil friction yet greater than the soil-steel friction value. The results showed a more realistic performance for the structural response of the test pipe and the surrounding soil inside the soil box. Figures 6.25-6.27 show the effective mean stress distribution for this analysis.

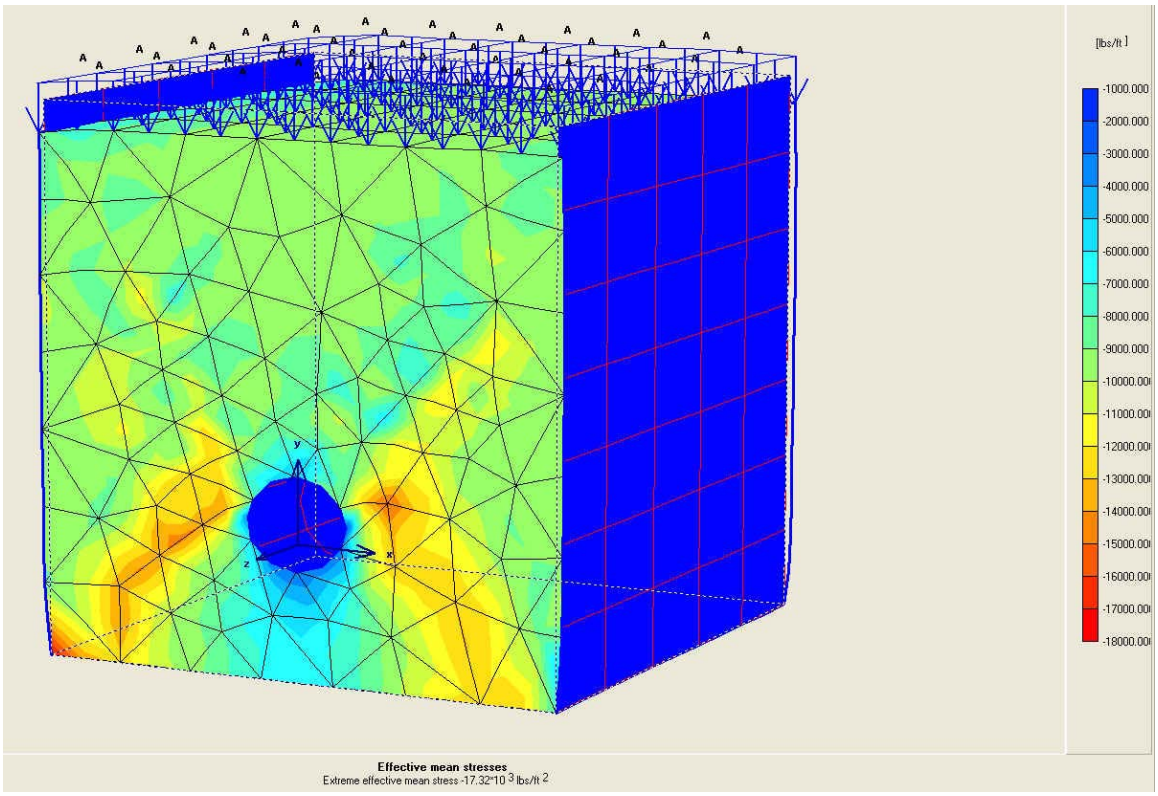

Figure 6.22 10’ Length Effective Mean Stress with Frictionless Sidewalls/ Pipe.

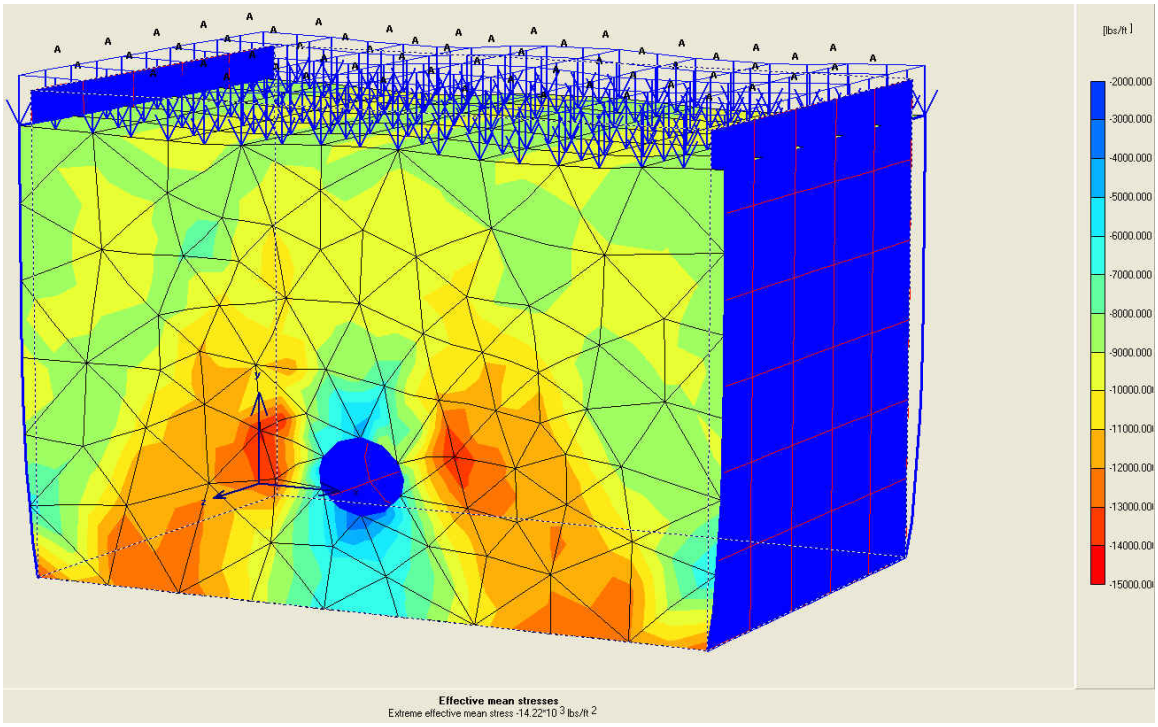

Figure 6.23 15’ Length Effective Mean Stress with Frictionless Sidewalls/ Pipe.

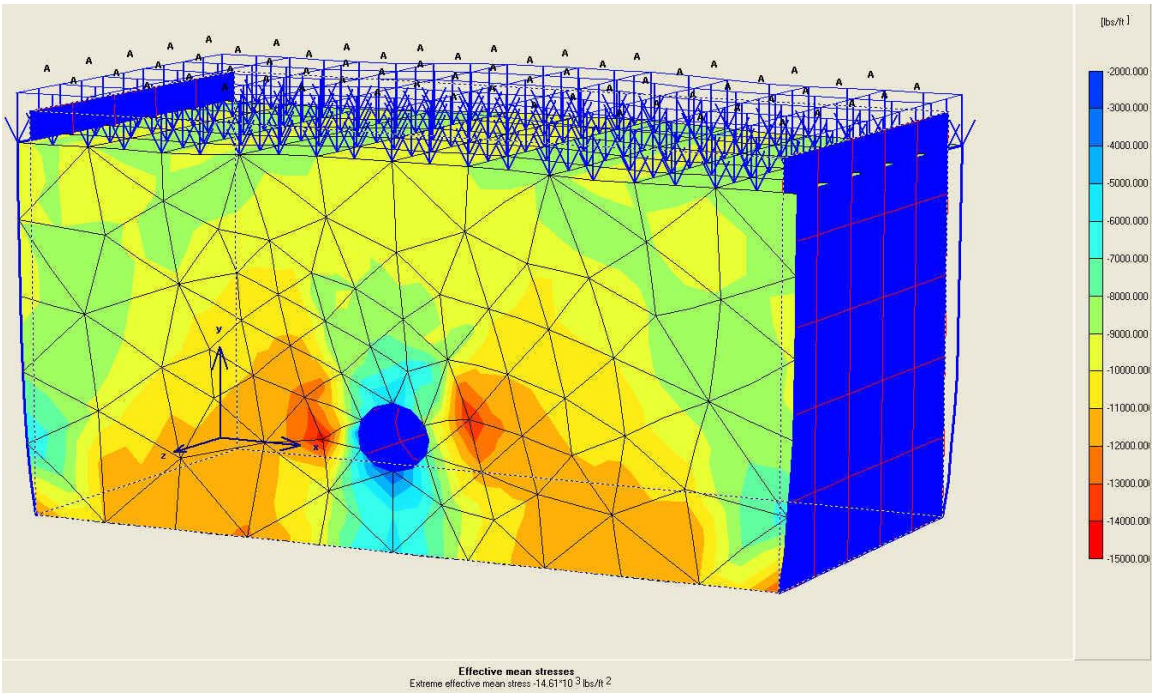

Figure 6.24 20’ Length Effective Mean Stress with Frictionless Sidewalls/ Pipe.

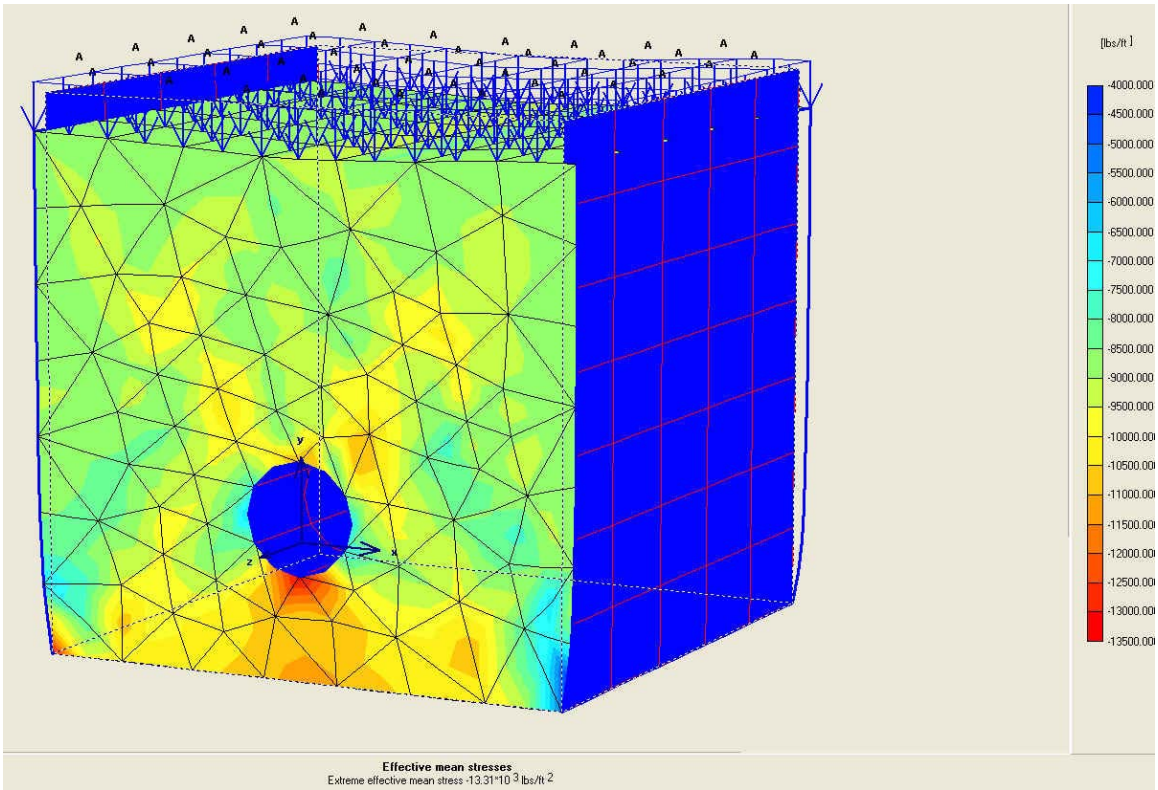

Figure 6.25 10’ length Effective Mean Stress with Frictionless Sidewalls and Friction Around Perimeter of Pipe.

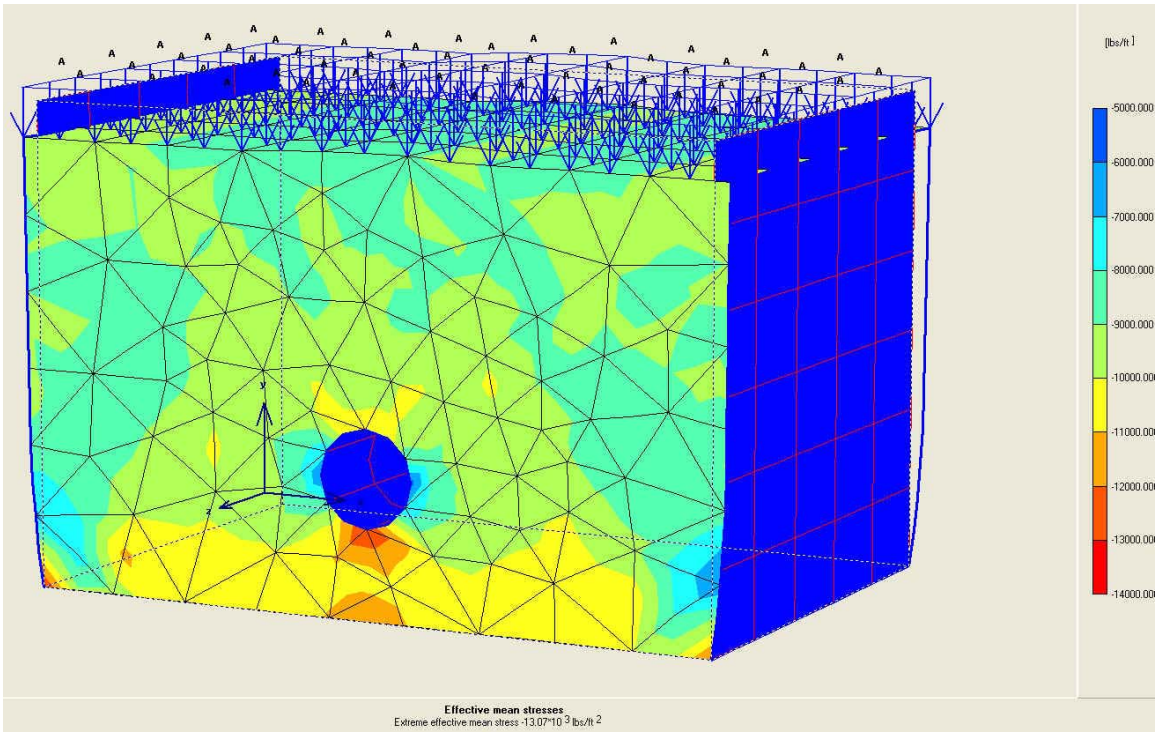

Figure 6.26 15’ length Effective Mean Stress with Frictionless Sidewalls and Friction Around Perimeter of Pipe.

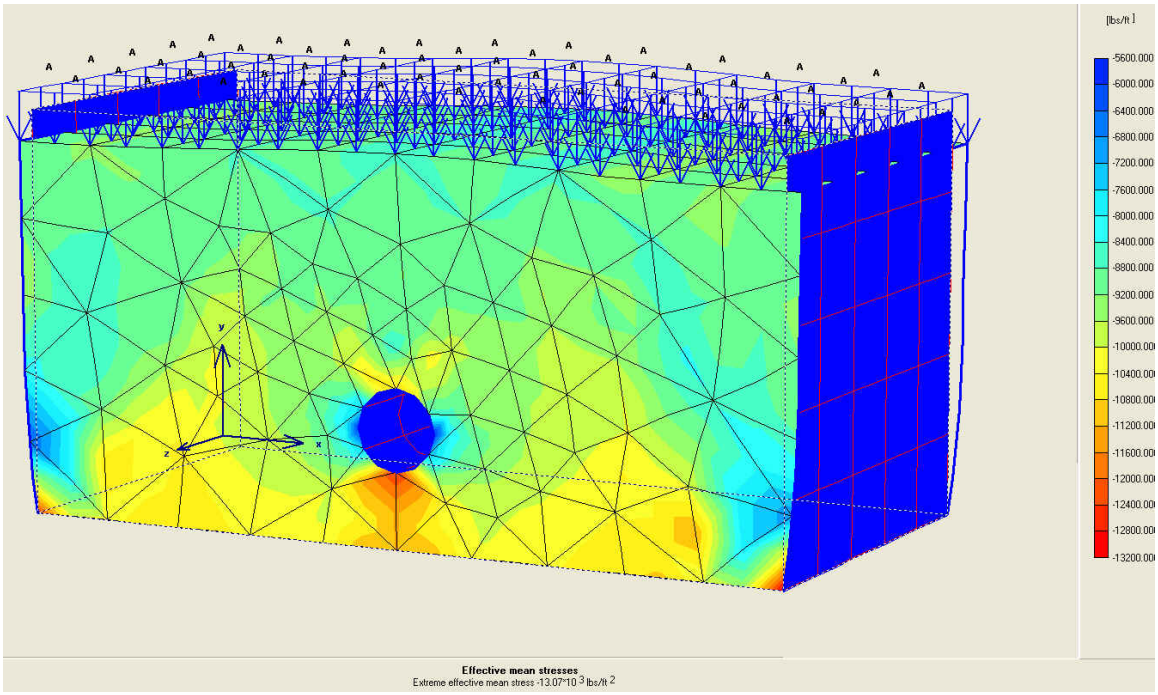

Figure 6.27 20’ length Effective Mean Stress with Frictionless Sidewalls and Friction Around Perimeter of Pipe.

The stress concentrations shown in Figures 6.25-6.27 portray a more accurate response from the soil and soil/ structure interaction. The assigned friction angles along the sidewalls and around the perimeter of the pipe effectively eliminate boundary effects. Results show no lateral stresses induce along the length of the pipe. This analysis shows a high stress concentration at the invert of the test pipe. With this high stress at the invert of the pipe, proper bedding compaction is necessary for maximum structural performance of the pipe.

Four Wall Friction Analyses

A three dimensional analysis examined the friction affects on the test pipe applied on all four walls of the soil box. Friction on the walls parallel to the pipe was assigned a value of 35 degrees. Though the two sidewalls were assigned friction angles, Plaxis is limited in that it does not allow friction angle specification for the front and rear walls. The test pipe was oriented perpendicular to the front and rear wall and parallel to the sidewalls. A concern was raised that if shear stress was induced on the ends of the pipe due to the test pipe sliding against the front and rear walls during loading, how would that shear stress affect the test pipe. Plaxis 3D was used to induce shear stress on the ends of the pipe and examine the effects of that stress along the length of the pipe and on the total displacement of the pipe. The friction on the front and rear wall was created using a beam element activated over a thin slice (0.01') in the z direction using the 3D mesh generation tool.

Shear stress induced on the ends of the pipe became a concern for the test pipe when attempting to simulate *in situ* conditions. An *in situ* pipe will experience very little shear stress on the ends of the pipe, where-as-in a test facility, the boundary conditions pose a concern for testing of the pipe. The stresses and displacements were examined

along the length of the pipe when the shear stress was induced on its ends as shown in Figure 6.28. Eight different analyses were performed using 18" and 24" diameter FRCP and SRCP compacted in dense soil backfill. Each diameter pipe was modeled using a sidewall friction angle of 35 degrees and less than 5 degrees. Displacements along the span length of the test pipe are shown in Table 6.7 with displacements at the front, middle, and rear of the pipe. As shown in Table 6.7, the displacements along the length of the pipe did not differ from the front to the rear. Shear stress induced at the ends of the pipe did not affect the displacements of the pipe.

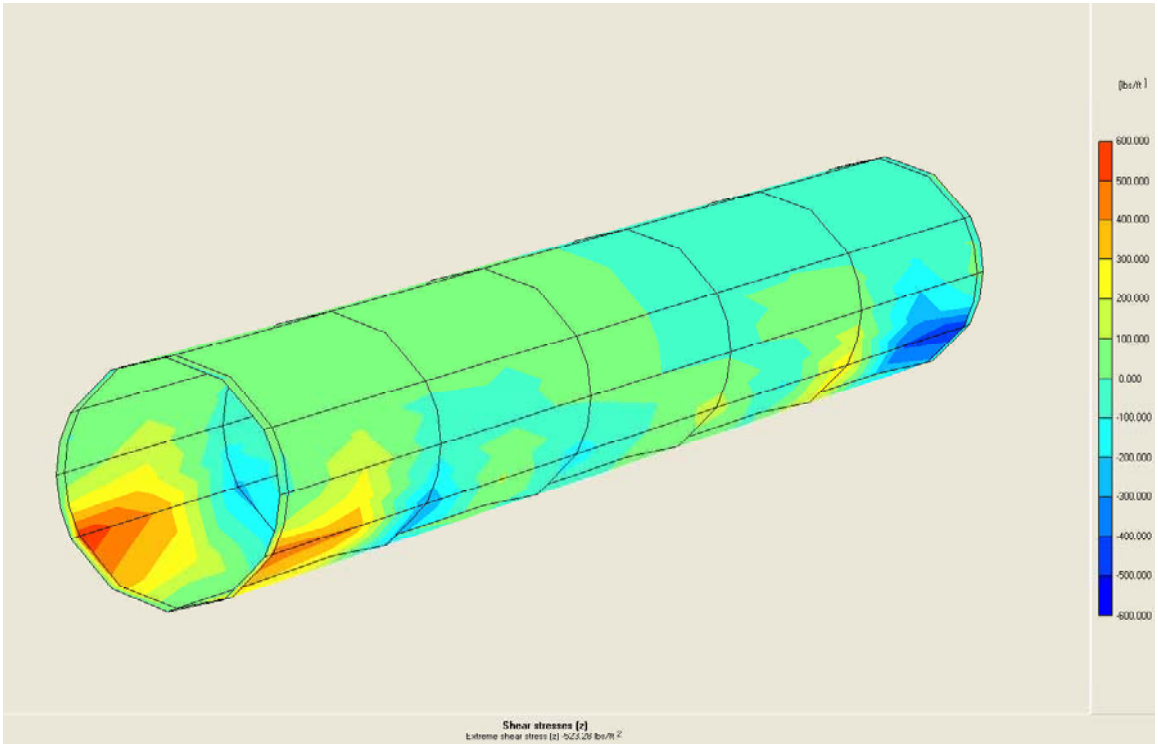

Figure 6.28 Plaxis 3D Test Pipe with Shear Stress Induced on Ends of Pipe

The stress at the middle of the pipe due to the shear stresses encountered at the ends of the pipe posed a concern. An area around the perimeter of the test pipe modeled the effective mean stress along the full length of the pipe. The eight analyses showed very little stress increase at the mid span of the pipe. Concerns of a stress increase at the mid

span of the pipe were analyzed using Plaxis 3D. Table 6.8 presents the extreme effective mean stress values around the mid span for each of the eight runs modeled. The stress values along the length of the pipe differed very little. To guarantee that no shear stresses are induced at the ends, the test pipe shall be 1-2 inches short of the depth of the box, allowing the pipe to settle without contact with the front or rear wall.

Table 6.7 Displacement of Pipe Length with Shear Stress Induced on the Ends.

Pipe	Dia.	R*	Disp F	Disp M	Disp R
FRCP	18"	1	0.050	0.050	0.050
SRCP	18"	1	0.050	0.050	0.050
FRCP	18"	0.05	0.019	0.019	0.019
SRCP	18"	0.05	0.019	0.019	0.019
FRCP	24"	1	0.067	0.067	0.067
SRCP	24"	1	0.067	0.067	0.067
FRCP	24"	0.05	0.035	0.035	0.035
SRCP	24"	0.05	0.029	0.029	0.029

* R is the Interface strength value representing the friction angle where R=1 is a friction angle equal to the soil and R=0.05 is near zero friction. Disp F, M, R represents the pipe displacement at the front (F), Midspan (M) and Rear (R) of the pipe in feet.

Table 6.8 Extreme Effective Normal Stresses Along the Length of Pipe with Shear Stress Induced on the Ends.

Pipe	Dia.	R*	EMS_1	EMS_2
FRCP	18"	1	-25750	-25620
SRCP	18"	1	-25760	-25625
FRCP	18"	0.05	-3860	-3860
SRCP	18"	0.05	-3860	-3860
FRCP	24"	1	-23220	-23540
SRCP	24"	1	-23510	-23490
FRCP	24"	0.05	-5050	-5050
SRCP	24"	0.05	-5100	-5110

* R is the Interface strength value representing the friction angle where R=1 is a friction angle equal to the soil and R=0.05 is near zero friction.

1. EMS is the extreme effective mean stress on the ends of the pipe in lbs/ft^2
2. EMS is the extreme effective mean stress at the middle span of the pipe in lbs/ft^2

CHAPTER 7
RECOMMENDATIONS

Two and three-dimensional analyses were performed using Plaxis Finite Element Analysis for Soil and Rock modeling soil structure interaction on buried pipes. A large soil test box was designed using the stress analysis from the finite element software. Plaxis 3D provided a good examination of stress and displacement analysis on buried pipes. In this research a two-dimensional approach was initially used, which limited the analysis in the z direction.

Plaxis 3D was used to analyze stress and displacements along the full length of the test pipe while buried and under loads from the cover soil and an applied distributed load. Plaxis 3D is a tunneling software program providing analysis in the z direction, the length of the test pipe. A three-dimensional approach is highly recommended for further analysis of any buried pipe research.

Another concept of interest for future research is the level of compaction around the haunch of the buried pipe. Plaxis 3D will allow the user to define the compaction throughout a defined distance in the z direction running parallel to the buried test pipe. Properties for analysis would be the normal stresses, shear stresses, displacements, axial forces and bending moments along the full length of the pipe. Plaxis 3D allows the user to input the stiffness of the soil in a desired geometry formation around the pipe. A finite element analysis is recommended for the area defining a loose compaction around the haunch of the pipe for a specified distance along the test pipe. A complete analysis is recommended on the effects of poor compaction around the haunch (loose pockets).

As shown in the third analysis, the highest stress concentrations occurred at the invert of the pipe assuming proper compaction. If poor compaction occurs the stress concentration locations could change, affecting the structural response of the pipe. Benefits of this analysis would include examination of the required trench width for installation of different size pipe diameters and also examination of the effect of the cover soil, whether compacted loose or dense.

Other recommended analyses for Plaxis 3D are the effects of soil-structure interaction between the test pipe and surrounding soil. Again the user can specify the stiffness of the soil surrounding the test pipe for analysis of the structural performance of the test pipe. Any geometry formation can be specified in the input program for Plaxis 3D to analyze a specified area of interest. Beam elements are used for the lining of the bored tunnel opening. The 3D mesh generation is a useful tool for specific analysis along the length of the pipe. The user specifies the distance into the z-axis for analysis and the thickness of the slice.

The structural performance of a test pipe can be analyzed looking at the effective normal stresses acting on the test pipe. Plaxis 3D does an excellent job of providing shaded images for the output of a finite element analysis. Stress distribution along the length of the pipe or any other material for analysis is displayed through the shading, allowing the user to visualize where the stress intensities vary in the analysis. Another good feature is the three-dimensional views in the output program. Having a three-dimensional view of a three-dimensional research project provides a better understanding of the results.

APPENDIX
PLAXIS 2D ANALYSIS AND RESULTS

Dimension Analysis

A two-dimensional finite element analysis was conducted with and without the pipe inside the soil box to analyze the box dimensions. In the two-dimensional analysis, an approximate height of ten feet was used based on the proper bedding needs of the 24" diameter pipe. Three different widths of soil box were analyzed, ten, fifteen and twenty feet. Each analysis was first run with no pipe inside the box and then with each of the 18" and 24" diameter concrete pipes. Symmetry was used in the size analysis of the box so that only the right half of the box need be included, as shown in Figure A.1.

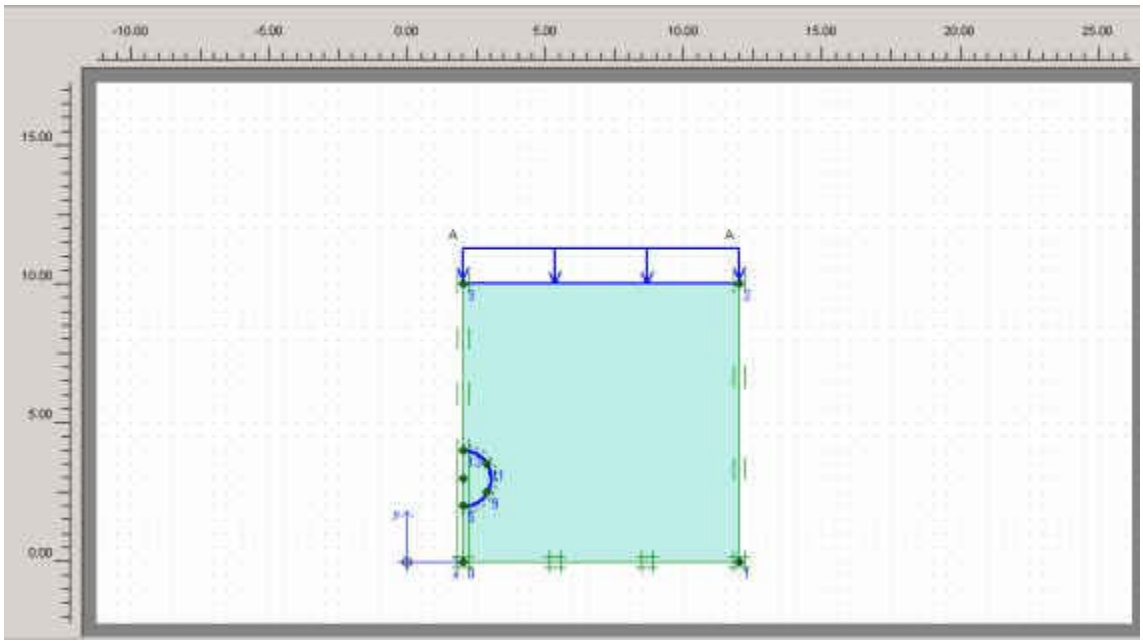

Figure A.1 Plaxis 2D Symmetry Model of 24" diameter FRCP.

Plaxis 2D modeling to determine the configuration that would minimize the sidewall stresses using the maximum load of 16,000 lbs/ft^2. The first analysis involved

three different widths with no pipe in the box, just the backfill soil. Figure A.2 shows the schematic of all three box analyses, for each length, executed in Plaxis 2D. Results showed the same extreme value for the sidewall stresses for each length as 7,270 lbs/ft^2. Modeling in only two dimensions, stresses are a direct result of the load applied and the unit weight of the soil. Plaxis 2D modeled with uniform compaction resulted in a uniform stress distribution along the sidewall. In order to obtain the sidewall stresses, a cross section was taken along the sidewall displaying the extreme effective normal stress. An example is shown in figure A.3.

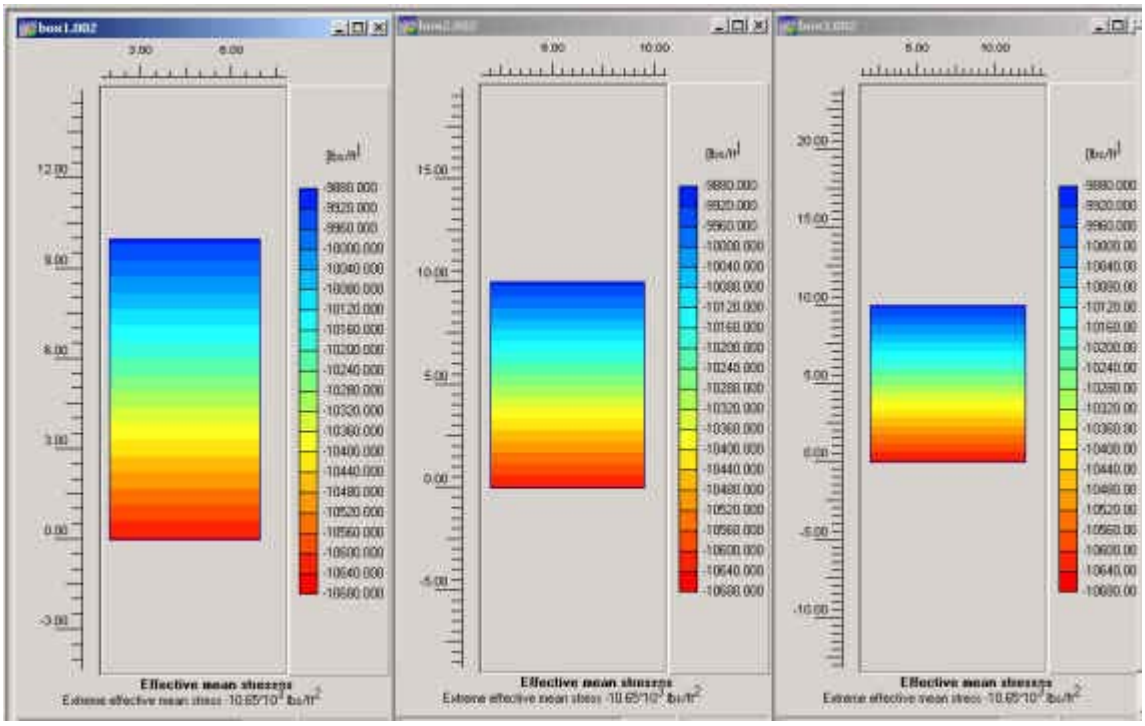

Figure A.2 Three Different Widths Modeled in Plaxis 2D: 10, 15, 20 feet wide.

A two-dimensional analysis was performed with a concrete pipe inserted in the soil box. Twenty-four inch diameter versions of both SRCP and FRCP were used to examine the stress on the sidewalls. The 24" diameter pipes were used because the stress on the sidewalls increases as the diameter of the pipe increases. Again, three different soil box

lengths were examined, with the right half of each of the FRCP and SRCP inserted into the soil model.

Stresses along the sidewalls for the ten, fifteen and twenty foot models with the FRCP are displayed in Figures A.4-A6. FRCP is displayed in the figure for illustration purposes only, both FRCP and SRCP were analyzed and resulted in similar stresses along the sidewalls. Results show that the stress decreases as box length increases, creating a maximum stress on the sidewall of 7,300 lbs/ft^2 for the twenty-foot length . For verification, a full-scale finite element analysis was done for the twenty-foot length soil box model. The full-scale model reported the same stress on the sidewalls as the model using symmetry with only the right half of the SRCP and FRCP. From the 24" diameter pipe analysis, the results showed that the stresses and boundary conditions were lowest for the 20' length.

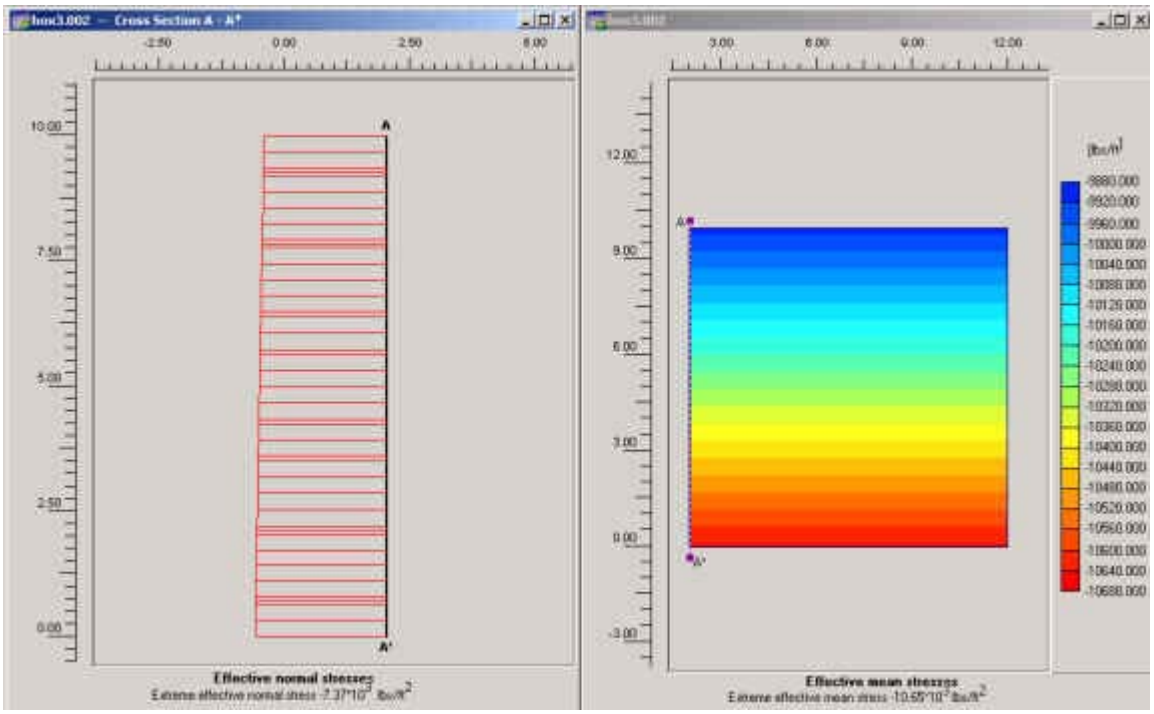

Figure A.3 Example of Cross Section Used to Examine the Sidewall Stresses (20' Width).

Wall Friction/ Soil Compaction Analysis

A two-dimensional analysis examined the sidewall friction of the selected box dimension length of twenty feet, altering the friction angle of the soil structure interface with the sidewalls and the perimeter area of the pipe using two different compacted backfills. Stresses and displacements were analyzed throughout the soil and along the specified areas of interest. Two different friction angles were assigned; a friction angle of 35 degrees and a friction angle less than five degrees. I. D. Moore conducted research, as discussed in chapter 2, that indicated a minimization of the friction angle to less than five degrees helps to reduce boundary effects from inducing lateral stresses on the test pipe. The purpose is to simulate *in situ* conditions by minimizing the boundary condition effect on the structural response of the test pipe. A total of 24 different analyses were done to examine the wall friction and the effects of different compacted soils on the structural response of the test pipe. Three different pipe size diameters were analyzed, 18", 24", and 48", with two types of concrete pipes, FRCP and SRCP, embedded in two different compacted backfills, loose and dense. Full-scale analyses were done to eliminate any doubt within the results. The extreme value results are presented in Table A.1.

It is apparent from the finite element modeling results that the dense compaction is more stable than the loose compaction. Referring to the total displacement in Table A.1, the displacement is twice as large for the loose compacted soil. Dense compacted soil will provide better bedding conditions for allowing the pipe to sustain a load. The dense compacted soil was modeled using a soil modulus value compacted to 90% proctor.

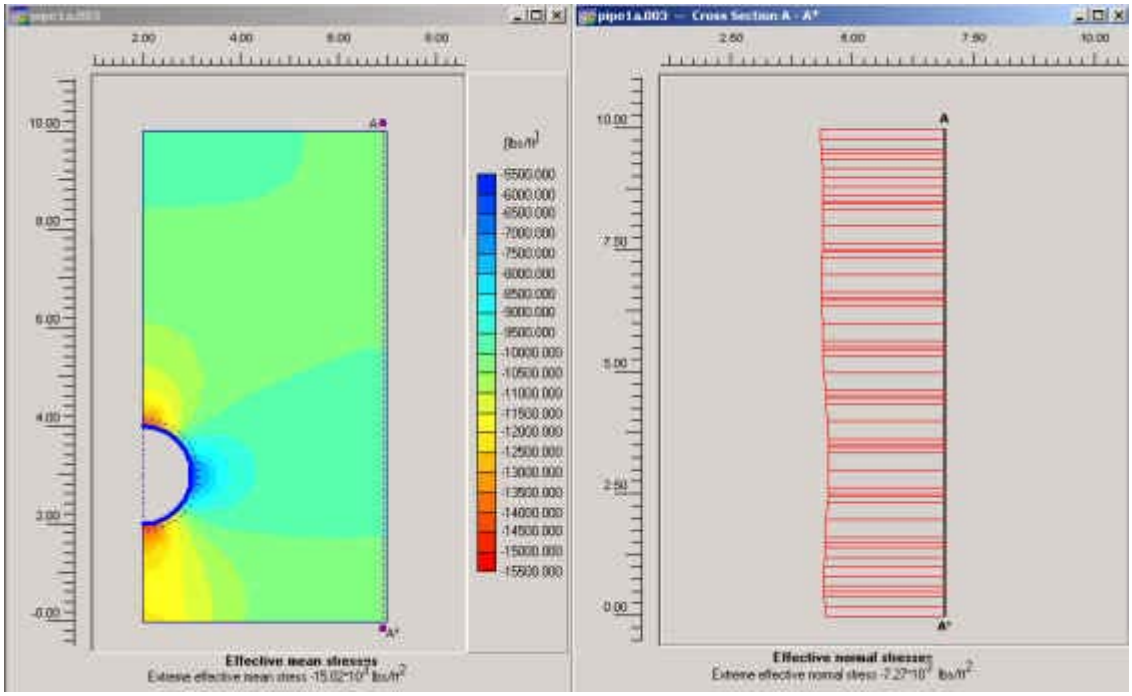

Figure A.4 Example FRCP Cross Section of Sidewall Stresses (10’ wide box).

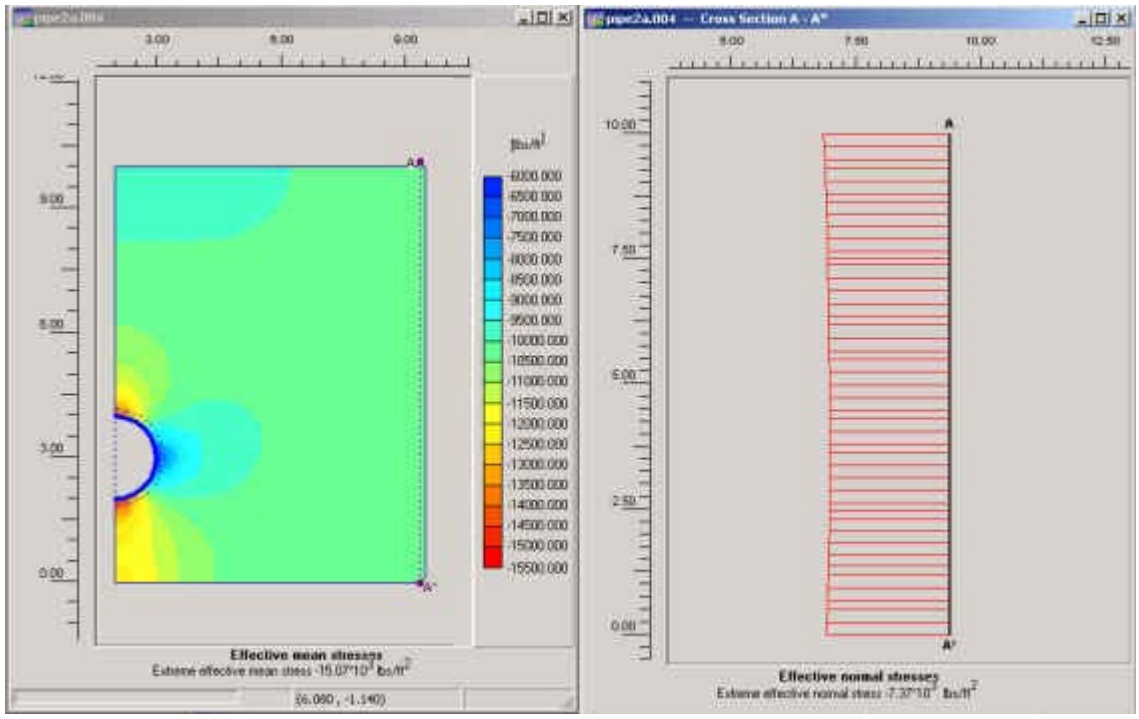

Figure A.5 Example FRCP Cross Section of Sidewall Stresses (15’ wide box).

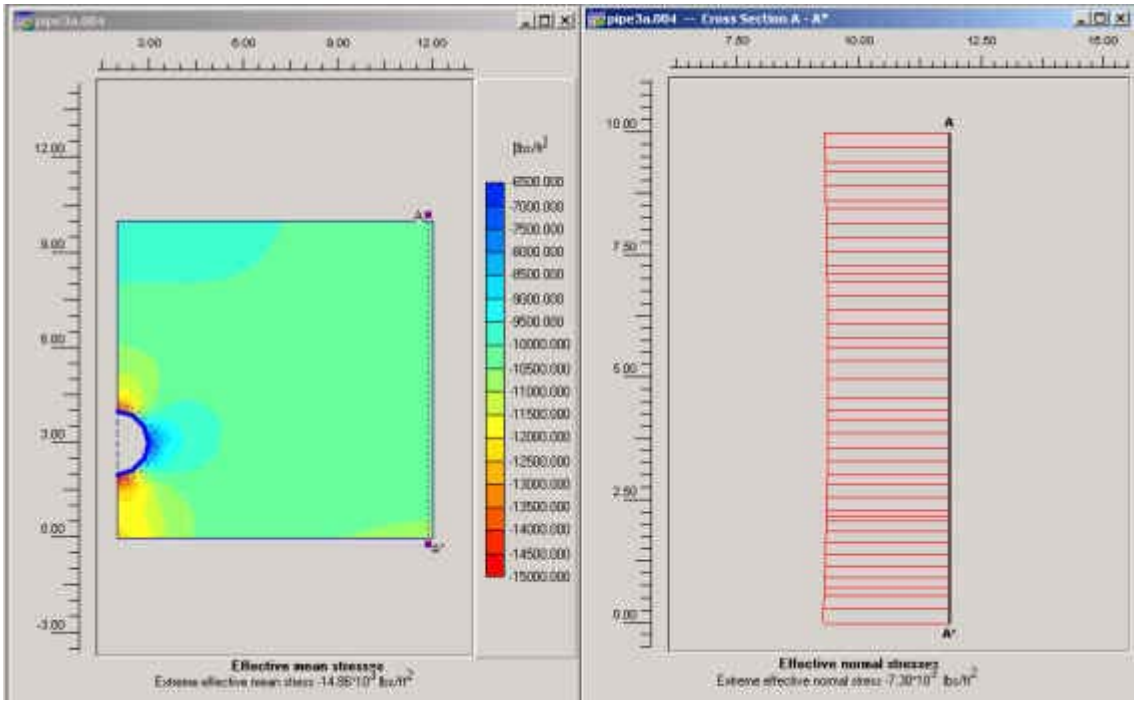

Figure A.6 Example FRCP Cross Section of Sidewall Stresses (20’ wide box).

In comparing both the FRCP and SRCP, the overall difference in results was minimal. The properties examined around the pipe, such as stress and displacements in the surrounding soil, showed minimal changes between the FRCP and SRCP. When comparing the variation in friction angle, the friction angle equal to the soil friction angle resulted in an effective normal stress along the sidewall that was twice the effective normal stress of the model with a friction angle less than five degrees. It should be noted that the negative stress values represent compression.

Table A.1 Wall Friction Analysis-Plaxis 2D Finite Element Analysis

Pipe	D[1]	C[2]	R[3]	EPS[4]	EMS[5]	$Disp_1$	IEWS[6]	IEPS[7]	$Disp_2$	PM[8]	$Disp_3$
SRCP	24"	Loose	1	-24560	-14720	0.523	-7360	-24990	-0.157	-10550	0.151
FRCP	24"	Loose	1	-24550	-14710	0.523	-7450	-24990	-0.157	-11100	0.152
SRCP	24"	Dense	1	-24550	-14710	0.231	-7380	-24980	-0.069	-10550	0.067
FRCP	24"	Dense	1	-24530	-14700	0.230	-7260	-24970	-0.070	-10950	0.067
SRCP	24"	Loose	0.05	-26430	-14760	0.755	-4790	-5800	-0.442	-2090	0.257
FRCP	24"	Loose	0.05	-26430	-14760	0.755	-4790	-5800	-0.442	-2190	0.257
SRCP	24"	Dense	0.05	-26430	-14760	0.333	-4790	-5800	-0.195	-2090	0.113
FRCP	24"	Dense	0.05	-26430	-14760	0.333	-4790	-5800	-0.194	-2190	0.113
SRCP	18"	Loose	1	-23690	-13850	0.535	-7340	-24660	-0.135	-5780	0.129
FRCP	18"	Loose	1	-23680	-13840	0.535	-7340	-24660	-0.135	-6070	0.129
SRCP	18"	Dense	1	-23680	-13840	0.236	-7340	-24650	-0.059	-5770	0.057
FRCP	18"	Dense	1	-23660	-13840	0.236	-7340	-24640	-0.059	-6070	0.057
SRCP	18"	Loose	0.05	-24430	-15400	0.750	-4840	-4590	-0.325	-884	0.204
FRCP	18"	Loose	0.05	-24430	-15400	0.750	-4840	-4590	-0.324	-961	0.204
SRCP	18"	Dense	0.05	-24430	-15400	0.331	-4840	-4590	-0.143	-884	0.090
FRCP	18"	Dense	0.05	-24430	-15400	0.331	-4840	-4590	-0.143	-941	0.090
SRCP	48"	Loose	1	-23300	-13840	0.483	-7120	-22920	-0.289	-40150	0.283
FRCP	48"	Loose	1	-23290	-13840	0.482	-7120	-22920	-0.289	-41560	0.282
SRCP	48"	Dense	1	-23290	-13840	0.213	-7120	-22910	-0.127	-40140	0.125
FRCP	48"	Dense	1	-23280	-13840	0.213	-7120	-22910	-0.127	-41550	0.125
SRCP	48"	Loose	0.05	-30550	-17710	1.230	-5130	-11990	-1.130	-18600	0.624
FRCP	48"	Loose	0.05	-30550	-17710	1.230	-5130	-11990	-1.130	-19370	0.624
SRCP	48"	Dense	0.05	-30550	-17710	0.541	-5130	-11990	-0.499	-18600	0.275
FRCP	48"	Dense	0.05	-30550	-17710	0.540	-5130	-11990	-0.499	-19240	0.275

**All values reported are extreme values (i.e., the maximum values).

1. D is the pipe diameter in inches.
2. C is the compaction of the backfill.
3. R is the interface value of strength. A value of 1 represents a friction angle the same as the backfill soil. A value of 0.05 represents a friction angle less than five degrees.
4. EPS is the effective principal stress for the entire model box in lbs/ft^2
5. EMS is the effective mean stress for the entire model box in lbs/ft^2
6. IEWS is the interface effective normal wall stress in lbs/ft^2
7. IEPS is the interface effective normal pipe stress in lbs/ft^2
8. PM is the pipe bending moment in lbs-ft/ft

$Disp_1$ is the total displacements for the entire box in feet.
$Disp_2$ is the total displacements for interface around the perimeter of the pipe in feet.
$Disp_3$ is the total displacement of the concrete pipe in feet.

LIST OF REFERENCES

American Society for Testing and Materials, Acoustic Emission. ASTM E 1932-97, Philadelphia, 2001.

Beattie Alan G, "Experimental methods-nondestructive evaluation techniques," Handbook on Structural Testing, Society for Experimental Mechanics, Inc., The Fairmont Press, Inc., Lilburn, GA, pp. 237-294, 1993.

Bishop, R R, Time dependent performance of buried PVC pipe. Underground Plastic Pipes, International Conference of Underground Plastic Pipe, March 30-April 1, 1981, New Orleans, Louisiana, pp. 202-212.

Bland, C E G, Sheppard, K J, "Investigations into the structural performance of clay pipes," Advances In Underground Pipeline Engineering, Proceedings of the International Conference, Jeyapalan, J K (ed), University of Wisconsin-Madison, 1985, pp. 100-116.

Brinkgreve R B J, Plaxis Manual. Plaxis, Rotterdam, Netherlands, 1998.

Brachman et al. R W I, Moore I D, Rowe R K, 2000, "The design of a laboratory facility for evaluating the structural response of small diameter buried pipes," Canadian Geotechnical Journal, 37: 281-295.

Brachman et al. R W I, Moore I D, Rowe R K, 2001, "The performance of a laboratory facility for evaluating the structural response of small diameter buried pipes," Canadian Geotechnical Journal, 37: 260-275.

Brachman et al. R W I, Moore I D, Rowe R K, 1996, "Interpretation of a buried pipe test: small diameter pipe in the Ohio University facility," Transportation Research Record 1541, Structures, Culverts, and Tunnels. pp. 64-70.

Fintel Mark 1974, Handbook of Concrete Engineering. Van Nostrand Reinhold Company, New York, NY.

Gaube, E, Mueller, W, "12 years of deformation measurement on plastic sewer pipes from Hostalen GM 5010," Underground Plastic Pipe, International Conference on Underground Plastic Pipe, March 30-April 1, 1981, New Orleans, Louisiana, pp. 288-297.

Minolta USA. “Minolta 3D Digitizer.” Minolta Co. Ltd. January 9, 2003 <www.minoltausa.com>

Molin, J, “Flexible pipes in buried clay,” Underground Plastic Pipe, International Conference on Underground Plastic Pipe, March 30-April 1, 1981, New Orleans, Louisiana, pp. 322-337.

Moser A P, 2001, Buried Pipe Design. 2nd Edition McGraw Hill, New York, NY, pp. 65-82.

Parmalee, R A, “A study of soil structure interaction of buried concrete pipe,” Concrete Pipe and the Soil-Structure System, ASTM STP 630, Bealey, M, Lemons, J D, editors, American Society for Testing and Materials, 1977, 99. 66-75.

Scott Ian G, 1991, Basic Acoustic Emission. Gordon and Breach Science Publishers, New York, pp. 43-83.

Selander, C E, Hickey, M E, Causey, F E, Howard, A K, “Evaluation of reinforced plastic mortar pipe – a government industry cooperative study,” REC-ERC-72-26, Bureau of Reclamation, United States Department of the Interior, 1972.

Singhal, A C, Veliz, V, “Experimental and field observation of dynamic behavior of buried pipelines,” Advances in Underground Pipeline Engineering, Proceedings of the International Conference, Jeyapalan, J K (ed), University of Wisconsin-Madison, 1985, pp. 302-310.

Todres, H A, McClinton, M, “Stress and strain responses of a soil-pipe system to vehicular traffic,” Advances In Underground Pipeline Engineering, Proceedings of the International Conference, Jeyapalan, J K (ed), University of Wisconsin-Madison, 1985, pp. 428-437.

Vary, Alex, 1988, “The acousto-ultrasonic approach,” Acousto-Ultrasonics Theory and Application. Plenum Press, New York and London.

BIOGRAPHICAL SKETCH

Melissa Kay Crosby was born April 30, 1978, in Naples, Florida, to Lacy Oler and Sandra Kay Crosby. She graduated from Santa Fe High School in May 1996 in the top 5% of her class and started her college career at Santa Fe Community College in Gainesville, Florida, on a full paid scholarship. She received her Associate of Arts degree in August 1999 and transferred to the University of Florida to pursue a Bachelor of Science in Civil Engineering in the summer of 1999. While attending the University of Florida full time, Melissa worked part time for a local civil engineering firm, Kelley Engineering, Inc., for two years interning and gaining valuable experience in the work field. She received her Bachelor of Science in Civil Engineering in December 2001, graduating with honors. Melissa continued with her education entering graduate school to pursue a Master of Engineering in the Materials Group of the Civil and Coastal Engineering Department in January 2002 immediately following her undergraduate completion. After graduating from the University of Florida with a Master of Engineering, Melissa plans on moving to Atlanta, Georgia, to pursue a career in the exciting and challenging field of civil engineering design. Melissa also plans to become licensed as a professional engineer in the state of Georgia.